Ion Signaling for Organ Size and Scaling During Zebrafish Fin Regeneration

by

Heather Kimberly Le Bleu

A dissertation accepted and approved in partial fulfillment of the

requirements for the degree of

Doctor of Philosophy

In Biology

Dissertation Committee:

Tory Herman, Chair

Kryn Stankunas, Advisor

Bruce Bowerman, Core Member

Karen Guillemin, Core Member

Adam C Miller, Core Member

Michael J Harms, Institutional Representative

University of Oregon

Winter 2024

DISSERTATION ABSTRACT

Heather Kimberly Le Bleu

Doctor of Philosophy in Biology

Title: Ion Signaling for Organ Size and Scaling During Zebrafish Fin Regeneration

Organs "know" how to develop to a specific size and shape conferring optimal function. In humans, very few organs and appendages show a natural ability to repair. Exemplifying this fundamental mystery, adult zebrafish fins regenerate to their original size and shape regardless of injury extent. Therefore, zebrafish fin regeneration provides a tractable system to investigate "organ scaling" mechanisms. Bioelectricity, or ion flow across cell membranes, is long-associated with both organ size control and regeneration. However, the links between ion signaling and their effectors to specific cell behaviors determining organ size are limited. Perturbed ion signaling, notably by elevated voltage-gated K^+ channel activity and inhibited Ca^{2+}-dependent calcineurin signaling, leads to dramatic overgrowth of regenerating zebrafish fins. A unique distal population of mesenchymal cells within the fin's regenerative blastema sustains fin outgrowth. The classic zebrafish mutant *longfin*^{t2} develops and regenerates dramatically elongated fins and underlying ray skeleton. We show ectopic expression of the *kcnh2a* K^+ channel in fin ray fibroblast-lineage cells enhances fin outgrowth in late regeneration rather than at early blastema establishment. Epistasis experiments suggest that Kcnh2a likely blocks Ca^{2+}-dependent calcineurin signaling to end fin outgrowth. Mechanisms of putative Ca^{2+} signaling during fin size acquisition has not been explored. Using a new Ca^{2+} responsive GCaMP6s transgenic reporter line, we show fibroblast-lineage cells are the nexus of dynamic voltage-gated Ca^{2+} channel activity and Ca^{2+} signaling events during zebrafish fin regeneration. Single cell transcriptomics identifies upstream voltage-gated Ca^{2+} channels *cacna1c* ($Ca_V1.2$, L-

type), *cacna1ba* (Cav2.2, N-type), and *cacna1g* (Cav3.1, T-type) as candidate mediators of fibroblast-lineage Ca^{2+} signaling in vivo. Dual chemical inhibition reveal that L/N-type voltage-gated Ca^{2+} channels are actively required for fin outgrowth during regeneration. Genetic analysis demonstrates *cacna1g* mutants regenerate extraordinarily long fins, indicating Cacna1g has a key in fin cessation and scaling. Accordingly, live imaging of regenerating animals suggests Cacna1g channel activity in distalmost mesenchymal cells is essential for Ca^{2+} flux. We conclude that a cadre of ion channels act within fibroblast-lineage cells to fine-tune Ca^{2+} signaling events and restore fin size and shape.

This dissertation includes previously published and unpublished co-authored material.

CURRICULUM VITAE

NAME OF AUTHOR: Heather Kimberly Le Bleu

GRADUATE AND UNDERGRADUATE SCHOOLS ATTENDED:

University of Oregon, Eugene, OR
University of Rochester, Rochester, NY
Sacramento City College, Sacramento, CA

DEGREES AWARDED:

Doctor of Philosophy, Biology, 2024, University of Oregon
Bachelor of Science, Cell and Development (Honors in Research), 2017, University of Rochester
Transfer credit, Biology, 2014, Sacramento City College

PROFESSIONAL EXPERIENCE:

Graduate Researcher, University of Oregon, 2017-2024
Graduate Teaching Assistant, Department of Biology, University of Oregon, 2017-2018
Undergraduate Researcher, Center for Musculoskeletal Research, University of Rochester Medical School, 2015-2017

GRANTS, AWARDS, AND HONORS:

F31HD103459 NIH Eunice Kennedy Shriver National Institute of Child Health and Human Development, Ion signaling and cell state transitions for organ size control of regenerating zebrafish fins, 2021-2024

5T32HD007348 NIH Ruth L. Kirschstein Institutional National Research Service Award Developmental Biology Training Program, 2018-2020

Raymond-Stevens Fellowship, University of Oregon, 2024

Developmental Biology Gordan Research Seminar Travel Funds, Mount Holyoke College, 2023

Outstanding Poster Award for Women in Graduate Science, Voltage-gated calcium channels control zebrafish fin size and shape, University of Oregon, 2023

Outstanding Graduate Student Poster Award, Voltage-gated calcium channels control zebrafish fin size and shape, University of Oregon, 2023

Peter O'Day Fellowship in Biological Sciences, Ion signaling for organ size control of regenerating zebrafish fins, University of Oregon, 2022

Donald Wimber Funds, University of Oregon, 2020

Best Talk Prize (2nd place), Ectopic expression of the *kcnh2a* slows intra-ray mesenchyme transitions to prolong fin outgrowth of *longfin*^{t2} zebrafish, 52nd Annual NW Developmental Biology Meeting, 2019

Adamson Memorial Scholarship, University of Oregon, 2017

Take Five Scholar, University of Rochester, 2016-2017

Phi Theta Kappa Transfer Scholarship, University of Rochester, 2014-2015

Outstanding Women Student Award, Sacramento City College, 2014

Hulda Mae Scholarship, Sacramento City College, 2014

Gallant J. Chin Scholarship, Sacramento City College, 2014

Training Award, Cell Culture Techniques Course, California State University Fresno, 2013

PUBLICATIONS:

Lewis, V.M., Le Bleu, H. K., Henner, A. L., Markovic, H., Robbins, A. E., Stewart, S. and Stankunas, K. (2023). Insulin-like growth factor receptor / mTOR signaling elevates global transition to accelerate zebrafish fin regeneration outgrowth. *Dev Biol* **502**, 1–13.

Stewart, S., Le Bleu, H. K., Yette, G.A., Henner, A. L., Robbins, A. E., Braunstein, J. A. and Stankunas, K. (2021). *longfin* causes *cis*-ectopic expression of the *kcnh2a ether-a-go-go* K+ channel to autonomously prolong fin outgrowth. *Development* **148**, dev199384.

Carlson, E. L., Karuppagounder, V., Pinamount, W. J., Yoshioka, N. K., Ahmad, A., Schott, E. M., Le Bleu, H. K., Zuscik, M. J., Elbarbary, R. A. and Kamal, F. (2021). Paroxetine-mediated GRK2 inhibition is a disease-modifying treatment for osteoarthritis. *Sci Transl Med.* **580**, eaau8491.

Le Bleu, H. K., Kamal, F. A., Kelly, M., Ketz, J. P., Zuscik, M. J. and Elbarbary, R. A. (2017). Extraction of high-quality RNA from human articular cartilage. *Anal Biochem*. **518**, 134–138.

ACKNOWLEDGMENTS

I wish to express sincere appreciation to Professor Kryn Stankunas for his assistance in the preparation of this dissertation and years of thoughtful mentorship and encouragement. This investigation was supported in part by the National Institutes of Health (NIH) NRSA fellowship (F31HD103459). The University of Oregon NIH-funded Developmental Biology Training Program (T32HD007348), and the Peter O'Day Fellowship and Undergraduate Research Opportunity Program provided additional trainee support. Furthermore, NIH (1R01GM127761 and 1R01GM149999) contributed research funds.

DEDICATION

This dissertation is dedicated to Kimberly Jo Le Bleu and Nickolas Norman Le Bleu, whose unconditional support and encouragement have been invaluable in fostering my intellectual creativity and discoveries. I am eternally grateful for your influence on my life. These writings are a tribute to both of you.

I also want to express my gratitude to Norman Aime Le Bleu for instilling a strong work ethic in me.

TABLE OF CONTENTS

Chapter Page

I. INTRODUCTION 12

II. LONGFIN CAUSES CIS-ECTOPIC EXPRESSION OF THE KCNH2A ETHER-A-GO-GO K^+ CHANNEL TO AUTONOMOUSLY PROMOTE FIN OUTGROWTH 15

Background 15

Results 19

Discussion 30

III. VOLTAGE-GATED CALCIUM CHANNELS GENERATE FIBROBLAST-LINEAGE BLASTEMAL MESENCHYME CA^{2+} FLUXES THAT RESTRAIN OUTGROWTH DURING ZEBRAFISH FIN REGENERATION 37

Background 37

Results 39

Discussion 52

Materials and Methods 56

Acknowledgements 62

Footnotes 62

Supplemental Figures 62

IV. CONCLUSION SUMMARY 74

REFERENCES CITED 75

LIST OF FIGURES

Figure Page

1. The *lof*^{t2} mutation causes *cis*-ectopic expression of *kcnh2a* 21

2. Fin overgrowth in *lof*^{t2} requires *kcnh2a*. 22

3. Kcnh2a actively prolongs the fin outgrowth period in *lof*^{t2} 24

4. *kcnh2a* acts fin autonomously and within the intra-ray mesenchyme lineage to promote overgrowth..... 27

5. *kcnh2a* is expressed ectopically in *lof*^{t2} intra-ray mesenchyme lineage cells during fin regeneration..... 28

6. Kcnh2a-disrupted calcineurin signaling gradually terminates fin outgrowth..... 31

7. The *tph1b:GCaMP6s* line enables visualization of Ca^{2+} fluxes in fibroblast-lineage distal blastemal cells..... 41

8. Voltage-gated Ca^{2+} channels actively contribute to dynamic Ca^{2+} fluxes in intra-ray fibroblast-lineage fin cells..... 43

9. Single cell transcriptomics identifies distinct spatial expression pattern of L-, N-, and T-type Ca^{2+} channels in fibroblast-lineage cells 45

10. Cilnidipine treatment reveals that L-and/or N-type Ca^{2+} channels act to promote the cessation of fin outgrowth..... 46

11. The T-type voltage-gated Ca^{2+} channel is essential for fin cessation and linked to the process of regeneration 48

12. Cacna1g actively decelerates the outgrowth rate of regenerating fins 50

13. Cacnalg controls Ca^{2+} dynamics in distal blastema and niche cells to terminate fin outgrowth and regeneration..... 51

14. Demarcating 7 dpa caudal fin cell clusters 63

15. Identifying voltage-gated Ca^{2+} channels expressed in the fibroblast/mesenchyme and osteoblast cluster. 64

16. *cacna1ba* is expressed in distal blastema *dachc*$^{+}$ cells..... 64

17. Exclusive co-expression of *cacna1c*, *cacna1ba*, and *cacna1g* to the distal blastema of regenerating fins..... 65

18. Cilnidipine promotes regenerative fin outgrowth cessation 66

19. *cacna1g* mutation causes a moderate increase in fin size and shape of developed adult zebrafish fins..... 66

20. Regenerative fin overgrowth phenotype in *cacna1g* CRISPants..... 67

21. *cacna1g* mutation in exon 3 causes an increase in the size of regenerative fins of adult fish..... 68

22. Fin scaling is disrupted in *cacna1g*$^{-/-}$ during regeneration..... 68

23. Prolong regenerative outgrowth of *cacna1g* caudal fins 69

24. All median and paired fins of *cacna1g*$^{-/-}$ fish regenerate to extraordinary sizes ... 70

25. Overgrown pectoral fin reinforces *cacna1g* acts to restrain regenerative fin outgrowth 71

26. *cacna1g*$^{-/-}$ regenerating caudal fins are comparable in size to *longfin*^{t2}..... 72

27. *cacna1g*$^{-/-}$ fish regenerate jointed rays 73

28. Excessive fin vascularization in *cacna1g*$^{-/-}$ regenerating adult caudal fin 73

CHAPTER I: INTRODUCTION

Chapter two comprises published work with co-authors Scott Stewart, Gabriel A. Yette, Astra L. Henner, Amy E. Robbins, Joshua A. Braunstein, and Kryn Stankunas. Chapter three comprises unpublished work with co-authors Rea G. Kioussi, Astra L. Henner, Scott Stewart, and Kryn Stankunas.

Most organs and limbs develop and grow to specific proportions that dictate their final form. Proper scaling of complex structures and their tissues is essential for optimal function. Select animals robustly regenerate damaged or lost tissues, including restoring organ size and shape. Such epimorphic regeneration is exemplified in adult teleost fish. The zebrafish *Danio rerio* serves as a powerful vertebrate model to study regeneration, as it can restore many organs including the heart, brain, spinal cord, and appendages/fins (Gemberling et al., 2013).

Zebrafish fins offer an attractive model for investigating the underlying mechanisms of organ size control due to their simply anatomy, ease of manipulation, and rapid regeneration. Although all fins regrow, the caudal fin is primarily used for regenerative studies. The caudal fin consists of eighteen tapering skeletal structures known as fin rays. After fin ray injury, developmental signal pathways coordinate fin outgrowth by finely tuned proliferation and differentiation (Wehner and Weidinger, 2015). New bone segments are sequentially added during regenerative outgrowth (Iovine and Johnson, 2000). How fin regeneration comes to an end with the original organ size restored remains a longstanding mystery.

Popular models accounting for fin scaling propose cells carry positional identities that direct differential proliferation in accordance with tissue demand (Nachtrab et al., 2013; Rabinowitz et al. 2017). Some groups attribute bioelectric signaling mechanisms as instructive cues that mediate changes in spatiotemporal patterns at the cell membrane and alter cellular

properties (Levin, 2014). Yet, mechanistic investigation of bioelectricity in zebrafish fin regeneration has been minimal due to limited insights into how ion channels and their activity feed into transcriptional and/or epigenetic cascades that trigger changes in fin cell behavior. The genetic tools needed to investigate coordinated ion signaling for large-scale tissue patterning throughout zebrafish fin regeneration are lacking.

This dissertation resolves barriers to understanding how ion signaling pathways regulate fin outgrowth. Here, we discover novel ion channels that act within fibroblast and mesenchymal cells at late periods of regeneration to restore fin size and shape. First, we resolve the mystery behind the eponymous *longfin*^{t2} phenotype. We discuss the implications of voltage-gated K^+ channel activity on Ca^{2+} -dependent calcineurin signaling in fin outgrowth. We then apply our new knowledge of the *longfin*^{t2} mutant to investigate the contribution of voltage-gated Ca^{2+} channels and Ca^{2+} signaling in restraining regenerative outgrowth. Our studies include the development of a newly stable transgenic line expressing the Ca^{2+}-responsive, GCaMP6s promoter in fibroblast-lineage cells to directly examine Ca^{2+} dynamics in regenerating fins. We focus on elucidating the specific types of voltage-gated Ca^{2+} channels mediating Ca^{2+} fluxes during regeneration. We conclude by discussing how our studies implicate Ca^{2+} as secondary messenger of electrical signaling in distalmost mesenchymal fin cells to promote fin cessation. In the case of the *longfin*^{t2}, we explain how ectopic activity of voltage-gated K^+ channels likely disrupt repolarization-depolarization dynamics, dampening Ca^{2+} levels and Ca^{2+} signaling events to prolong outgrowth and delay fin cessation.

These findings advance our understanding of upstream mechanisms in fin growth control. However, the mechanisms explaining how Ca^{2+} channel activity and Ca^{2+} signaling alters cellular behaviors for fin cessation remain unresolved. However, we present the hypothesis that

Ca^{2+} channel activity and dynamic Ca^{2+} levels activate calcineurin signaling to promote cell state transitions and end fin regrowth. Lastly, this body of work was not aimed at interrogating existing questions of bioelectricity in organ size control; however, we present new findings that have the potential to expand upon and/or reshape opinions of a bioelectric code in tissue growth and regenerative repair.

CHAPTER II: LONGFIN CAUSES CIS-ECTOPIC EXPRESSION OF THE KCNH2A ETHER-A-GO-GO K^+ CHANNEL KCNH2A TO AUTONOMOUSLY PROMOTE FIN OUTGROWTH

From **Stewart, S., Le Bleu, H. K., Yette, G.A., Henner, A. L., Robbins, A. E., Braunstein, J. A. and Stankunas, K.** (2021). *longfin* causes *cis*-ectopic expression of the *kcnh2a ether-a-go-go* K+ channel to autonomously prolong fin outgrowth. *Development* **148**, dev199384.

BACKGROUND

Animal organs develop to and maintain a species-specific size and shape in scale with the individual's overall body. Remarkably, regenerating organs can sense injury extents to restore their original proportions. Fish fins neatly demonstrate both organ size establishment and regeneration mysteries. Fins display tremendous morphological diversity to optimize swimming, predator avoidance, and courtship, while also contributing to fishes' aesthetic appeal (Nelson et al., 2016). Further, most fins, including those of the zebrafish model organism, regenerate to their original form, providing a striking example of organ size control and scaling.

Zebrafish fin skeletons comprised of segmented, cylindrical bony rays define the overall fin form. Each ray segment embodies two opposing hemi-cylindrical bones produced by tightly associated osteoblasts. A stratified epidermis lines and vasculature, sensory axons, and fibroblasts reside within rays. During larval development, fins initiate rapid asynchronous allometric growth culminating in their mature forms, including the familiar bi-lobed shape of the well-studied caudal fin (Goldsmith et al., 2006). Adult fins switch to isometric growth, slowly expanding in scale with the rest of the body throughout the animal's life. Adult fin regeneration engages the appropriate extent of rapid allometric growth to restore a properly proportioned appendage (Goldsmith et al., 2006; Iovine and Johnson, 2000).

The zebrafish fin regeneration model affords a tractable platform to determine fin size control mechanisms. No matter where a fin is amputated, the regenerated fin restores its original size and shape (Chen and Poss, 2017; Sehring and Weidinger, 2020). Fin amputation triggers a wound epithelium formed by migrating epidermal cells. De-differentiation of mature cells to lineage-restricted progenitors then generates a regenerative blastema for each ray (Knopf et al., 2011; Singh et al., 2012; Sousa et al., 2011; Stewart and Stankunas, 2012; Tu and Johnson, 2011). Heterogeneous blastemas organize by cell lineage and state to enable progressive regeneration (reviewed in (Wehner and Weidinger, 2015)). De-differentiated, proliferative osteoblasts (pObs) migrate to blastema peripheries and hierarchically arrange along the distal-to-proximal axis of the blastema, with the most progenitor "state" cells distally concentrated (Stewart et al., 2014). Similarly, fibroblasts residing between hemi-rays de-differentiate, form the major blastema mesenchyme population radially interior to pObs, and then contribute to regenerated intra-ray tissue (Tornini et al., 2016). An outgrowth phase follows that integrates spatially segregated proliferation (distal) and differentiation (proximal) activities for the progressive restoration of replacement tissue.

Developmental signaling pathways promote tissue interactions and cell behaviors to replace lost cells and re-form mature, patterned tissue (Wehner and Weidinger, 2015). A distal blastema "organizing center" produces essential Wnt signals that coordinates other pathways including FGFs and BMPs (Wehner et al., 2014). FGFs likely are the primary mitogens (Lee et al., 2005; Lee et al., 2009; Poss et al., 2000; Shibata et al., 2016), whereas BMP signaling is implicated in osteoblast differentiation (Quint et al., 2002; Smith et al., 2006; Stewart et al., 2014). Yet, cell behaviors and their mechanistic control that ensure cessation of regrowth once the proper fin size is reached are unresolved. Prevailing models for fin size restoration suggest

positional identities of cells at an injury site establish appropriate outgrowth-determining blastema pre-patterns (Lee et al., 2005; Rabinowitz et al., 2017; Tornini et al., 2016). The nature of such cellular memories, how they establish blastema positional information, and how those pre-patterns are converted into outgrowth extents all remain largely mysterious.

Genetic studies of adult viable zebrafish mutants with abnormally sized fins provide an entry for molecular insights into fin growth control (Van Eeden et al., 1996). These studies universally implicate ion signaling as a major determinant of fin size. Gain-of-function mutations in the K^+ channel *kcnk5b* in *another longfin* (*alf*) develop and regenerate long fins (Perathoner et al., 2014). Further, fin overgrowth in the *schleier* mutant is caused by loss of *kcc4a/ slc12a7a*, a K^+ Cl^- cotransporter (Lanni et al., 2019). Ectopic expression of *kcnj13*, coding for a K^+ channel, caused by a viral insertion or transgene-mediated expression of the Kcnj1b, Kcnj10a, and Kcnk9c K^+ channels also causes overgrowth (Silic et al., 2020). Finally, loss of *gap junction protein alpha 1b* (*gja1*, also known as *connexin 43*) in *shortfin* mutants suggests involvement of intercellular ion exchange (Iovine and Johnson, 2000). This literature, together with studies in other animals, points to central roles of ion signaling, or "bioelectricity" in organ size establishment (McLaughlin and Levin, 2018). However, how ion signaling dynamics directly alter cell states and behaviors to instruct and/or enable scaled growth is poorly understood.

Cooperating factors that promote and effect ion signaling dynamics for fin size control are unresolved. As one key insight, small molecule inhibition of the Ca^{2+}-dependent phosphatase calcineurin causes dramatic fin overgrowth (Kujawski et al., 2014). As a decoder of the ubiquitous cytosolic Ca^{2+} second messenger, calcineurin links ion signaling and protein effector phosphorylation (Crabtree, 1999). Calcineurin may act directly upstream of Kcnk5b (*alf*) to temper outgrowth and restore fin proportions (Daane et al., 2018; Yi et al., 2020). In mammals,

diverse stimuli activate calcineurin by elevating intracellular Ca^{2+}, including antigen engagement of the T-cell receptor complex (Rao, 2009), depolarization of cardiomyocytes (Parra and Rothermel, 2017), and neuronal ion channel activity (Baumgärtel and Mansuy, 2012). Calcineurin dephosphorylates multiple proteins, including ion channels and transcription factors, to promote context-dependent cell behaviors. Characterizing calcineurin's upstream regulators and downstream effectors in the fin is a promising path to reveal organ size control mechanisms.

The classic dominant *longfin*^{t2} (*lof*^{t2}) mutant also develops and regenerates exceptionally long fins, producing a "schleierform", or flowing veil-like appearance (Elias, 1984; Van Eeden et al., 1996) (Fig. 1A and B). Notably, the widely used stock strain *Tüpfel-Longfin* (*TL*) contains compound *lof*$^{t2/t2}$*; leopard*$^{t1/t1}$ (*leo*) mutations, whose respective fin and pigmentation phenotypes allow visual identification of mixed genotypes (Haffter et al., 1996). Developing fins of *lof*^{t2} fish do not have a greater maximal growth rate (Iovine and Johnson, 2000). Rather, *lof*^{t2} fins fail to return to isometric growth as animals reach maturity (Goldsmith et al., 2006; Iovine and Johnson, 2000). Unlike *kcnk5b* (*alf*) and *kcc4a/ slc12a7a* (*schlier*) mutants as well as calcineurin inhibition, *lof*^{t2} overgrown fins lack other defects such as tissue hyper-vascularization and elongated ray segments (Kujawski et al., 2014; Lanni et al., 2019; McMillan et al., 2018; Perathoner et al., 2014; Silic et al., 2020). The latter phenotype likely reflects the independent disruption of joint formation rather than overgrowth since ray segment number and fin size are not correlated; *evx1* mutants, devoid of all fin joints, have normal fin sizes (Schulte et al., 2011; Ton and Iovine, 2013). Regardless, *lof*^{t2} provides a uniquely clean model to explore fin size control.

Further motivated by the historical significance and prominence of *lof*^{t2}, we sought to identify the cause of its eponymous phenotype. We show the dominant *lof*^{t2} fin overgrowth

phenotype is caused by *cis* ectopic expression of *kcnh2a*, a K^+ channel-encoding gene mapping near the *lof* locus. During regeneration, the activity of ectopic Kcnh2a, an ortholog of cardiac arrhythmia-associated *ether-a-go-go* channels, promotes fin overgrowth exclusively by extending the outgrowth period. Labeled *lof*^{t2} genetic chimeras demonstrate Kcnh2a acts tissue autonomously within size-determining intra-ray mesenchymal lineage cells. Finally, we provide evidence Kcnh2a disrupts a $Ca^{2+/}$calcineurin pathway that gradually terminates allometric fin outgrowth. Our results suggest readily tunable ion signaling alters organ size by modulating growth periods rather than establishing growth-defining positional information or directly impacting cell cycling rates.

RESULTS

The dominant *lof*^{t2} allele that specifically causes dramatic fin overgrowth maps to an essential ~250 kilobase region (Fig. 1 A-C) of chromosome 2 (chr2) (Iovine and Johnson, 2002). Therefore, *lof*^{t2} likely results from a dominant negative or gain-of-function mutation rather than haploinsufficiency. One explanation is that *lof*^{t2} alters a transcriptional regulatory element causing over- or ectopic expression of a gene(s) within or near the *lof* region (Fig. 1C). We explored this possibility using mRNA sequencing (RNA-seq) to identify differentially expressed genes (DEGs) from 4 days post-amputation (dpa) caudal fin regenerates (Fig. 1D). We reasoned 4 dpa regenerates would highlight primary transcriptional changes because *lof*^{t2} and wildtype fin sizes were indistinguishable at this stage of regeneration (data not shown). We identified 39 increased and 111 decreased DEGs (+/- 2-fold change) in *lof*^{t2} fins (data not shown). Confining the DEG analysis to the *lof*^{t2} region and surrounding genes (Fig. 1C), a single transcript roughly 1 megabase from *lof*^{t2}, *potassium voltage-gated channel, subfamily H (eag-related), member 2a* (*kcnh2a*), was greatly elevated in *lof*$^{t2/+}$ animals (+ 25.8 fold) (Fig. 1D). One gene, *csrnp1a*,

showed decreased transcript levels (- 3.9 fold). Quantitative RT-PCR (RT-qPCR) confirmed *kcnh2a* was expressed uniquely in *lof*$^{t2/+}$ fin regenerates, at levels similar to the *runx2b* osteoblast-lineage transcription factor (Fig. 1D).

To determine if *lof*^{t2} affects *kcnh2a* expression in *cis* or *trans*, we leveraged sequence polymorphisms (Butler et al., 2015) in the 5' UTR that distinguish *kcnh2a* from *TL* and *WIK* (*kcnh2a*$^{WIK\text{-}TL}$) versus our wildtype *AB* (*kcnh2a*^{AB}) strains (Fig. 1E). We used allele-specific primers and RT-qPCR to observe that *kcnh2a*$^{WIK\text{-}TL}$ transcripts accounted for nearly all *kcnh2a* expression in *lof*^{t2} *kcnh2a*$^{WIK\text{-}TL}$*; lof*$^{+}$ *kcnh2a*^{AB} regenerating caudal fins. The apparent 10% residual contribution of *kcnh2a*^{AB} to total *kcnh2a* expression likely reflects partial primer cross-hybridization. We conclude most, if not all, *kcnh2a* expression in *lof*^{t2} regenerating fins arises from *cis* effects of the *lof*^{t2} mutation.

We used CRISPR/Cas9 to mutate *kcnh2a* in the *TL* (*leo*$^{t1/t1}$*; lof*$^{t2/t2}$) background to determine if overexpressed *kcnh2a* causes *lof*^{t2} fin overgrowth. We outcrossed founders to wildtype fish and identified numerous obligatory *lof*$^{t2/+}$ F_1 animals with normal sized fins carrying germline-transmitted *kcnh2a* loss-of-function alleles. One of these, *kcnh2a*^{b1391}*,* contained an 8 bp deletion causing a frameshift at codon 3 of the predicted polypeptide. Homozygous *lof*$^{t2/t2}$*; kcnh2a*$^{b1391/b1391}$ fish were phenotypically normal with fin sizes indistinguishable from wildtype clutchmates (Fig. 2A and B). Since *lof*^{t2} *kcnh2a*^{b1391}*; lof*$^{+}$ *kcnh2a*$^{+}$ and *lof*^{t2} *kcnh2a*^{b1391}*; lof*^{t2} *kcnh2a*$^{+}$ fish developed normal and long fins, respectively, the *kcnh2a*^{b1391} allele uniquely suppresses *lof*^{t2} in *cis*. Regenerative outgrowth also was identical between wildtype and *lof*$^{t2/t2}$*; kcnh2a*$^{b1391/b1391}$ caudal fins (Fig. 2C-F). Finally, *lof*^{t2}-linked *kcnh2a* had no exon or intron/exon boundary non-synonymous mutations or unappreciated SNPs.

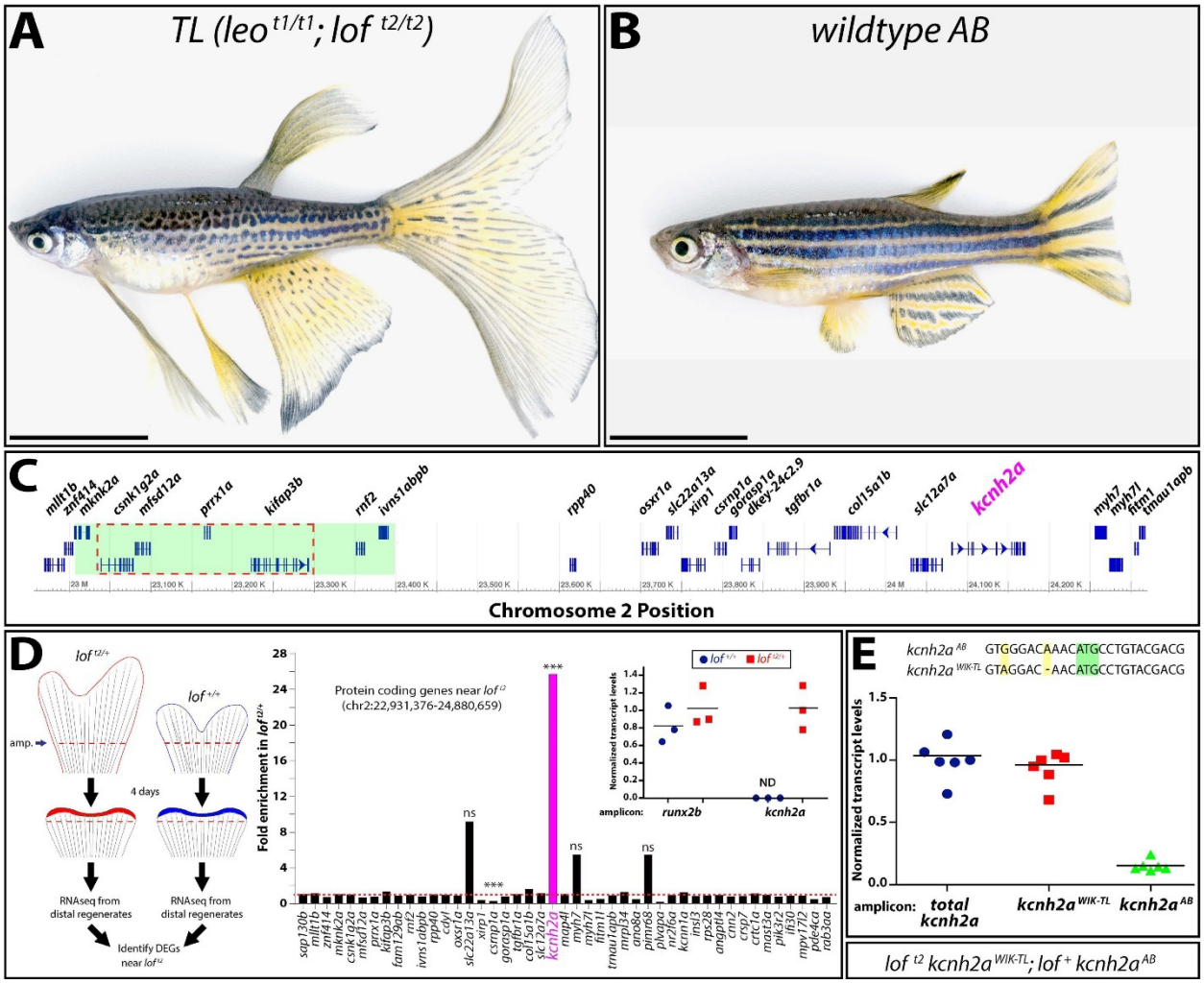

Figure 1. The *lof*^{t2} mutation causes *cis*-ectopic expression of *kcnh2a*. (A, B) Brightfield images of adult *TL (Tüpfel longfin: leo*$^{t1/t1}$*; lof*$^{t2/t2}$*)* and wildtype *AB* zebrafish. The scale bar represents 1 cm. (C) Schematic diagram of 1.5 Mb region of zebrafish chromosome 2 (chr2). The putative location of the *lof*^{t2} mutation is outlined with a dashed red line and the region deleted in the suppressed *lof*^{tg1} is highlighted by a green box as determined in (Iovine and Johnson, 2002). (D) Left. Schematic of RNA-Seq experimental design to identify genes mis-expressed in regenerated *lof*^{t2}. Right. RNA-Seq data showing gene expression at chr2:22,931,376-24,880,659 from *lof*$^{t2/+}$ relative to clutchmate *lof*$^{+/+}$ controls. The asterisks indicate the two differentially expressed genes ($p < 10^{-4}$). ns: not significant. Inset. Expression of *kcnh2a* in *lof*$^{t2/+}$ (in red) and *lof*$^{+/+}$ (in blue) clutchmates determined by RT-qPCR using 4 dpa fin cDNA. Data were normalized to *rpl8* reference expression levels and presented as fold change relative to *lof*$^{t2/+}$. *runx2b* expression levels are shown for comparative purposes and were not significantly changed between the two genotypes. Expression of *kcnh2a* was below limits of detection in *lof*$^{+/+}$ fish (indeterminate, ND). Each point represents a cohort of 3 animals. (E) RT-qPCR on 4 dpa caudal fin cDNA from *lof*^{t2} *kcnh2a*$^{WIK\text{-}TL}$*; lof*$^{+}$ *kcnh2a*^{AB} fish to detect chromosome-specific expression *kcnh2a.* Sequences of non-coding *kcnh2a* polymorphisms that specifically amplify either *kcnh2a*$^{WIK\text{-}TL}$, located on the *lof*^{t2} mutant chr2 (red squares), or *kcnh2a*^{AB}, located on *AB* chr2 (green triangles). Data were normalized to total *kcnh2a* (blue circle) levels determined using primers that amplify both alleles indiscriminately. Each data point represents data from an individual fish. RT-qPCR statistical analyses used one-way ANOVA with Tukey's multiple comparisons tests.

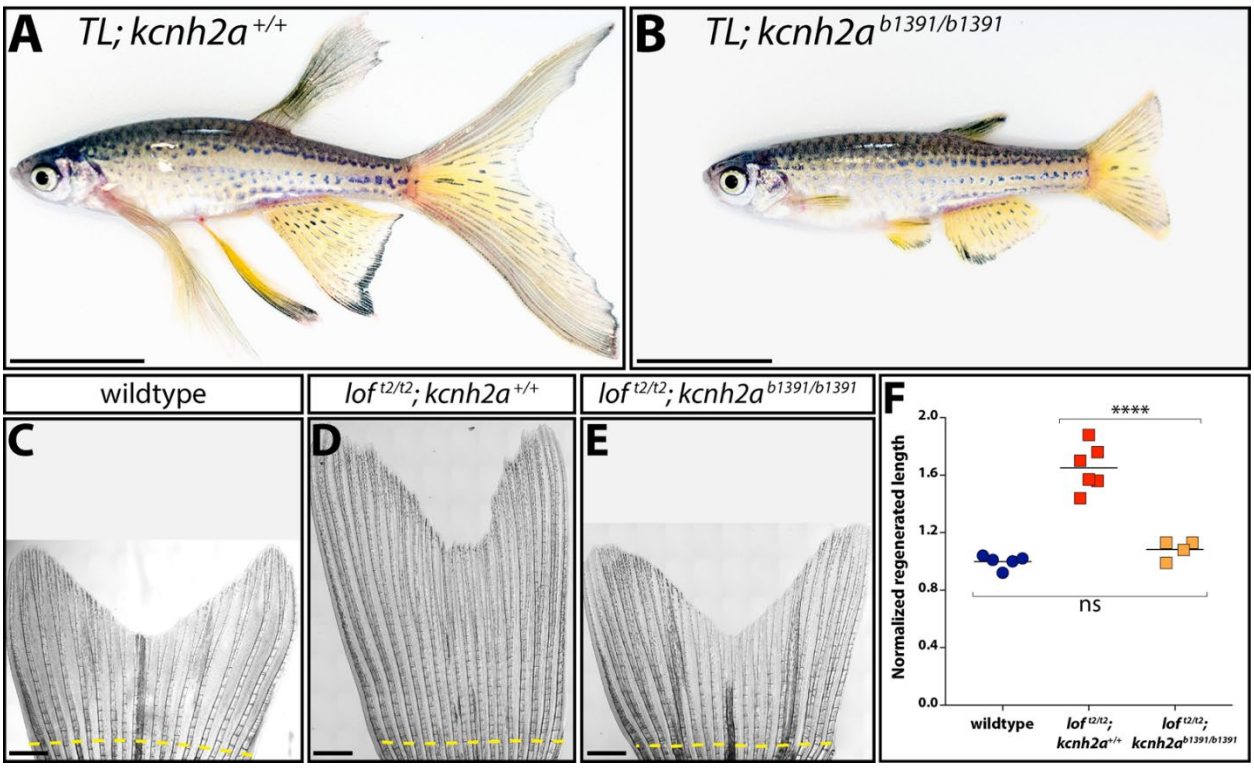

Figure 2. Fin overgrowth in *lof*^{t2} requires *kcnh2a*. (A, B) Brightfield images of clutchmate *TL; kcnh2a*$^{+/+}$ (panel A) and *TL; kcnh2a*$^{b1391/b1391}$ (panel B) adult zebrafish. The scale bars represent 1 cm. (C-E) Representative images of regenerated caudal fins at 27 days post-amputation (dpa) from (C) wildtype control, (D) *lof*$^{t2/t2}$*; kcnh2a*$^{+/+}$, and (E) *lof*$^{t2/t2}$*; kcnh2a*$^{b1391/b1391}$ fish. The dashed yellow line indicates the site of fin resection and scale bars represent 1 mm. (F) Quantification of fin ray outgrowth of wildtype (blue circles), *lof*$^{t2/t2}$*; kcnh2*$^{+/+}$ (red squares), and *lof*$^{t2/t2}$*; kcnh2a*$^{b1391/b1391}$ (orange squares) fish at 27 dpa. Each data point represents the normalized length of ray 3 from an individual animal of the indicated genotype. Asterisks indicate $p < 0.005$ determined by a one-way ANOVA with Tukey's multiple comparisons tests. ns: not significant.

We conclude *cis*-ectopic expression of *kcnh2a* on the *lof*^{t2} chr2 causes the dominant *lof*^{t2} fin overgrowth phenotype. Therefore, *lof*^{t2} likely is a regulatory *kcnh2a* neomorphic allele.

We measured regenerating fin outgrowth of wildtype and clutchmate *lof*^{t2} fish over a 30 day period to explore temporal effects of ectopic *kcnh2a* on fin overgrowth. For each genotype, regenerated lengths over time fit well to a logistic growth curve, consistent with a lag for blastema establishment prior to a prolonged outgrowth phase. Wildtype and *lof*^{t2} fish had indistinguishable maximal growth rates reached between 3 and 5 dpa (Fig. 3A and B). Growth rates then gradually declined, approximating an exponential decay equation. However, the growth rate declined slower in *lof*^{t2} fish, progressively increasing the fin length difference with wildtype animals. Wildtype fins largely ceased regenerative outgrowth by 21 dpa whereas *lof*^{t2} fins continued to extend through the 30 dpa period. This prolonged outgrowth dynamic matches that of *lof*^{t2} fin development (Iovine and Johnson, 2000). We conclude fin overgrowth in *lof*^{t2} fish is due to an extended outgrowth period beginning around 6 dpa rather than elevated maximum growth.

Kcnh2a is related to *ether-a-go-go* voltage-gated K^+ channels (Vandenberg et al., 2012) whose channel activity is blocked by the small molecule astemizole (Sanguinetti and Tristani-Firouzi, 2006; Suessbrich et al., 1996; Zhou et al., 1999). We treated *lof*$^{t2/+}$ fish with astemizole from 7-30 dpa to determine if ectopic Kcnh2a actively extends fin outgrowth period. This inhibitor regimen fully suppressed excessive *lof*$^{t2/+}$ fin outgrowth to wildtype levels (Fig. 3C-F). Further, starting astemizole treatment at 6 dpa was as effective as administration throughout regeneration (data not shown). Therefore, although *lof*$^{t2/+}$ fins express *kcnh2a* relatively early during regeneration, as seen in Figure 1, its functional impact on growth at these times is negligible. Further, consistent with wildtype-sized *kcnh2a*$^{b1391/b1391}$ caudal fins, Kcnh2a activity

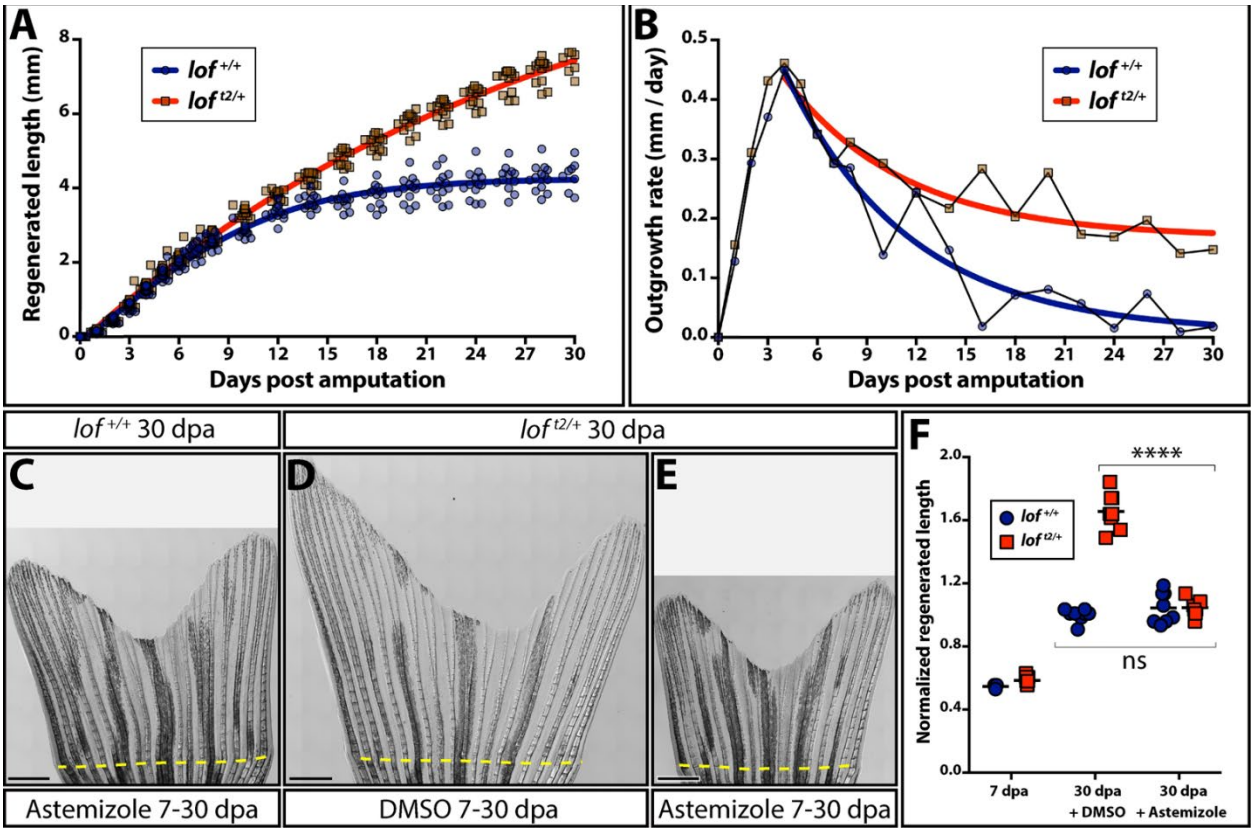

Figure 3. Kcnh2a actively prolongs the fin outgrowth period in *lof*^{t2}. (A) Plots comparing the growth (A) and growth rate (B) of regenerating *lof*$^{t2/+}$ (blue) and clutchmate *lof*$^{+/+}$ (red) caudal fins. Curves show actual data fit to a (A) logistic equation reflecting establishment and then progressively slowing outgrowth phases and (B) exponential decay equation using time points after the peak growth rate is reached. All data points (≥ 12 fish per time) are shown in panel A and mean values are used in panel B. (C-E) Stitched DIC images showing clutchmate *lof*$^{+/+}$ astemizole-treated (panel C; 500 nM), DMSO-treated *lof*$^{t2/+}$ (panel D) and *lof*$^{t2/+}$, astemizole-treated (panel E; 500 nM) fish at 30 days post caudal fin amputation (dpa). The dashed yellow line indicates the amputation plane and the scale bars denote 1 mm. (F) Quantification of normalized caudal fin regenerative outgrowth from control and astemizole-treated animals. Data points represent individual *lof*$^{+/+}$ (blue circles) and *lof*$^{t2/+}$ (red squares) animals prior to treatment (7 dpa) and post-treatment (30 dpa) with DMSO or astemizole (500 nM). Graph shows mean lengths of the third ventral regenerated ray normalized to DMSO-treated controls at 30 dpa. Each point is an individual animal. $p < 0.0001$ DMSO-treated from 7-30 dpa comparing wildtype and *lof*$^{t2/+}$ fin lengths, no significant differences between genotypes at 7 dpa or comparing 7-30 dpa astemizole-treated wildtype and *lof*$^{t2/+}$ regenerative outgrowth. Statistical tests used one-way ANOVA with Tukey's multiple comparisons tests.

normally does not contribute to regenerative outgrowth. We conclude ectopic Kcnh2a exclusively causes regenerative fin overgrowth by actively preventing growth termination during late-stage outgrowth (~7 dpa and onward).

Kcnh2a could function fin autonomously or systemically (e.g., via circulating endocrine factors) to prolong *lof*^{t2} fin outgrowth periods. We used F_0 CRISPR/Cas9 targeting to induce mosaic *kcnh2a* mutations to discriminate between these scenarios. The tissue autonomous model predicts fin size heterogeneity depending on the extent of *kcnh2a* targeting across rays of a given fin and between different fins. In contrast, the systemic hypothesis anticipates *kcnh2a* loss-of-function mutations always would equally suppress *lof*$^{t2/+}$ fin overgrowth. We injected embryos from a wildtype x *lof*$^{t2/+}$ cross with Cas9 and a *kcnh2a*-targeting gRNA and scored reared adults for fin overgrowth. Roughly half of uninjected control animals displayed long fins, as anticipated (51:40 wildtype:overgrown). In contrast, 21.8% of *kcnh2a* crispants showed partial, regionalized fin overgrowth (17 of 78, of which half would be *lof*$^{t2/+}$ fish). A representative partially overgrown caudal fin is shown in Figure 4A. Another striking example displayed one pectoral fin rescued to wildtype length with the other exhibiting pronounced overgrowth indicative of *lof*^{t2} (Fig. 4B). Therefore, ectopic Kcnh2a likely functions within fin tissue rather than systemically to disrupt the cessation of fin outgrowth.

We generated chimeras by blastula cell transplantations (Kimmel et al., 1990) to examine *lof*^{t2} tissue autonomy further. We introduced EGFP-labeled *lof*$^{t2/+}$ blastula-stage cells into *AB* wildtype host embryos and raised them to adulthood (Fig. 4C). 13% of transplants (39 fins with overgrowth from 28 of 214 screened chimeras) exhibited EGFP^{+} fin tissue with notable overgrowth indicative of chimerism (Fig. 4D). Several fins had strong EGFP^{+} overgrown rays flanked by intermediate length rays with minimal EGFP expression. We attribute these neighbor

effects to diffusible factors emanating from the primary overgrown ray, anatomical influences on growth between adjacent rays, or scarce $EGFP^+$ cells sufficient to cause lesser overgrowth. In a few cases, chimeric animals displayed asymmetrically sized pectoral fins, as observed with *kcnh2a* CRISPR-targeted F_0 lof^{t2} mosaic fish (data not shown). All overgrown chimeric rays contained $EGFP^+$ intra-ray mesenchymal cells (n=30 overgrown fins containing only $EGFP^+$ mesenchyme), although some also displayed EGFP-expressing osteoblasts and/or epidermis (n=5 $EGFP^+$ mesenchyme/osteoblast; n=2 $EGFP^+$ mesenchyme/epidermis; n=2 $EGFP^+$ mesenchyme/osteoblast/epidermis). We immunostained sections from representative overgrown fins for the mesenchymal marker Msx (Akimenko et al., 1995) to confirm overgrown chimeric fins always included $EGFP^+$ $lof^{t2/+}$-derived intra-ray mesenchyme (Fig. 4F). In contrast, chimeras harboring only $EGFP^+$ $lof^{t2/+}$ epidermal cells were of normal length (n=3, data not shown). We conclude ectopic Kcnh2a functions in intra-ray mesenchyme and/or blastema cells derived from this lineage to disrupt outgrowth-slowing mechanisms.

We used RNAscope (Wang et al., 2012) to localize *kcnh2a* mRNA in 4 dpa *TL* caudal fin sections. As predicted from our transplant studies, *kcnh2a* was expressed in *TL* regenerating intra-ray mesenchyme, including at lower levels in growth-promoting distal blastema cells of shared lineage (Tornini et al., 2017; Wehner et al., 2014) (Fig. 5A). We did not detect *kcnh2a* in *AB* control fins, as expected from RNA-Seq and qRT-PCR (Fig. 5B). We next combined *kcnh2a* RNAscope with immunostaining for the intra-ray mesenchyme lineage markers Msx (Akimenko et al., 1995) or *tph1b:mCherry* (Tornini et al., 2016). *kcnh2a* was expressed in Msx^+ or *tph1b:mCherry*$^+$ cells in proximal regenerating tissue (Fig. 5C-F) with lower levels in *tph1b:mCherry*$^+$ distal blastema cells (data not shown), reinforcing that ectopic Kcnh2a acts in this lineage to promote fin overgrowth.

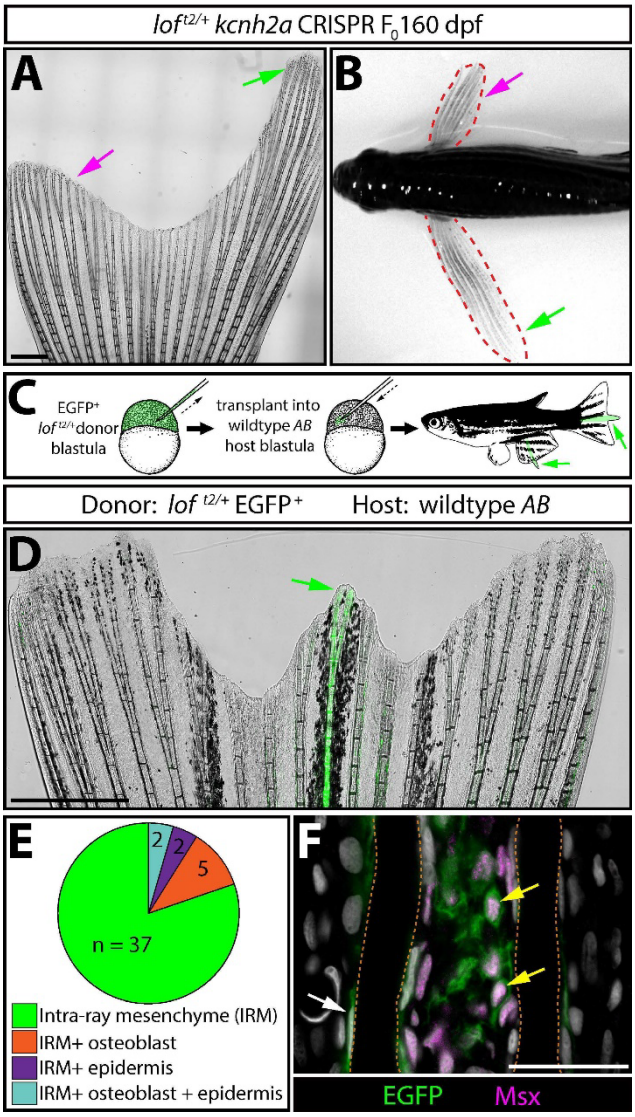

Figure 4. *kcnh2a* acts fin autonomously and within the intra-ray mesenchyme lineage to promote overgrowth. (A) Representative whole mount image of a F_0 *kcnh2a* CRISPR *lof*$^{t2/+}$ adult caudal fin at 160 days post-fertilization. The magenta arrow points to suppressed overgrowth in otherwise long fins (green arrow). The scale bar represents 1 mm. (B) Pectoral fin asymmetry in a *kcnh2a* F_0 CRISPR *lof*$^{t2/+}$ animal. The magenta arrow points to a wildtype-sized fin indicative of phenotypic suppression. The green arrow points to the overgrown contralateral fin expected of the *lof*$^{t2/+}$ genotype. (C) Upper panel schematic highlighting the nature of the blastula stage transplant experiment. EGFP$^+$ *lof*$^{t2/+}$ blastula cells were transplanted into wildtype *AB* embryos. Reared adults with partial or complete fin overgrowth were scored for cell type(s) with EGFP expression. (D) A representative example of a caudal fin displaying overgrown EGFP$^+$ fin rays. The green arrow points to overgrown EGFP$^+$ fin rays and the scale bar represents 1 mm. (E) The pie chart indicates the EGFP$^+$ lineage(s) present in 39 overgrown regions across 30 total fins with extended rays. (F) Caudal fin section of an overgrown chimeric fin ray immunostained with EGFP and Msx antibodies. Yellow arrows point to EGFP$^+$/Msx$^+$ intra-ray mesenchymal cells. The white arrow highlights an EGFP$^+$ osteoblast. Fin rays are outlined with a dashed orange line. Hoechst-stained nuclei are in gray. The scale bar represents 50 µm.

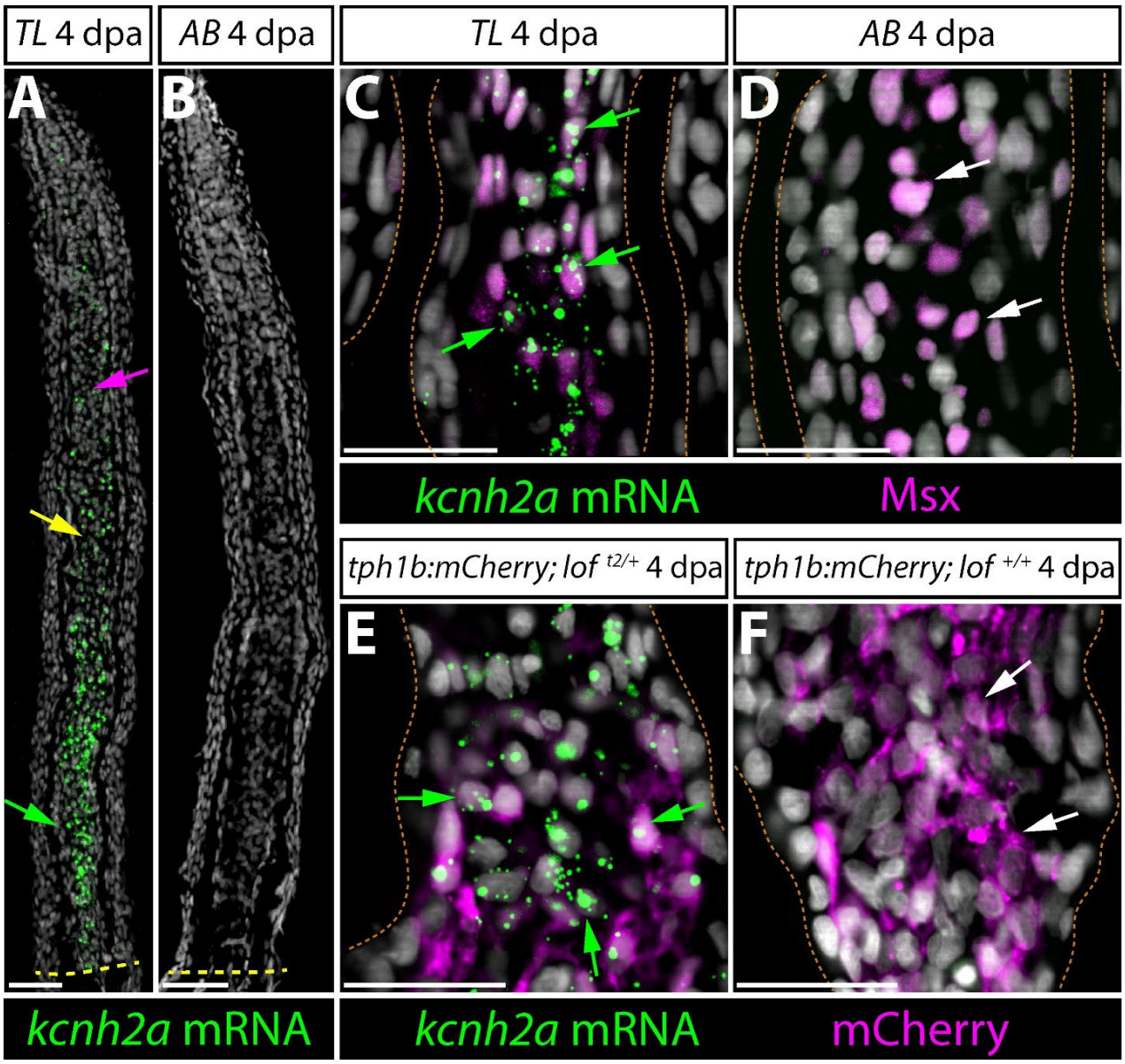

Figure 5. *kcnh2a* is expressed ectopically in *lof*^{t2} intra-ray mesenchyme lineage cells during fin regeneration. (A, B) *kcnh2a* mRNA localization (in green) detected by RNAscope in longitudinal caudal fin sections from 4 day post amputation (dpa) *TL* (*lof*$^{t2/t2}$, panel A) and *AB* (panel B) animals. The green arrow points to proximal intra-ray cells expressing high levels of *kcnh2a*, which is also detected in medial mesenchyme (yellow arrow) and distal cells (magenta arrow) of *TL* fish. The dashed yellow line denotes the site of amputation. Hoechst stained nuclei are in gray and scale bars indicate 50 µm. (C, D) Double *kcnh2a* RNAscope (green) and Msx immunostaining (magenta) of 4 dpa caudal fin sections from *TL* (panel C) and *AB* (panel D) fish. (E, F) Combination *kcnh2a* RNAscope (green) and mCherry immunostaining (magenta) of 4 dpa fin sections from (E) *tph1b:mCherry; lof*$^{t2/+}$ and (F) *tph1b:mCherry; lof*$^{+/+}$ fish. For panels C-F, green arrows highlight Msx^{+} or *tph1b:mCherry*$^{+}$ cells with overlapping *kcnh2a* mRNA in proximal regenerating *lof* tissue. White arrows show Msx^{+} or *tph1b:mCherry*$^{+}$ nuclei in corresponding regions from control fins lacking *kcnh2a* expression. Fin rays are outlined with a dashed orange line. Hoechst-stained nuclei are in gray. Scale bars represent 50 µm.

Intra-ray mesenchymal cell proliferation rates monitored by EdU incorporation were similar in 4 dpa wildtype and *lof*$^{t2/+}$ regenerating fins (data not shown). Cell cycling was distally concentrated in both genotypes. The fraction of proliferating cells was significantly higher in 10 dpa *lof*$^{t2/+}$ fin regenerates, being only modestly reduced from 4 dpa (data not shown). EdU-incorporating intra-ray cells remained largely confined to the distal blastema of *lof*$^{t2/+}$ fin regenerates in spite of ectopic *kcnh2a* throughout ray mesenchyme. Further, the *wnt5a* growth factor remained distal-enriched in 10 dpa *lof*$^{t2/+}$ regenerating fins (Stoick-Cooper et al., 2007, Stewart et al., 2014). Therefore, matching our outgrowth rate measurements, an extended outgrowth period leading to accumulated cell proliferation rather than an increased maximum cycling rate causes *lof*^{t2} fin overgrowth. Further, *kcnh2a* prolongs outgrowth without being autonomously sufficient to drive cell cycling and/or a growth factor-producing distal blastema cell state.

Inhibiting the Ca^{2+}/calmodulin-dependent phosphatase calcineurin with the immunosuppressants FK506 or cyclosporin leads to pronounced fin overgrowth (Daane et al., 2018; Kujawski et al., 2014). Maximal growth rates in calcineurin-inhibited regenerating caudal fins are the same as wildtype (Daane et al., 2018; Kujawski et al., 2014), implying that, like *lof*$^{t2/+}$, such fins do not properly terminate growth. We treated fish with FK506 at various time points post-caudal fin amputation to test this hypothesis. Optimization experiments demonstrated that daily 4 hour immersion from 1-21 dpa in water containing 500 nM FK506 was sufficient to overgrow fins to the same degree as *lof*$^{t2/t2}$ with no apparent adverse effects on animal health (data not shown). We treated regenerating animals from either 1-5, 6-21, or 1-21 dpa following this acute drug delivery regimen and measured regeneration extents at 21 dpa. Treating animals with FK506 from 1-5 dpa had no effect on fin outgrowth but still prevented joint formation (Fig.

6A and B), a known additional phenotype upon calcineurin inhibition (Kujawski et al., 2014). In contrast, FK506 treatment from 6-21 or 1-21 dpa caused the same extent of pronounced fin overgrowth (Fig. 6C and E). Thus, like ectopic Kcnh2a in *lof*^{t2} mutants, calcineurin inhibition appears uniquely to cause fin overgrowth by disrupting growth cessation.

We hypothesized ectopic Kcnh2a disrupts calcineurin signaling given *lof*^{t2} and FK506 experiments highlight similar growth dynamic effects and temporal functions during fin regeneration. If so, *lof*^{t2} should not enhance FK506-induced fin regenerative overgrowth. Accordingly, we observed no difference in caudal fin overgrowth in wildtype vs *lof*$^{t2/t2}$ fish treated with FK506 from 7-21 dpa (Fig. 6F-J). The *lof*$^{t2/t2}$ genetic background did not alter FK506 bio-availability because joint formation remained dramatically disrupted (Fig. 6H, I). Additionally, treating *lof*$^{t2/+}$ with both astemizole and FK506 from 7-21 dpa still produced FK506-induced fin overgrowth (Fig. 6K-O). Therefore, Kcnh2a activity, unlike Kcnk5b/*alf* (Daane et al., 2018), is not downstream of calcineurin. Further, *lof*^{t2}-ectopic Kcnh2a throughout fin development, and even the first week of fin regeneration, does not impact how an amputated fin responds to calcineurin inhibition. We conclude ectopic Kcnh2a likely disrupts calcineurin signaling, which otherwise impacts fin size by gradually terminating outgrowth.

DISCUSSION

lof^{t2} was one of the first zebrafish mutant lines used scientifically (hence, its "t2" – Tübingen 2 – designation), having been originally isolated by tropical fish hobbyists (Elias, 1984; Haffter et al., 1996; Van Eeden et al., 1996). *lof*^{t2} remains widely used because its highly specific fin overgrowth provides a convenient phenotypic marker to discriminate zebrafish of mixed genotypes. We demonstrate *lof*^{t2} is a regulatory neomorphic allele of *kcnh2a* (*kcnh2a*^{lof}) that causes its ectopic expression in fin mesenchyme, resolving the basis of its remarkable and

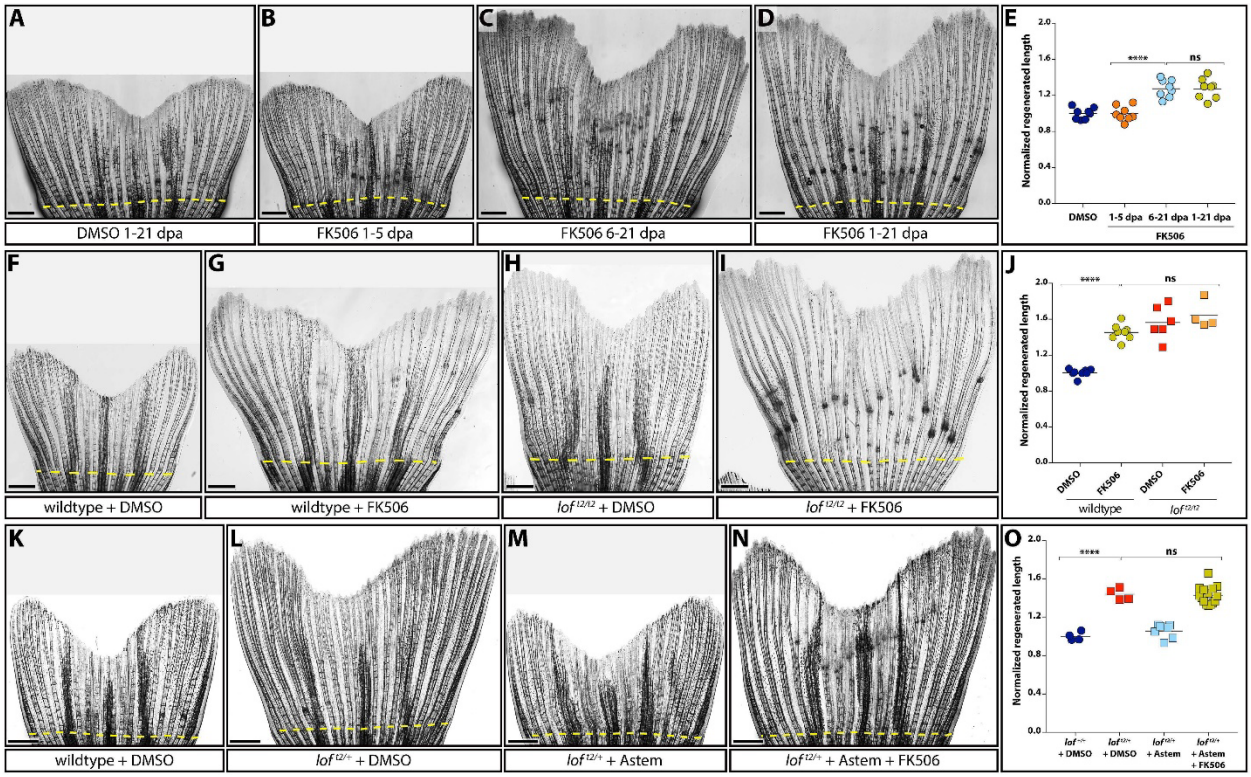

Figure 6. Kcnh2a-disrupted calcineurin signaling gradually terminates fin outgrowth. (A-D) Calcineurin gradually ends the fin outgrowth period. Stitched DIC images showing wildtype 21 day post amputation (dpa) caudal fins treated with DMSO (A) or 500 nM FK506 from either 1-5 (B), 6-21 (C), or 1-21 dpa (D). (E) Quantification of the experiment presented in A-D. Data are the average regenerated lengths of the third ray normalized to DMSO-treated controls at 21 dpa. Each point is a single wildtype animal treated with either DMSO 1-21 dpa (dark blue circles) or FK506 for the indicated times (orange circles 1-5 dpa, light blue circles 6-21 dpa, gold circles 1-21 dpa). (F-I) Ectopic Kcnh2a and FK506 treatment do not cooperate during overgrowth. DIC-imaged regenerated caudal fins from wildtype (F, G) and *lof*$^{t2/t2}$ (H, I) animals treated with DMSO (F, H) or 500 nM FK506 (G, I) daily from 1-23 dpa. (J) Graph showing relative regenerate lengths of ray 3 at 23 dpa from wildtype fish treated with DMSO or FK506 (blue or gold circles, respectively), and *lof*$^{t2/t2}$ fish treated with DMSO or FK506 (red or orange squares respectively). Each data point is an individual fish. (K-N) Kcnh2a activity is not required for FK506-induced overgrowth. Images showing wildtype (K) and *lof*$^{t2/+}$ clutchmate (L-N) caudal fin regenerates at 21 dpa. Animals were treated from 7-21 dpa with DMSO vehicle (K, L), 500 nM astemizole (M), or 500 nM astemizole + 500 nM FK506 (N). (O) Plot showing relative regenerative fin growth of ray 3 from the samples described in (K-N). Data points represent individual animals: DMSO-treated *lof*$^{+/+}$ or *lof*$^{t2/+}$ (dark blue circles and red squares, respectively), astemizole-treated *lof*$^{t2/+}$ (light blue squares), and *lof*$^{t2/+}$ treated with both FK506 and astemizole (gold squares). Data are normalized to DMSO-treated wildtype samples. Dashed yellow lines indicate amputation sites. Each data point represents an individual animal and asterisks indicate $p < 0.001$; ns: not significant. Scale bars are 1 mm. One-way ANOVA with Tukey's multiple comparisons tests tested differences between regenerated fin lengths.

long-appreciated phenotype. The genetic lesion is likely a chromosomal inversion linking *kcnh2a* to a displaced enhancer, explaining why *kcnh2a* lies just outside of the originally mapped *lof* region (Daane et al., 2021; Iovine and Johnson, 2000).

kcnh2a encodes an *ether-a-go-go* (EAG)-related voltage-gated K^+ channel. EAG/KCNH channels support membrane repolarization in various excitable cells, including neurons and myocytes (Vandenberg et al., 2012). The human ortholog KCNH2 produces I_{Kr}, the rapid component of the cardiac delayed rectifier current (Curran et al., 1995; Noble and Tsien, 1969; Sanguinetti et al., 1995). The voltage-dependent gating properties of KCNH2, namely slow opening and closing but fast inactivation, uniquely enables it to repolarize cardiac tissue and terminate action potentials (Bohnen et al., 2017; Vandenberg et al., 2012). *KCNH2* mutations are a frequent cause of inherited arrhythmias known as long QT syndrome whereby patients exhibit prolonged cardiac action potentials (Bohnen et al., 2017; Curran et al., 1995; Sanguinetti et al., 1995). KCNH2 is also a notorious pharmaceutical "off-target", leading to withdrawal of many drugs due to arrhythmia side effects. We find homozygous loss of *kcnh2a* has no overt effects on zebrafish development to adulthood, including fin length, although we have not assessed cardiac function. Ectopic expression of *kcnh2a* in *lof*^{t2} may be confined to fin mesenchyme, explaining the highly specific phenotype and otherwise healthy fish. However, we have not explored if *kcnh2a* is misexpressed in other *lof*^{t2} tissues, where it could adversely impact cardiac or other excitable cell functions. If so, *lof*^{t2} likely should be avoided as a "wildtype" strain.

Our study of fin overgrowth in *lof*^{t2} advances a mechanistic view of fin growth control centered on growth cessation rather than acceleration or potency. Ectopic Kcnh2a in *lof*^{t2} does not alter initial or maximal growth rates during caudal fin regeneration, similar to *lof*^{t2} fin development growth dynamics (Iovine and Johnson, 2000). Rather, Kcnh2a expression dampens

growth rate deceleration, effectively extending the allometric growth period. Kcnh2a specifically may enhance later outgrowth phases because mitogenic drive is saturated during the initial regenerative growth response (3-6 dpa), overshadowing Kcnh2a growth-promoting effects. Alternatively, upstream signals activating Kcnh2a or the ion signaling pathways disrupted by Kcnh2a may be inactive early in regeneration.

Our CRISPR and transplant chimera studies indicate ectopic Kcnh2a within fins and their intra-ray mesenchyme lineage is necessary and sufficient for fin overgrowth. Concordantly, *lof*^{t2} fish ectopically express *kcnh2a* in blastema fin mesenchyme but not other cell types with transcripts nearly undetectable in wildtype regenerating caudal fins. *alf* transplant experiments suggest hypermorphic Kcnk5b also acts within the mesenchyme lineage to cause fin overgrowth (Perathoner et al., 2014). Further evidence indicating this population is growth-determining include lineage tracing experiments showing intra-ray mesenchyme contributes to the growth-promoting distal blastema (Tornini et al., 2016). Finally, we recently proposed a model explaining slowing fin outgrowth by the progressive depletion of these distal blastema cells by biased differentiation vs. self-renewal (Stewart et al., 2019). Therefore, Kcnh2a may disrupt ion signaling that normally promotes mesenchyme lineage cell transitions from a growth-promoting to differentiated state.

Alternatively, ectopic Kcnh2a may prolong or enhance the production of pro-growth signaling molecules during the slowing outgrowth phase of fin regeneration. In support, Wnts and FGFs are produced by mesenchyme-derived “organizing center” or “niche” cells at the distal blastema (Stewart et al., 2019; Tornini et al., 2016; Wehner et al., 2014) and new observations suggest the Kcn5b (*alf*) K^+ channel cell autonomously promotes growth factor production (Yi et al., 2020). We observed *kcnh2a* expression throughout regenerating mesenchyme, highest near

the amputation site but still detectable in medial and distal blastema. However, we did not observe elevated proliferation or ectopic *wnt5a*, a representative distal growth factor, in proximal *kcnh2a*-expressing *lof*^{2} mesenchyme. Nevertheless, ectopic Kcnh2a could prolong growth factor production by acting directly in distal blastema/niche cells or in more proximal mesenchyme by disrupting negative feedback to the distal cells.

Mutations in *kcnk5b* (K^+ channel, (Perathoner et al., 2014)), *kcc4a*/*slc12a7A* (K^+ Cl^- co-transporter, (Lanni et al., 2019)), or over/ectopic expression of the K^+ channels *kcnj13, kcnj1b*, *kcnj10a*, *kcnk9c* (Silic et al., 2020), and now *kcnh2a* (this study) all cause fin overgrowth. Each model may disrupt a common "ion signaling" pathway featuring the fin outgrowth-restraining Ca^{2+}-dependent phosphatase calcineurin (Daane et al., 2018; Harris et al., 2020; Kujawski et al., 2014; Lanni et al., 2019; Yi et al., 2020). Here, we found fin overgrowth in regenerating *lof*^{2} fins was not enhanced by the calcineurin inhibitor FK506, suggesting ectopic Kcnh2a also inhibits calcineurin signaling. Ectopic Kcnh2a in *lof*^{2} could derail calcineurin output either upstream or downstream of calcineurin itself. Supporting the former, calcineurin's phosphatase activity is modulated by sustained elevated cytosolic Ca^{2+} (Klee et al., 1998; Rao, 2009; Timmerman et al., 1996) and KCNH2 effectively shortens Ca^{2+} fluxes during the cardiac conduction cycle (Bohnen et al., 2017; Vandenberg et al., 2012). Further, recent work indicates reduced calcineurin activity in *lof*^{2} fins (Cao et al., 2021). Alternatively, ectopic Kcnh2a could short-circuit calcineurin-promoted ion signaling dynamics mediated by Kcnk5b inhibition (Daane et al., 2018; Yi et al., 2020). These possibilities could be distinguished by determining if expressing constitutively active calcineurin in the intra-ray mesenchyme lineage suppresses *lof*^{2} fin overgrowth.

Bioelectricity is widely linked to organ size control and regeneration (McLaughlin and Levin, 2018). Bioelectric fields are suggested to pre-pattern undifferentiated tissue (including the

fin blastema) to establish positional information instructing correct amount of growth. However, *lof*^{t2} does not seem to change positional information established at the outset of fin regeneration because inhibiting ectopic Kcnh2a only during the late outgrowth phase restores a normal sized fin. Likewise, calcineurin need only be inhibited late during regeneration to maximally overgrow fins. Therefore, elevated Kcnh2a and calcineurin inhibition appear to disrupt growth deceleration mechanisms tuned to interpret, rather than set, positional information and thereby help establish (and re-establish) correct proportions. Regeneration has the additional challenge that outgrowth has to "read" some form of memory within cells or in higher tissue-level organization to direct correct amount of outgrowth while also re-establishing said memories. At least proximally, *lof*^{t2} overgrown caudal fins do not carry abnormal positional memory as fins amputated here regenerate normally when ectopic Kcnh2a is inhibited. Similarly, clonal analyses show calcineurin inhibition does not alter blastema pre-patterning (Tornini et al., 2016) and re-amputation of previously FK506-treated animals results in normal fin size (Daane et al., 2018). The nature of fin positional information and memory is unresolved but, as mentioned, likely reflects properties of intra-ray fibroblasts and derived blastema mesenchyme cells and/or their population sizes (Stewart et al., 2019).

Identifying and characterizing ectopic *kcnh2a* as the cause of the classic *lof*^{t2} zebrafish allele provides a framework to consider bioelectric control of organ size and shape through ion-mediated intracellular signaling. Subtle changes in calcium dynamics that tune signaling output and then growth period durations could produce profound changes in organ scale while retaining overall form and function. More local expression changes in ion signaling components (therefore, acting as effectors of "positional information") could then readily alter organ proportions supporting evolutionary innovations and phenotypic diversity. Extending this

concept, intersecting systemic gene regulatory signals including hormones could underlie sexual dimorphic traits or environmental effects on organ morphology arising after embryonic development. Swordtail fish provide a compelling example by their male-specific, dramatically elongated rays (the "sword") on the ventral edge of the caudal fin. Strikingly, the swordtail phenotype was recently linked to the *kcnh2a*-related gene *kcnh8* (Schartl et al., 2020). How fin growth periods are highly sensitive to alterations in K^+ channels and Ca^{2+}/calcineurin is unclear.

From these findings, we posit that ectopic *kcnh2a* in *longfin*^{t2} causes fin overgrowth by reducing Ca^{2+} levels and effectively inhibiting Ca^{2+}-dependent phosphatase calcineurin. Calcineurin may normally act to promote cell state transitions in fin mesenchyme, thereby progressively terminating fin outgrowth. This model implies fibroblast and mesenchymal cells undergo membrane depolarization to alter intracellular Ca^{2+} dynamics. Importantly, it underscores the role of Ca^{2+} as a critical second messenger ion in transducing signaling cascades, thereby initiating a cellular-level response that promotes fin regeneration. The mechanisms that ensure adequate Ca^{2+} signaling in fin regeneration have not been explored. Future direction is to elucidate a role for Ca^{2+} channel signaling in regenerative fin outgrowth.

CHAPTER III: VOLTAGE-GATED CALCIUM CHANNELS GENERATE FIBROBLAST-LINEAGE BLASTEMAL MESENCHYME CA^{2+} FLUXES THAT RESTRAIN OUTGROWTH DURING ZEBRAFISH FIN REGENERATION

The materials described in this chapter are co-authored by Rea G. Kioussi (R.G.K.), Astra L. Henner (A.L.H.), Scott Stewart (S.S.), and Kryn Stankunas (K.S.). Experiments were designed by me or by S.S. and K.S. Experimental procedures were performed by me or R.G.K., A.L.H., S.S., and K.S. The manuscript was prepared and written by me with editorial assistance by S.S. and K.S.

BACKGROUND

Developmental growth ends once an organ reaches an optimal size in scale with the individual organism. Robust organ regeneration exemplifies and extends this organ scaling phenomenon by restoring lost or damaged tissue to their original proportions. Adult zebrafish, like many teleosts, regenerate fins to the original size and pattern, providing a tractable vertebrate model to explore mechanisms of scaled organ growth.

Zebrafish fins are defined by tapering and segmented skeletal structures termed lepidotrichia or fin rays. Each fin ray segment comprises two opposing hemi-ray bones produced by lining osteoblasts. The apposed hemi-rays surround sensory nerves, blood vessels, and fibroblast cells (Sehring and Weidinger, 2019). Fin injury triggers regeneration including through cellular dedifferentiation (Wehner and Weidinger, 2015). Lineage-restricted progenitor cells then migrate, proliferate, and organize to establish ray-associated regenerative blastemas (Knopf et al., 2011; Singh et al., 2012; Sousa et al., 2011; Stewart and Stankunas, 2012; Tu and Johnson, 2011). Distal fibroblast-derived blastemal mesenchyme transitions to a Wnt and other growth factor-producing “niche” state to initiate outgrowth around 3 days post-amputation (Stewart et al., 2014;

Stewart et al., 2019; Tornini et al., 2016; Wehner et al., 2014). Outgrowth progressively slows until the original fin size is restored (Morgan, 1900). Zebrafish mutants with disrupted fin scaling provide an entry to investigate fin outgrowth control (van Eeden et al., 1996). Strikingly, all such mutants implicate ion signaling. *shortfin* (*sof*) fish with disrupted gap junction protein *connexin43* (*cx43/gja1*) develop small fins with shortened bony ray segments (Iovine et al., 2005). Long-finned zebrafish genetic models all reflect gain-of-function of potassium K^+ channels. *another longfin* (*alf*^{y86d}) fish develop and regenerate long fins due to a gain-of-function mutation in the K^+ channel *kcnk5b* (Perathoner et al, 2014; Daane et al., 2018). *longfin*^{t2} (*lof*^{t2}) fin overgrowth is caused by ectopic expression of *kcnh2a*, an ether-a-go-go (EAG)-related voltage-gated K^+ channel in fin fibroblast-lineage cells (Stewart et al., 2021, Daane et al., 2021). Further, transgenic overexpression of K^+ channels *kcnj13*, *kcnj1b*, *kcnj10a*, and *kcnk9* all lead to overgrown fins (Silic et al., 2020). Roles for both gap junctions and voltage-gated and membrane potential setting K^+ channels suggest "bioelectricity" patterns and/or modulates the extent of fin outgrowth. However, mechanisms linking ion channels and altered membrane potential dynamics to cell behaviors impacting outgrowth are unclear.

Calcineurin inhibition during fin regeneration leads to dramatically overgrown fins similar to genetic long-finned models (Kujawski et al., 2014; Stewart et al., 2021). Calcineurin, a Ca^{2+}-dependent protein phosphatase, likely is an ion signaling node for fin outgrowth control, acting upstream (Yi et al., 2021) or downstream (Stewart et al., 2021) of K^+ channels and modulated membrane potentials. Support the latter role, intracellular Ca^{2+} levels and spike dynamics govern calcineurin signaling output (Rao, 2009). Further, K^+ channels like *kcnh2a* modulate cell membrane potentials to produce specific patterns of intracellular Ca^{2+} fluxes, for example during the cardiac cycle (Bohnen et al., 2017; Sanguinetti and Tristani-Firouzi, 2006; Vandenberg et al.,

2012). Calcineurin activity acts only during the outgrowth phase to gradually slow and then end growth as fin size is restored (Stewart et al., 2021). Likewise, fibroblast-lineage ectopic Kcnh2a in *longfin*^{t2} mutants acts uniquely during regenerative outgrowth to drive fin overgrowth. However, Ca^{2+} fluxes and their control, including by Ca^{2+} channels, in fibroblast-lineage regenerating fins have not been examined.

We explored if membrane potential-regulated Ca^{2+} signaling in fibroblast-lineage blastemal cells during zebrafish fin regenerative outgrowth contributes to growth cessation and therefore fin size control. We developed a regenerating fin fibroblast GCaMP6s reporter line to determine that isolated fibroblast-lineage fin cells flux Ca^{2+} in response to membrane depolarization and dependent on voltage-gated Ca^{2+} channels. We used single cell transcriptomics and *in situ* transcript expression studies to localize expression of specific L-, N-, and T-type voltage-gated Ca^{2+} channels to fibroblast-lineage blastema mesenchyme during the outgrowth phase of fin regeneration. In vivo pharmacological inhibition implicates L- and/or N- type voltage-gated Ca^{2+} channels in fin outgrowth suppression. Genetic loss-of-function of the T-type *cacna1g* channel produces a new, recessive long-finned zebrafish model with strikingly exaggerated overgrowth upon regeneration. Live imaging of regenerating adult fins demonstrates that Cacna1g enables endogenous Ca^{2+} fluxes in fibroblast-lineage blastema cells. We conclude voltage-gated Ca^{2+} channel activity within fibroblast-derived blastemal mesenchyme actively sets a tuned rate of outgrowth slowing and the outgrowth period, thereby ensuring the restoration of scaled fin size.

RESULTS

K^+ channel gain-of-function and inhibited calcineurin likely disrupt the same ion signaling mechanism to produce long-finned zebrafish (Stewart et al., 2021), suggesting Ca^{2+} as

a second messenger moderating fin outgrowth. Further, spatiotemporal gene function studies indicate ion signaling acts within fibroblast-lineage cells to gradually terminate fin regenerative outgrowth (Stewart et al., 2021; Daane et al., 2021). We generated a transgenic line using the *tryptophan hydroxylase 1b* (*tph1b*) promoter (Kapsimali et al., 2011) driving GCaMP6s (Chen et al., 2013) expression to monitor Ca^{2+} dynamics within fibroblast-lineage cells of regenerating fins (Stewart et al., 2021; Tornini et al., 2016). 3 day post-amputation (dpa) *tph1b:GCaMP6s* regenerating fins showed GCaMP6 fluorescence specifically in blastemal tissue extending from each ray (Fig. 7A). Whole mount antibody staining confirmed GCaMP6s expression in fibroblast-lineage (Mardon et al., 1994; Shen and Mardon, 1997) distal blastema cells by co-expression of the *Dachshund* (*Dach*) transcription factor (Stewart et al., 2021; Lewis et al., 2023) (Fig. 7B). We imaged GCaMP6s dynamics in 3 dpa regenerating fins of anesthetized zebrafish by spinning disc confocal microscope and measuring volumetric GCaMP6 fluorescence of individual cells. Many blastemal cells exhibited fluctuating GCaMP6s levels, including spikes of variable duration and occasional oscillatory behaviors (Fig. 7C, D). We conclude fibroblast-lineage distal blastema cells flux Ca^{2+} levels in vivo and such dynamics could represent the nexus of ion signaling modulating the fin outgrowth period and therefore fin size.

We next turned to an in vitro system to confirm and expand upon these observations. Time-lapse imaging of isolated *tph1b:GCaMP6s* cells prepared from regenerating fins revealed sporadic Ca^{2+} fluxes (data not shown). Voltage-gated Ca^{2+} channels are activated by membrane depolarization and facilitate flow of extracellular Ca^{2+} into the cytoplasm (Catterall, 2011). We depolarized *tph1b:GCaMP6s* primary cells with KCl to investigate if the observed Ca^{2+} fluxes are controlled by voltage-gated Ca^{2+} channels. We found 56% of *tph1b:GCaMP6s*-

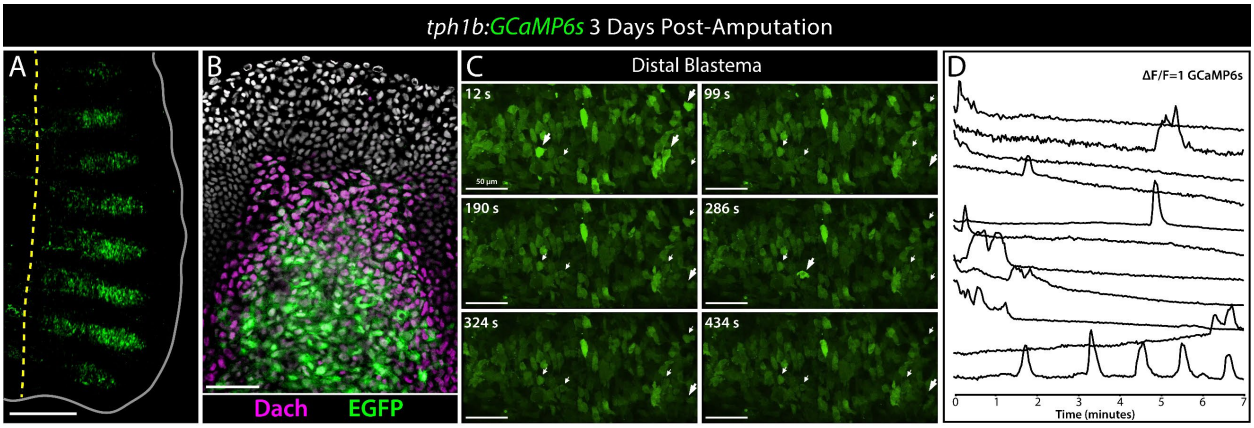

Figure 7. The *tph1b:GCaMP6s* line enables visualization of Ca^{2+} fluxes in fibroblast-lineage distal blastemal cells. (A) Whole mount image of a 3 dpa *tph1b:GCaMP6s* caudal fin. Yellow dashed is the amputation plane and scale bar is 500 µm. (B) GCaMP6s expression includes distalmost blastemal cells. Confocal maximum intensity projection image showing antibody stained 3 dpa fin section from *tph1b:GCaMP6s* animals. Dach and endogenous GFP are in magenta and green, respectively. Hoechst-stained nuclei are grey. (C) Representative 3D-rendered timelapse still images of intact distal fin of *tph1b:GCaMP6s* adult fish at 3 dpa; scale bars are 50 µm. A large white arrow indicates the event of a spike or sustained Ca^{2+} levels captured overtime (individual cells can be tracked by small white arrows). (D) Plot of normalized GCaMP6s intensity traces over a 7-minute period corresponding to individual cells in panel C shows heterogenous Ca^{2+} dynamics.

responsive cells spiked GCaMP6s fluorescence upon membrane depolarization (Fig. 8A, B). Therefore, voltage-gated Ca^{2+} channels are likely active in fibroblast-lineage regenerating fin cells.

We treated *tph1b:GCaMP6s* primary cells with the Ca^{2+} channel blockers amlodipine (L-type) (Nayler and Gu, 1991), cilnidipine (L/N-type) (Yamaura et al., 1986), and PD1732122 (N-type) (Hu et al., 1999) prior to depolarization to determine whether high voltage-sensitive L- and/or N-type Ca^{2+} channels contributed to the observed Ca^{2+} spikes. Approximately 39% of DMSO-treated control cells were excitable (Fig. 8C). Each of amlodipine ~ 12% (15/127 cells), cilnidipine ~ 4% (4/103 cells), and PD17132 ~ 20% (29/147 cells) significantly reduced the fraction of excited cells (Fig. 8D-F). We conclude L- and N-type voltage-gated Ca^{2+} channels jointly contribute to dynamic Ca^{2+} fluxes in fibroblast-lineage cells.

The *longfin*^{t2} (ectopic Kcnh2a) and inhibited calcineurin long-finned models are due to disrupted ion signaling that normally acts after 5 dpa and onwards to slow and eventually terminate outgrowth (Stewart et al., 2021). We re-analyzed single cell RNA-seq data collected from 7 dpa regenerating caudal fins using an expanded transcriptome to identify voltage-gated Ca^{2+} channels expressed in fibroblast-lineage blastemal fin cells during fin outgrowth (Lawson et al., 2020; Lewis et al., 2023). We identified 11 clusters (Farnsworth et al., 2020; Hou et al., 2020; Lewis et al., 2023), including co-clustered fibroblast- and osteoblast-lineage cells (Stewart et al., 2014; Lewis et al., 2023), by literature-established marker genes enriched within each cluster (Cao et al., 2019) (Fig. 9A-D; Fig. S14). We surveyed the expression of genes encoding α1 subunit pores of L-, P-, N-, and T-type Ca^{2+} channels (Catterall, 2011) (Fig. S15). Of all candidates, L-type *cacna1c*, N-type *cacna1ba*, and T-type *cacna1g* transcripts were specifically expressed within the fibroblast/osteoblast cluster (Fig. 9E-G). *cacna1g* and *cacna1c* expression

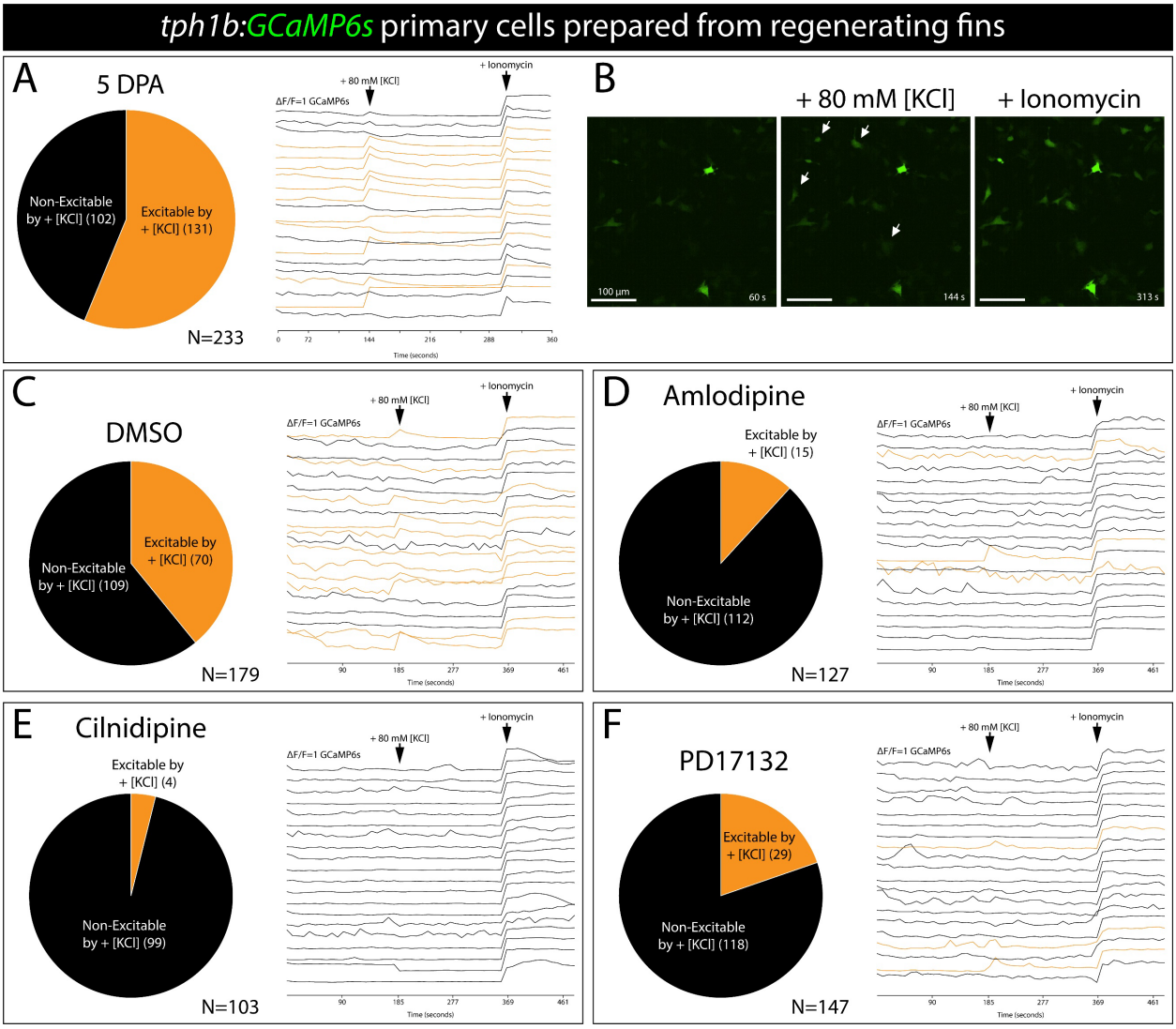

Figure 8. Voltage-gated Ca^{2+} channels actively contribute to dynamic Ca^{2+} fluxes in intra-ray fibroblast-lineage fin cells. (A, B) Intra-ray fibroblast-lineage cells are *tph1b:GCaMP6*s expressing and susceptible to depolarization events. Primary cells were prepared from adult *tph1b:GCaMP6s* reporter fish caudal fins at 5 dpa. (A) The pie chart indicates the fraction of *tph1b:GCaMP6s* expressing primary cells excited by addition of 80 mM KCl at ~ 144 seconds(s). Candidate cells were positively controlled for by the addition of ionomycin at ~313 s and referred to as responsive. Plot of normalized GCaMP6s intensity traces over 360 s corresponding to twenty randomly selected responsive cells out of N=233. We show that all cells can respond to Ca^{2+}, however only a subset is excitable and show an amplitude spike in GCaMP6s level by the addition of 80 mM KCl. (B) Representative 3D-rendered timelapse still images of cells showing Ca^{2+} spikes at 144 s (+ 80 mM KCl) and 313 s (+ Ionomycin). White arrows point to an excited cell. Scale bars are 100 µm. (C-F) Excitable cells (C) are highly sensitive to voltage-gated Ca^{2+} channels blockers Amlodipine 500 nM (D), cilnidipine 500 nM (E), and PD17132 500 nM (F). The pie charts indicate the fraction of excitable cells from the total count of responsive cells (N) for each experimental group. Plot of normalized GCaMP6s intensity traces over 480 s corresponding to twenty randomly selected responsive cells. Black arrows indicate the time primary cells were exposed to 80 mM KCl and Ionomycin. Individual Ca^{2+} traces indicate excitable cells in orange or non-excitable cells in black.

was relatively broad across the cluster, including mature and maturing fibroblasts (*rgs5a*- and *fhl1a*-expressing) (Fig. S15). In contrast, *cacna1ba* was enriched in distal blastema mesenchyme based on overlapping expression with *msx3*, *dachc*, *wnt5a*, and *robo3* (Lewis et al., 2023; Fig. 9B; Fig. S15).

We assessed the *in situ* spatial distributions of *cacna1c*, *cacna1ba*, and *cacna1g* transcripts by RNAScope (Wang et al., 2012) on 7 dpa fin sections (Fig. 9H-K). As predicted by the scRNA-seq analysis, *cacna1ba* exclusively was expressed in *dachc* co-expressing distal blastema (Lewis et al., 2023; Stewart et al., 2019) (Fig. 9H and I; Fig. S16; Fig. S17). *cacna1c* and *cacna1g* transcripts were enriched in all fibroblast-lineage cells as well as osteoblasts (Fig. 9H, J, and K; Fig. S17). The distal blastema mesenchyme co-expressed *cacna1c*, *cacna1ba*, and *cacna1g* transcripts (Fig. S17). We conclude these voltage-gated Ca^{2+} channels likely contribute to the observed cytosolic Ca^{2+} dynamics within intra-ray fibroblast-lineage cells.

We hypothesized voltage-gated Ca^{2+} channel activity, acting after 7 dpa (Stewart et al., 2019), mediates size restoration during fin regeneration. We first employed a small molecule approach by treating fish with cilnidipine, the dual N/L-type Ca^{2+} channel blocker most potent in the in vitro assays. Daily 5 µM cilnidipine from 5-28 dpa caused significant fin overgrowth in otherwise healthy fish (Fig. 10A-E; Fig. S18). Regenerated fins of cilnidipine-treated fish also had fewer ray segments, similar to calcineurin inhibition and *another longfin* (*alf*) long-finned models (Kujawski et al., 2014, Perathoner et al., 2014) (Fig. 10F-H, Fig. S18). We conclude L- and/or N- type Ca^{2+} channels actively promote fin outgrowth cessation, consistent with *cacna1c* and *cacna1ba* expression in Ca^{2+}-fluxing and outgrowth-regulating blastema mesenchyme.

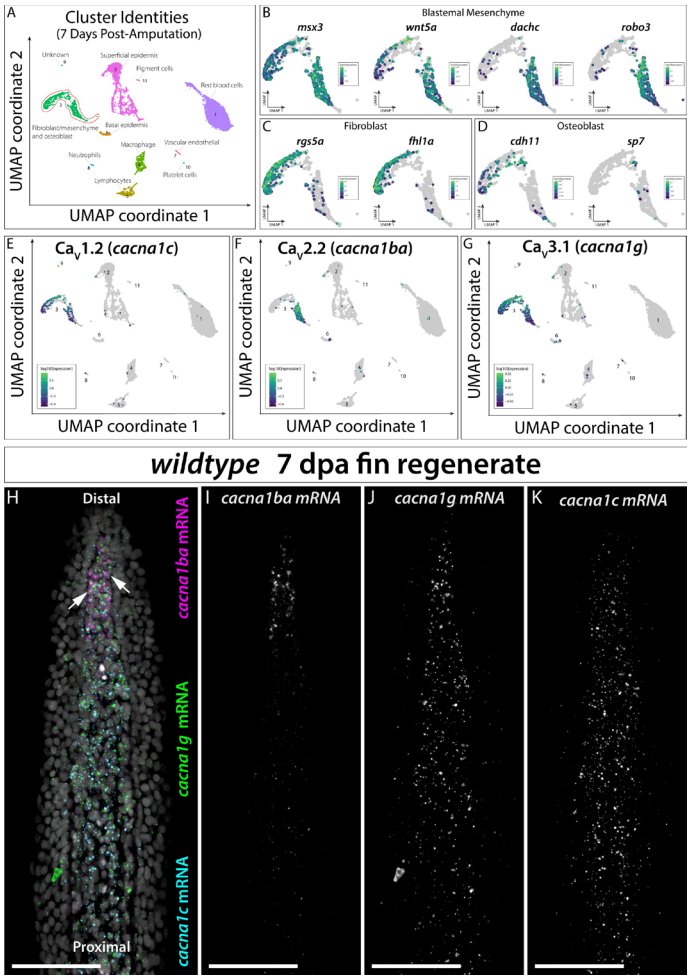

Figure 9. Single cell transcriptomics identifies distinct spatial expression pattern of L-, N-, and T-type Ca^{2+} channels in fibroblast-lineage cells. (A-G) UMAP projection of the 12,298 cells from our 7 dpa scRNA-seq dataset (Lewis et al., 2023) projected in 11 clusters from Louvain clustering and annotated on the basis of unique marker genes (Supplemental Figure 14) and/or literature such as, cluster 1: red blood cell genes *epb41b*, *klf1*, *gata1a*, and *fech*; cluster 2: superficial epidermis genes *krt4/5/91*; cluster 3: blastemal mesenchyme, fibroblast, and osteoblast genes in (B-D); cluster 4: macrophage genes *cd74a*, *mpeg1.1*, and *mfap4*; cluster 5: lymphocytes genes *sal2*, Ick, and *dusp2*; cluster 6: basal epidermis genes *apoeb* and *fras1*; cluster 7: vascular endothelial genes *plvapb*, *podxl*, *flt4*, and *clec14a*; cluster 8: neutrophils genes *lyz*, *mpx*, and *npsn*; cluster 9: unknown; cluster 10: Platelet cell gene *itga2b*; lastly cluster 11: pigment cell genes *pax7a/b*, *mlpha*, and *plin6*. Red dashed line outlines cluster 3 containing fibroblast-lineage cells. (E-G) UMAP projections showing high expression levels of α_1 subunit gene for voltage-gated Ca^{2+} channels L-type $^{+}$, *cacna1c* (E), N-type, *cacna1ba* (F), and T-type, *cacna1g* (G), which show specificity for cluster 3. (H-K) 7 dpa longitudinal section of wildtype caudal fin ray analyzed by RNAscope for *cacna1c*, *cacna1ba*, and *cacna1g* mRNA abundance. (I) The white arrows point to cells co-expressing *cacna1ba* (magenta), *cacna1c* (cyan), and *cacna1g* (green) solely in distal fibroblast-lineage cells. Hoechst-stained nuclei are marked in gray. Individual max intensity projections for *cacna1ba* (I), *cacna1g* (J), and *cacna1c* (K) mRNA are shown in greyscale. Heterogeneity exists in the spatial expression of voltage-gated Ca^{2+} channels, with discrete expression levels of *cacna1ba* in distal intra-ray, variable expression levels of *cacna1c* throughout the intra-ray (highest levels in the proximal position), and consistent expression levels of *cacna1g* across the entire intra-ray. Scale bars are 50 µm.

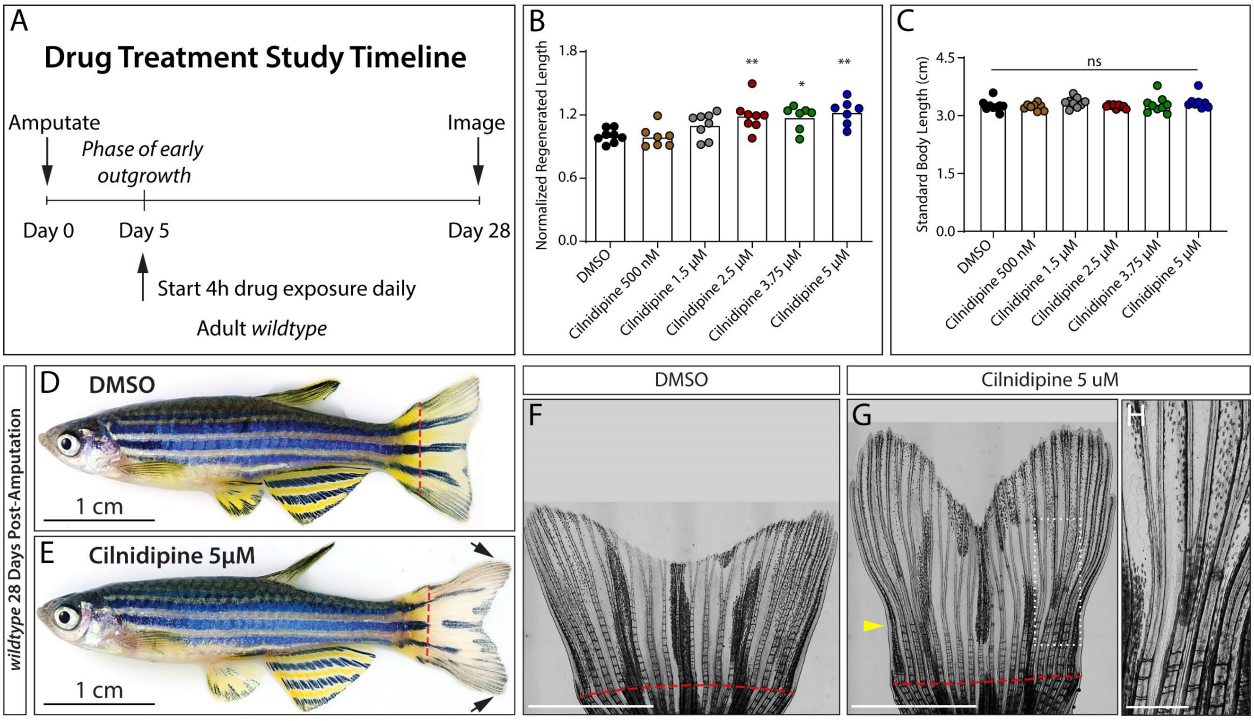

Figure 10. Cilnidipine treatment reveals that L-and/or N-type Ca^{2+} channels act to promote the cessation of fin outgrowth. (A) Schematic representation of timeline drug treatment following wildtype animals treated from 5-28 dpa; fish received daily 4-hour exposure of DMSO (n=8), 500 nM (n=7), 1.25 µM (n=8), 2.5 µM (n=8), 3.75 µM (n=7), or 5 µM (n=7) cilnidipine. (B) Quantification of fin length measurements from third ray normalized to wildtype-DMSO treated samples. Each point represents an individual fish. (C) Standard body length measurements from the tip of the mouth to the caudal peduncle. Shown are adult wildtype treated with DMSO (black circle) or cilnidipine at indicated dosages (brown circles 500 nM, gray circles 1.25 µM, red circles 2.5 µM, green circle 3.75 µM, and blue circles 5 µM). *$P < 0.05$ and **$P < 0.01$ vs. the wildtype-DMSO treated group using a one-way ANOVA; ns: not significant. (D and E) Representative brightfield images of lateral whole animal view of wildtype-DMSO (D) and cilnidipine 5 µM (E) treated zebrafish at 28 dpa. The black arrows point to overgrown caudal fin tissue. The dashed red line indicates amputation plane. The scale bars are 1 cm. (F-H) Representative stitched brightfield images of regenerative caudal fin at 28 dpa corresponding to fish in (D and E); scale bars are 4 mm. A red dashed line indicates the amputation plane. A yellow arrow in (G) indicates the start of a joint defect that begins approximately at the start of cilnidipine treatment. Dashed white box in (G) shows a zoomed in region in (H), scale bar is 200 µm.

The prominent *cacna1g* expression fibroblast-lineage blastema mesenchyme implicates low-voltage-regulated T-type channel activity in outgrowth control. Therefore, we used CRISPR/Cas9 technology to generate loss-of-function alleles of *cacna1g*. F0 cacna1g CRISPants displayed mosaic developmental and, sometimes dramatically, regenerative overgrowth across all fins (Fig. S19 and S20). We outcrossed founders to identify two putative *cacna1g* loss-of-function alleles (Fig. S19 and S21). Homozygous *cacna1g* mutants developed modestly overgrown fins with slightly longer ray segments but appeared otherwise normal (Fig. S19). Strikingly, *cacna1g*$^{-/-}$ fish regenerated exceptionally long caudal fins that greatly exceeded their developed length (Fig. 11A-G; Fig. S22 and S23). *cacna1g* heterozygotes displayed only modest regenerative overgrowth (Fig. S23). *cacna1g*$^{-/-}$ fish also greatly overgrew other median as well as paired fins, including pectoral fins upon regeneration (Fig. S24 and S25). The degree of caudal fin regenerative overgrowth even exceeded that of *longfin*$^{t2/+}$ fish amputated in parallel (Fig. S26). Joint length was only modestly increased in *cacna1g*$^{-/-}$ regenerated caudal fins, more closely resembling the *longfin*^{t2} than calcineurin-inhibition or *alf* models (Fig. S27). We also observed pronounced vascularization and blood pooling in the distal fin tip of late regenerating *cacna1g*$^{-/-}$ fish (Fig. S28), phenotypes associated with other long-finned models (Kujawski et al., 2014; Lanni et al., 2019). *cacna1g*$^{-/-}$ uniquely establishes a recessive, loss-of-function long-finned model that centrally and specifically implicates T-type voltage-gated Ca^{2+} channels in restraining regenerative fin outgrowth.

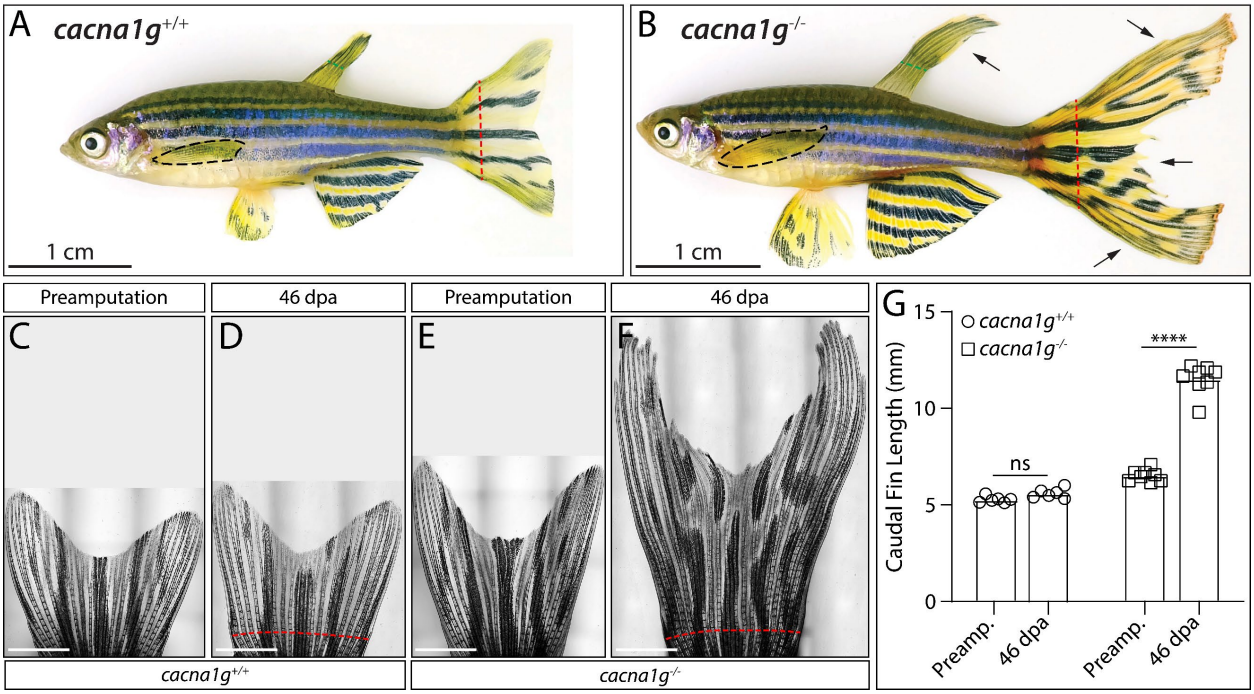

Figure 11. The T-type voltage-gated Ca^{2+} channel is essential for fin cessation and linked to the process of regeneration. (A and B) Representative brightfield images of lateral whole animal view of regenerated F2 *cacna1g*$^{+/+}$ (A) and *cacna1g*$^{-/-}$ (B) adult zebrafish at 66 dpa. Black dashed lines outline the pectoral fin, green dashed lines indicate clipped dorsal fin for genotyping, and the red dashed lines indicate amputation site. Scale bars are 1 cm.(C-F) Representative brightfield stitched images showing caudal fin outgrowth in *cacna1g*$^{+/+}$ before and after at 46 dpa (C and D), as well as, in *cacna1g*$^{-/-}$ fish (E and F). Red dashed lines indicate amputation site and scale bars are 2 mm. (G) Plotted are measurements along the third fin ray starting from the pre-current position (also the amputation site) to the fin tip. Data points of individual genotypes are denoted by circles (*cacna1g*$^{+/+}$) or squares (*cacna1g*$^{-/-}$). ****$P < 0.0001$ vs. the Preamputation (preamp.) group using paired two-way ANOVA; ns: not significant.

We hypothesized Cacna1g-containing channels ($Ca_V3.1$) may control fin size by progressively slowing and then terminating fin outgrowth, as seen with *longfin*^{t2} and calcineurin-inhibited long finned models (Stewart et al., 2021). We defined the outgrowth characteristics of *cacna1g*$^{-/-}$ and wildtype clutchmates by measuring regenerated fin length over the course of regeneration (Fig. 12; Fig. S23). The size of *cacna1g* mutant regenerating fins was unchanged through approximately 5 days of regeneration. From that point, the outgrowth rate increasingly exceeded that of control animals thereby leading to progressively longer fins, matching the outgrowth kinetics of *lof*$^{t2/+}$ regenerating fins (Iovine and Johnson, 2000; Stewart et al., 2021) (Fig. 12A, C-H). The maximum rate of outgrowth peaked at ~3-4 dpa for *cacna1g*$^{+/+}$ and *cacna1g*$^{-/-}$ then gradually declined, with the rate curve past that point closely fitting to a one-phase exponential decay curve with differential decay rate (Fig. 12B). As with other ion signaling molecules implicated by long-finned models, we conclude Cacna1g establishes a steadily decreasing outgrowth rate that helps restore fins to their original size.

We performed live, time-lapse, GCaMP6s imaging of *cacna1g*$^{-/-}$ regenerating caudal fins to determine if Cacna1g influences the Ca^{2+} dynamics we observed in fibroblast-lineage blastemal mesenchyme. We observed heterogenous GCaMP6s reporter activity across distal fibroblast-lineage cells of 5 dpa wildtype regenerating fins, as seen at 3 dpa (Fig. 13A, D). In contrast, very few *cacna1g*$^{-/-}$ fin regenerate cells showed Ca^{2+} transients and even those cells showed only rare and modest Ca^{2+} spikes over a 5 minute time course (Fig. 13B-D). We conclude the Cacna1g T-type channel centrally enables Ca^{2+} dynamics in the distal fibroblast-lineage blastemal mesenchyme. These Ca^{2+} fluxes appear specifically coupled to unknown cell behaviors that tune the period of fin outgrowth and thereby restore regenerated fin size.

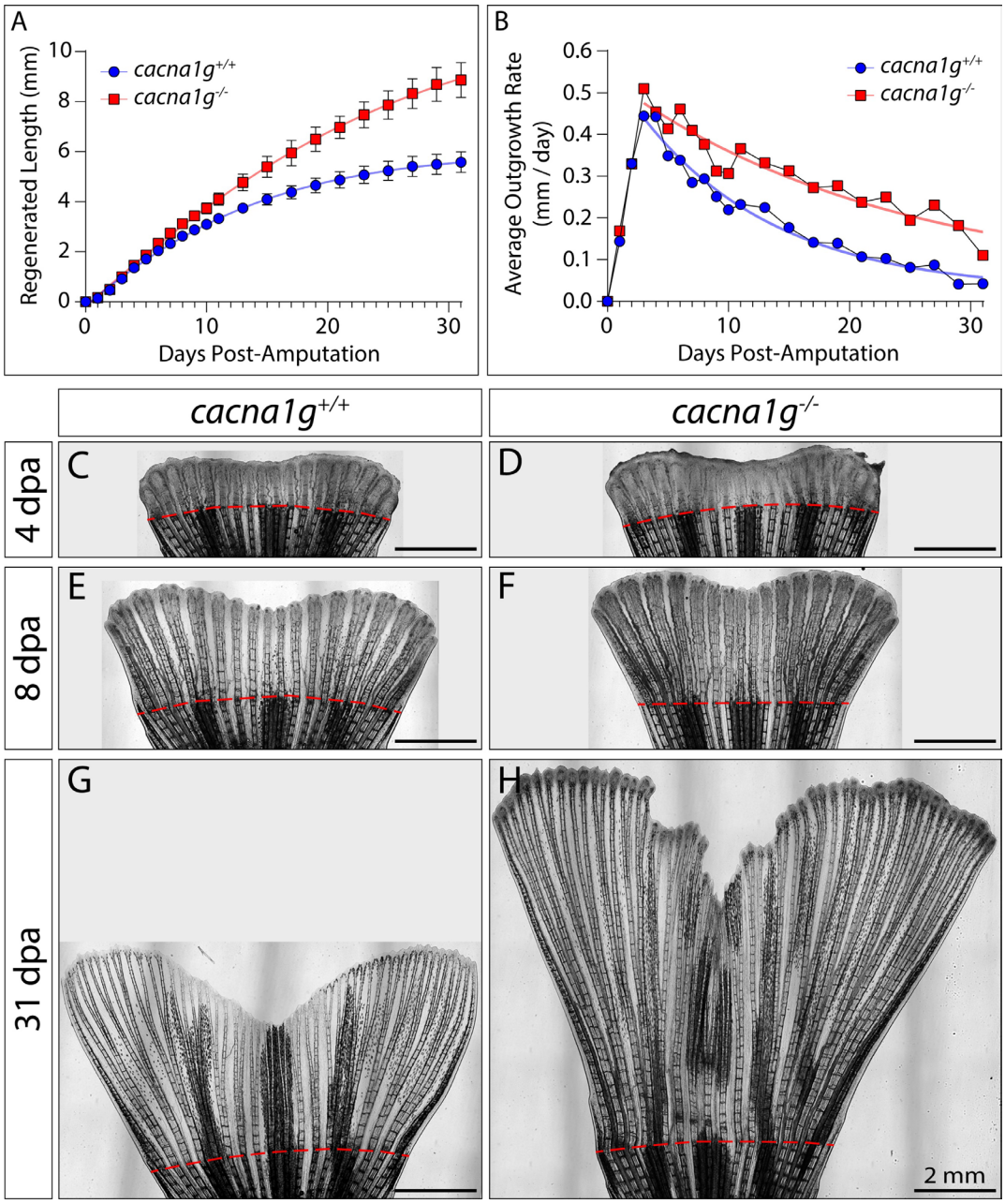

Figure 12. Cacna1g actively decelerates the outgrowth rate of regenerating fins. (A and B) Graphs display regenerated fin growth rates for *cacna1g*$^{+/+}$ (data points are circles in blue) and *cacna1g*$^{-/-}$ (data points are squares in red) fish over the course of 31 days. (A) Sigmoidal logistic growth curve is fitted to regenerated fin length to reflect blastema establishment and the observed slow decline in late-stage outgrowth. Mean ± SD are plotted for each timepoint (N=14 fish per genotype). (B) One phase exponential decay curve is fitted to the average outgrowth rate starting at 3 dpa when the peak rate of fin outgrowth is achieved for both *cacna1g*$^{+/+}$ and *cacna1g*$^{-/-}$ groups. (C-H) Representative brightfield stitched images of caudal fins at 4, 8, and 31 dpa for *cacna1g*$^{+/+}$ (C, E, and G) and *cacna1g*$^{-/-}$ (D, F, and H). Early regenerative outgrowth is similar in *cacna1g*$^{+/+}$ and *cacna1g*$^{-/-}$ animals but fails to decelerate in *cacna1g*$^{-/-}$ fish by 31 dpa. Mild outgrowth phenotype was observable in *cacna1g*$^{+/-}$ fish only during very late-stage outgrowth period at 31 dpa (representative whole mount fin not shown). Scale bars are 2 mm.

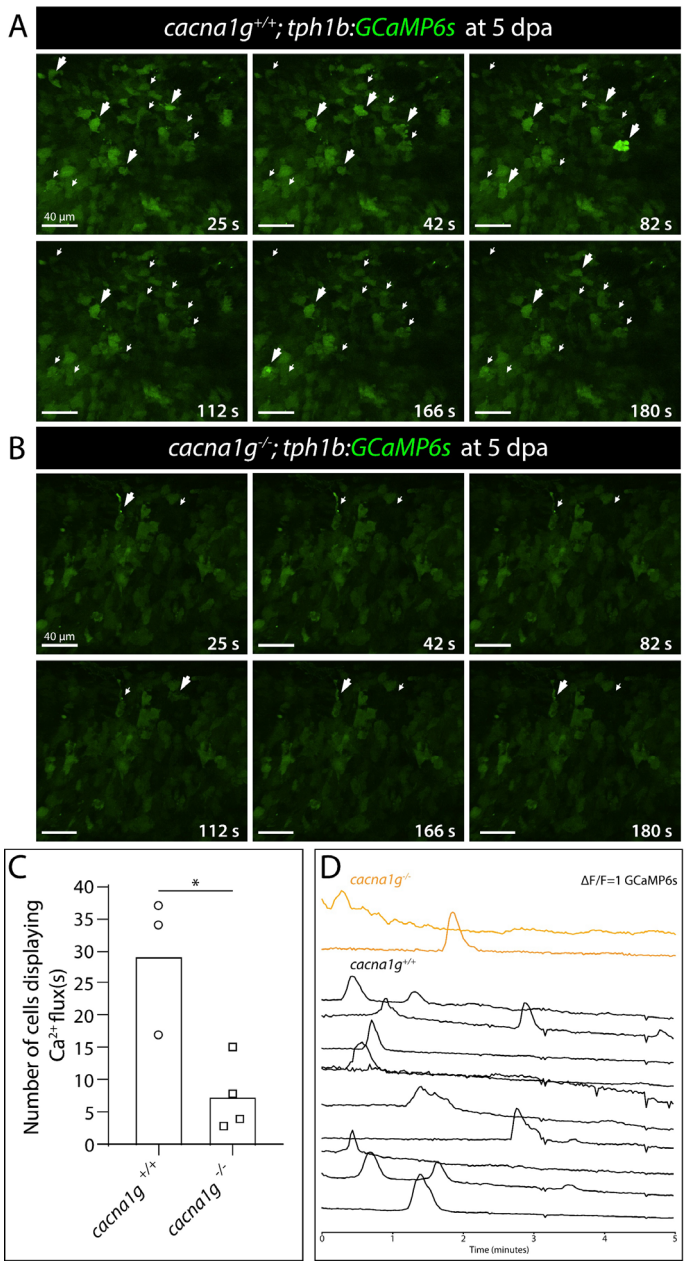

Figure 13. Cacnalg controls Ca^{2+} dynamics in distal blastema and niche cells to terminate fin outgrowth and regeneration. (A and B) Representative 3D-rendered timelapse still images of intact distal fins of *cacna1g*$^{+/+}$ (A) and *cacna1g*$^{-/-}$ (B) fish expressing the reporter *tph1b:GCaMP6s* at 5 dpa, also considered as the early phase of regenerative outgrowth. A large white arrow indicates the event of a spike or sustained Ca^{2+} levels captured overtime (individual cells can be tracked by small white arrows). Here we show the scale bars are 40 µm. (C) The total number of distal fibroblast-lineage cells displaying dynamic Ca^{2+} flux was diminished in *cacna1g*$^{-/-}$ fish. Each data point represents an individual animal with *cacna1g*$^{+/+}$ denoted as circles and *cacna1g*$^{-/-}$ denoted as squares. *$P > 0.05$ vs. clutchmate *cacna1g*$^{+/+}$ using unpaired t-test. (D) Representative plot of normalized GCaMP6s intensity traces over a 5-minute period corresponding to individual cells in panels A and B. Orange traces are *cacna1g*$^{-/-}$ cells (N=2) and black traces are *cacna1g*$^{+/+}$ cells (N=10). Each cell has a unique amplitude, duration, and frequency of Ca^{2+} spike, revealing heterogenous response in Ca^{2+} signaling in fin outgrowth.

DISCUSSION

We link voltage-gated Ca^{2+} channels and associated cytosolic Ca^{2+} flux within blastemal fibroblasts to cessation of fin outgrowth. Live GCaMP6s reporter imaging of regenerating fins indicates distal fibroblast-lineage blastemal cells undergo dynamic and variable cytosolic Ca^{2+} fluxes. Isolated regenerating fin fibroblasts spontaneously and autonomously produce heterogeneous Ca^{2+} fluxes. Further, their membrane depolarization causes cytosolic Ca^{2+} spikes, indicating at least some fibroblast-lineage blastemal cells are in an "excitable" state. Inhibitor studies indicate the excitability is mediated by voltage-gated Ca^{2+} channels. In vivo, fibroblast-lineage distal blastemal cells express *cacna1c* (L-type), *cacna1ba* (N-type), and *cacna1g* (T-type) voltage-gated Ca^{2+} channels. Temporal inhibition indicates L- and/or N-type Ca^{2+} channels actively restrain fin outgrowth during late stages of regeneration. Dramatic regenerative fin overgrowth and GCaMP6s studies in *cacna1g* loss-of-function mutants reveals a central and specific role for T-type channel-dependent Ca^{2+} fluxes in fibroblast-lineage distal blastemal mesenchyme. We propose voltage-gated ion channel activity in distal fibroblast-lineage cells culminates in intracellular signaling by the classic second messenger Ca^{2+}. Ca^{2+}-regulated proteins, likely the calcineurin phosphatase, then progressively restrain outgrowth and eventually terminate fin regeneration.

We generated a Ca^{2+} reporter line expressing GCaMP6s under the control of the *tph1b* promoter and therefore expressed in fibroblast-lineage blastema cells (Tornini et al., 2016). Live-imaged, regenerating adult fins at 3 dpa and 5 dpa showed frequent flashes of GCaMP6s reporter activity, indicative of cytosolic Ca^{2+} flux. Such cells were largely distally concentrated, suggestive of growth factor-producing "niche"-state, or "organizing center" cells (Stewart et al. 2019, Wehner et al. 2014). The amplitude, duration and frequency of fluxes were qualitatively

heterogeneous and not overtly coordinated, arguing against the transmission of bioelectric signals across a blastema field. However, coordinated spikes may initiate at later outgrowth periods than we could assay (5 dpa), corresponding to when calcineurin activity is required, or in distalmost blastema cells where the *tph1b:GCaMP6s* line expresses poorly.

Primary cells prepared from regenerating *tph1b:GCaMP6s* fins showed voltage-gated Ca^{2+} channel-dependent Ca^{2+} fluxes, indicating the autonomous initiation of membrane potential fluxes. Further, membrane depolarization by addition of KCl rapidly spiked cytosolic Ca^{2+}, again dependent on voltage-gated Ca^{2+} channels. This excitability as well as the GCaMP6s intensity and frequency was notably heterogenous, similar to in vivo observations. Plausible explanations for cell-to-cell variability Ca^{2+} signaling among fibroblast-lineage cells include heterogeneous voltage-gated ion channel gene expression, differences in resting membrane potentials, or the variable establishment of gap junction intercellular connections.

N- and/or L- as well as T-type voltage-gated Ca^{2+} channels contribute to the observed Ca^{2+} fluxes and restoration of fin size. The L- and N-type Ca^{2+} inhibitor, cilnidipine, displayed the most potent block of depolarization-induced Ca^{2+} flux in isolated regenerating fibroblasts. Cilnidipine administration to regenerating animals then resulted in significant fin overgrowth. However, regenerating fin overgrowth was considerably more dramatic in T-type channel *cacna1g* homozygous mutants. Further, fibroblast-lineage blastemal mesenchyme Ca^{2+} fluxes were almost completely lost in *cacna1g*$^{-/-}$ regenerating fins. Single cell transcriptomics and *in situ* hybridizations of 7 dpa caudal fins revealed expression of *cacna1c* (L-type) and *cacna1g* (T-type) primarily in fibroblast-lineage blastema and osteoblasts. In contrast, *cacna1ba* (N-type) transcripts were exclusively found in far distal fibroblast-lineage cells. The possible cooperation between all three channel types suggests their uniquely overlapping expression in these

distalmost cells may define where ion signaling is most critical. Regardless, upregulation of voltage-gated Ca^{2+} channels and other ion signaling molecule transcripts (including *kcnk5b*) appears a key component of fibroblast cell state transitions underpinning regeneration (Tornini et al., 2016, Lewis et al., 2023).

Cilnidipine timing-of-administration experiments revealed that at least L- and/or N-type channels are actively required to terminate fin outgrowth. These results, along with temporal calcineurin inhibition that exclusively defined calcineurin's role in fin size restoration to the outgrowth phase (Stewart et al. 2021), are inconsistent with alternative models whereby bioelectric signals either "pre-pattern" the blastema and/or modulate initial growth rates after fin resection.

The extent of developmental fin overgrowth *cacna1g*$^{-/-}$ fish is less than seen with either *longfin*^{t2} or *alf*^{ty86d}. However, after fin amputation, *cacna1g* mutant fins regenerate to extreme lengths comparable to *longfin*^{t2}. Growth rates of regenerating *cacna1g*$^{-/-}$ fins peaks around 3-4 dpa, similar to *longfin*^{t2} (Stewart et al., 2021). We conclude *cacna1g* preferentially restrains overgrowth during fin regeneration. A simple explanation could be functional redundancy. For example, a redundant and/or compensatory voltage-gated Ca^{2+} channel could be expressed in developing, but not regenerating, fins. Alternatively, different outgrowth and/or scaling mechanisms could act in developing vs. regenerating fins, with only the latter requiring Cacna1g-modulated Ca^{2+} dynamics.

Cacna1g is remarkably specific for outgrowth cessation as its loss-of-function otherwise does not overtly disrupt fin pattern, including bony ray branching and segmentation. *cacna1g*$^{-/-}$ ray segments were only slightly longer than wildtype counterparts. In contrast, cilnidipine-treated fins regenerate without ray junctions, reminiscent of *alf*^{ty86d} and calcineurin-inhibited fish

(Perathoner et al., 2014, Kujawski et al., 2014). This result further indicates ray segmentation and outgrowth are orthogonal processes. Extending this idea, Ca^{2+} and calcineurin may have distinct functions in fibroblast-lineage (outgrowth control) and osteoblast-lineage (joint formation) cells. Perturbations that disrupt ion signaling in both cell lineages (*alf*, FK506 treatment, cilnidipine) then produce both phenotypes. In contrast, long-finned models that disrupt ion signaling exclusively in the fibroblast-lineage (*longfin*^{t2}, with fibroblast-specific ectopic Kcnh2a; *cacna1g* homoyzgous mutants) lead to excessive outgrowth but normal segmentation. Considering *cacna1c* expression in osteoblast-lineage blastemal cells and cilnidipine specificity for L-type channels, Cacna1c is likely a primary determinant of cytosolic Ca^{2+} signaling for ray joint formation. Loss-of-function studies of *cacna1c* as well as the N-type *cacna1ba* channel will help resolve distinct, pathway, or redundant roles of each of the three blastema-expressed channels.

Live imaging of GCaMP6s in regenerating fins demonstrates Cacna1g enables heterogeneous Ca^{2+} fluxes of distal fibroblast-derived cells. A likely effector of cytosolic Ca^{2+} flux in fibroblasts is the Ca^{2+}-dependent phosphatase calcineurin given its pharmacologic inhibition also produces regenerative fin overgrowth. Further, calcineurin is controlled by voltage-gated Ca^{2+} channels in other contexts. This model places the gain-of-function effects of K^+ channels upstream, whereby promiscuous K^+ channel activity hypopolarizes fibroblasts, preventing normal Ca^{2+} channel activity and associated cytosolic Ca^{2+} flux culminating in reduced calcineurin activity. Alternatively, calcineurin has been proposed to act upstream of the *alf*^{ty86d}/Kcnk5b K^+ channel to negatively regulate growth factor expression through unresolved gene regulatory mechanisms (Yi et al., 2021). Conceivably, calcineurin could act both upstream and downstream of K^+ channel-modulated ion signaling by contributing to a feedback network.

Additionally, fin excavation ("hole punch") experiments suggest calcineurin acts early to specify the posterior edge of fin damage site (Cao et al. 2021). However, this tissue polarity role for calcineurin may be distinct from its role in restraining the fin outgrowth period. Regardless, these results are at odds with observations a) calcineurin inhibition does not change the maximum outgrowth rate (Stewart et al. 2021), b) alter the blastema pre-pattern (Tornini et al. 2016), and c) calcineurin inhibitors must be administered late in regeneration to override growth cessation mechanisms (Stewart et al., 2021).

We conclude ion signaling or bioelectricity contributes to organ size during fin regeneration by promoting Ca^{2+} dynamics serving as second messengers activating calcineurin. Calcineurin then slows fin outgrowth, possibly by promoting gradual depletion of the distal growth-promoting fibroblast-lineage blastemal cells – which we term "niche" cells for simplicity and to reflect their pro-growth effects on surrounding cell lineages, including osteoblasts. By this model, bioelectricity does not produce a growth-determining pre-pattern while the blastema is established and therefore does not provide positional information itself. However, the Ca^{2+}/calcineurin signaling could reflect feedback output "sensing" size restoration or, more simply, provide robustness circuitry maintaining a "tuned" countdown timer to precisely readout positional information – which could simply be cell numbers – established at the onset of regeneration (Stewart et al. 2019).

MATERIALS AND METHODS

Zebrafish were housed in the University of Oregon Aquatic Animal Care Services facility at 28-29°C. The University of Oregon Institutional Animal Care and Use Committee oversaw animal use. Wildtype *AB* (University of Oregon Aquatic Animal Care Services) and *TL* (Haffter

et al., 1996), lines were used. For all experiments, adult fish (>3 months old) of equal size and sex were used for analysis.

We generated a Tol2 kit compatible (Kwan et al., 2007) 5E_tph1b promoter (Kapsimali et al., 2011) by PCR amplification and molecular cloning. Next, we used Gateway Cloning, ME_GCaMP6s (Chen et al., 2017) and Tol2 kit components to generate the tph1b:GCaMP6s_polyA_cmlc2_ECFP vector. This construct was co-injected with capped RNA coding for the Tc transposase (Kawakami et al., 2000) into one stage AB embryos at a concentration of 25 ng/µl. Animals positive for EGFP expression in the heart at 48 dpa were selected, reared to adulthood, and screened for GCaMP6s expression in regenerative fin rays at 3 dpa. Founders were then outcrossed to AB fish and progeny were selected for EGFP+ hearts, reared to adulthood, screened, and scored for robust GCaMP6s expression in all 18 bony fin rays at 3 dpa. Multiple generational out-crossing isolated a stable *tph1b:GCaMP6s* line, which is maintained in heterozygous state by outcrossing to AB fish and selecting animals with EGFP heart expression.

We designed guide RNAs (gRNA) targeting the 5′ UTR and/or exon 3 of *cacna1g* using ChopChopV3 (Labun et al., 2019). We adapted Bassett et. al (Bassett et. al, 2013) method to create gRNAs DNA templates. gRNA quality was assessed prior to injecting into one-stage AB wildtype embryos at a concentration of 100 ng/µl gRNA(s) and 500 ng/µl Cas9 protein (Thermo). F0 fish were screened for fin outgrowth in uninjured and injured states and then outcrossed to wildtype AB fish. F1 clutches harboring unique mutant alleles were identified by isolating and sequencing DNA from fin clips, then reared to adulthood and outcrossed to AB. Genotyping F1 *cacna1g* mutants identified a 6 bp deletion in the 5′ UTR along the gRNA target site (gRNA underlined and deleted base pairs in bold)

(GGAGCGCGCAATTGGGGATTGGGA). F1 *cacna1g* mutants were in-crossed to generated F2 *cacna1g* families that were genotyped at adulthood by amplifying genomic DNA as described in Bhattacharya et. al (Bhattacharya and Van Meir, 2019) using cacna1g_sg1_for and cacna1g_sg1_rev primers.

Whole animal images were captured using a homemade light box made from a fenestrated styrofoam container, an AmScope LED-8WD Led Spot Light, and a consumer Fujifilm X-A1 camera with Fujinon 28mm 1.4R lens. High resolution fin images were obtained from tricaine-euthanized adult fish mounted with water on a glass slide. Stitched differential interference contrast (DIC) images were then captured using a motorized Nikon Eclipse Ti widefield microscope with a 4X objective and NIS-Elements software.

Single cell RNA-seq data (Lewis et al., 2023) was processed using the 10X Genomics Cell Ranger pipeline (version 5.0.1) and zebrafish reference genome GRCz11_104. To accommodate scRNA-seq 3′ end-sequencing bias, reads were mapped to the comprehensive zebrafish transcriptome V4.3.2 (Lawson et al., 2020). Cell Ranger output files (barcodes, genes, and matrix files) were loaded into Monocle3 (1.0.0) for pre-processing, visualization, and clustering in R (version 4.1.2). An estimated 12,298 cells with a median of 296 genes per cell were used for downstream data analysis. For dimensionality reduction, PCA on log transformed expression matrix with 16 dimensions was applied. UMAP dimensionality projection grouped similar cells according to global expression profiles in 2 dimensions (Becht et al., 2018; McInnes et al., 2018). The UMAP parameters were set to: metric = cosine, distance = 0.05, and neighbor = 50. Clustering using default parameters (except for cluster_cells: method = ‘louvain’, res = 1e-6), produced 11 clusters. Clusters or cell types were assigned by two approaches, first was identifying what genes make each cluster unique by calling the top_markers() function in

Monocole3 using default parameters (except for group_cells_by=”cluster”, reference_cells=500, top_n(6)) (Cao et al., 2019). The second approach was performing a literature review to identify well-known genes associated with cell-types we expected to isolate from our fins. We annotated clusters to be red blood cells (5,092 cells), superficial epidermis (3,330 cells), fibroblast and osteoblast (1,673 cells), macrophage (852 cells), lymphocytes (738 cells), basal epidermis (289 cells), vascular endothelial (105 cells), neutrophils (92 cells), unknown (45 cells), platelet cells (42 cells), and pigment cells (40 cells).

Cilnidipine (Cayman Chemicals) was dissolved in DMSO (Sigma) and diluted to a working stock of 50 mM. From 5 dpa onwards, fish were treated 4 hours a day with DMSO (0.01%) or the indicated concentration of cilnidipine and then returned to normal water flow conditions. For in vitro experiments, compounds were dissolved in DMSO and added to cell culture media in chamber slides at least 15 minutes prior to time-lapse imaging using a stage-mounted incubation system on a Nikon TiE inverted microscope and a Yokogawa CSU-W1 spinning disk confocal microscope.

All fin lengths and segments were measured along the third ray using stereomicroscope images and FIJI software (NIH). Fin length measurements started from the position of the first procurrent ray to the tip of the fin in both injured and uninjured animals. Standard body length was measured from the tip of the mouth to the caudal peduncle using whole animal images.

RNAscope probes to detect *cacna1ba*, *cacna1c*, *cacna1g*, and *dachc* mRNA were designed and synthesized by ACD Bio. RNAscope was performed using the Multiplex Fluorescent kit (ACD Bio) according to manufacturer’s recommendations for paraffin embedded sections with minor modifications. Nuclei were visualized by Hoechst staining (Thermo Fischer). Imaging used Zeiss LSM 880 or LSM 710 laser scanning confocal microscopes.

For in vivo fin regeneration studies, fish were anesthetized in 0.02% tricaine methanesulfonate (MS-222, Syndel) and mounted with fish water on the bottom of a chambered cover glass system (C1-1.5H-N, Cellvis). Fins were positioned with a single-hair paint brush and distal ventral rays imaged using a Nikon/Yokogawa CSI-W1 spinning disk confocal microscope equipped with a 40X water immersion objective lens and NIS-Elements software. The distance between confocal planes was set at 2.5 μm for Z-stack, and a time-lapse of 5 to 6 Z-stacks was conducted with an interval of 1 second between each stack for duration of 10 minutes. Post time-lapse imaging, fish were returned to tanks to recover to normal swimming behavior. Time-lapse recording of regenerated fins was processed for data acquisition using Imaris (v9.9.1). Prior to counting fibroblast fin cells, videos were corrected for translational drift. 3D surfaces were manually drawn onto cells of interest to measure the average GCaMP6s fluorescence and output as an Excel file for each video. Python scripts were used to normalize raw calcium trace data using the formula [$\Delta F/F = (Ft - Fmin)/ F(max - Fmin)$, where Fmin and Fmax are the maximum and minimum trace values, respectfully] developed by Ho et al. (Ho et al., 2021) and plot data.

For in vitro studies, regenerated caudal fins from *tph1b:GCaMP6s* animals were collected, and cells isolated as previously described (Stewart et al., 2014) with minor modifications. Cells were plated on glass coverslips and cultured overnight at 30 degrees in an air incubator in L-15 media (Thermo Fisher) containing 10% Fetal Bovine Serum (Sigma). The following day cells were equilibrated in Tyrode's solution (10 mM HEPES, 127 mM NaCl, 12 mM NaHCO3, 5 mM KCl, 5 mM glucose, 1 mM MgCl2; Boston Bioproducts) for 1 hour at 30 degrees containing the indicated small molecule(s) or an equal volume of DMSO. GCaMP6s+ cells were imaged using a stage-mounted, temperature colored imaging chamber and spinning disk confocal microscopy. Cells were depolarized by adding KCl to a final concentration of 80

mM and imaged for 5 min followed by adding ionomycin (1 μM final concentration) and 1 min of further imaging. Raw calcium trace data was normalized to the highest signal timepoint (=1) using custom Python scripts and output as an Excel file. Normalized data was further analyzed using Python. We defined calcium-responding cells as cells that reached a maximum GCaMP6s fluorescent intensity of >= 0.9 after ionomycin addition. From these filtered responding cells, we identified the fraction of "excitable" cells susceptible to depolarization at a final concentration of 80 mM KCl. We defined excitable cells as cells showing a normalized GCaMP6s fluorescent intensity >= 0.25 immediately after KCl administration. Twenty such Ca^{2+} responding cells were randomly sampled and plotted for each condition.

Fin outgrowth analyses used paired or unpaired Student's T-tests or one-way ANOVA. For ANOVA, Tukey's post-hoc tests were used to determine statistically significant differences between groups. A sigmoidal logistic curve was fit to regenerated ray length over time to account for the establishment phase of blastema formation (Sehring and Weidinger, 2020). A one phase exponential decay curve was fit to outgrowth rate over time starting with the 3 dpa timepoint to isolate the outgrowth phase. All summary statistics, including mean, standard deviation and/or sample size are described in the figure legends. All calculations were performed using GraphPad Prism Version 8.4.3. The lower triangle matrix of significant values in Fig. S26 was plotted as a heatmap in Python. Pie charts for fraction of excitable cells were generated using Python packages.

The following primers were used:

- cacna1g_sg1_for 5'AGGCGTGTATTGGAAGTTGAAT 3'
- cacna1g_sg1_rev 5' AAGCAGTCCAAATGATGGTTCT 3'
- cacna1g_sg2_for 5' GAGATACCCATAAACCTGCTCG 3'

- cacna1g_sg2_rev 5’ GGCTGGTAGGTAGGGAGAAGTT 3’

ACKNOWLEDGMENTS

We thank the University of Oregon Aquatic Animal Care Services for animal husbandry, Drs. Marika Kapsimali and Lilianna Solnica-Krezel for reagents, the University of Oregon Microscopy Core for imaging, and Pete Batzel for assisting with scRNA-sequence analysis.

FOOTNOTES

We report no competing interests. The National Institutes of Health (NIH) provided research funding (R01GM127761 and (K. S. and S. S.)). Heather Kimberly Le Bleu (H. K. L.) was funded by NIH NRSA fellowship (F31HD103459). The University of Oregon NIH-funded Developmental Biology Training Program (T32HD007348) provided H. K. L. with additional trainee support. A Peter O’Day Undergraduate Research Fellowship from the University of Oregon supported R. G. K.

Requests for data and materials should be addressed to K. S.

SUPPLEMENTAL FIGURES

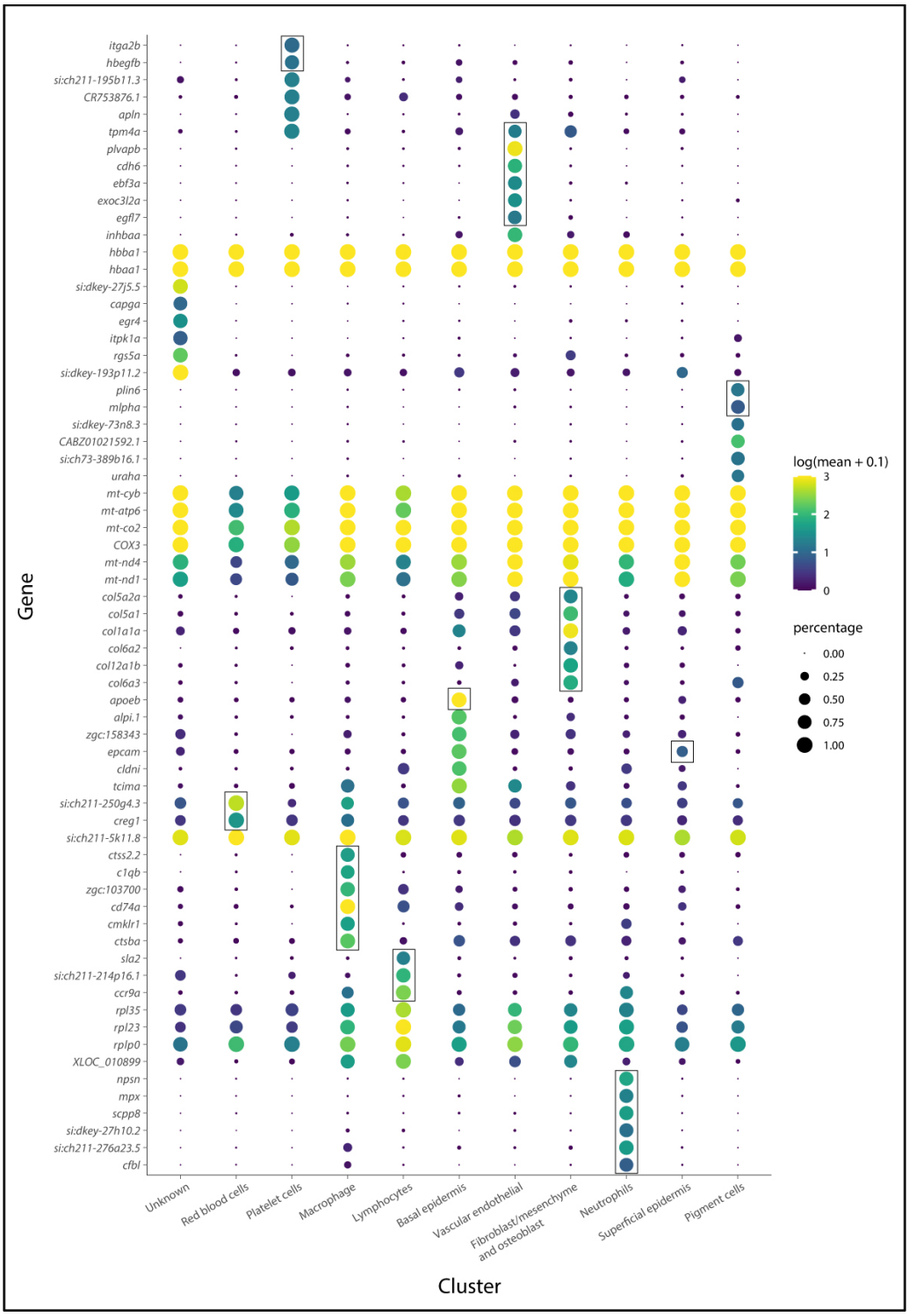

Figure S14. Demarcating 7 dpa caudal fin cell clusters. Dot plot showing expression of six genes selected to be unique to each of the 11 clusters identified from Louvain clustering in Fig 9A. Dot size encodes the percentage of cells within a cluster in which that gene was detected, and its color encodes its average expression level. Black box highlights the unique gene(s) used to infer cluster identities. Cell-types were confirmed using known markers from literature as well.

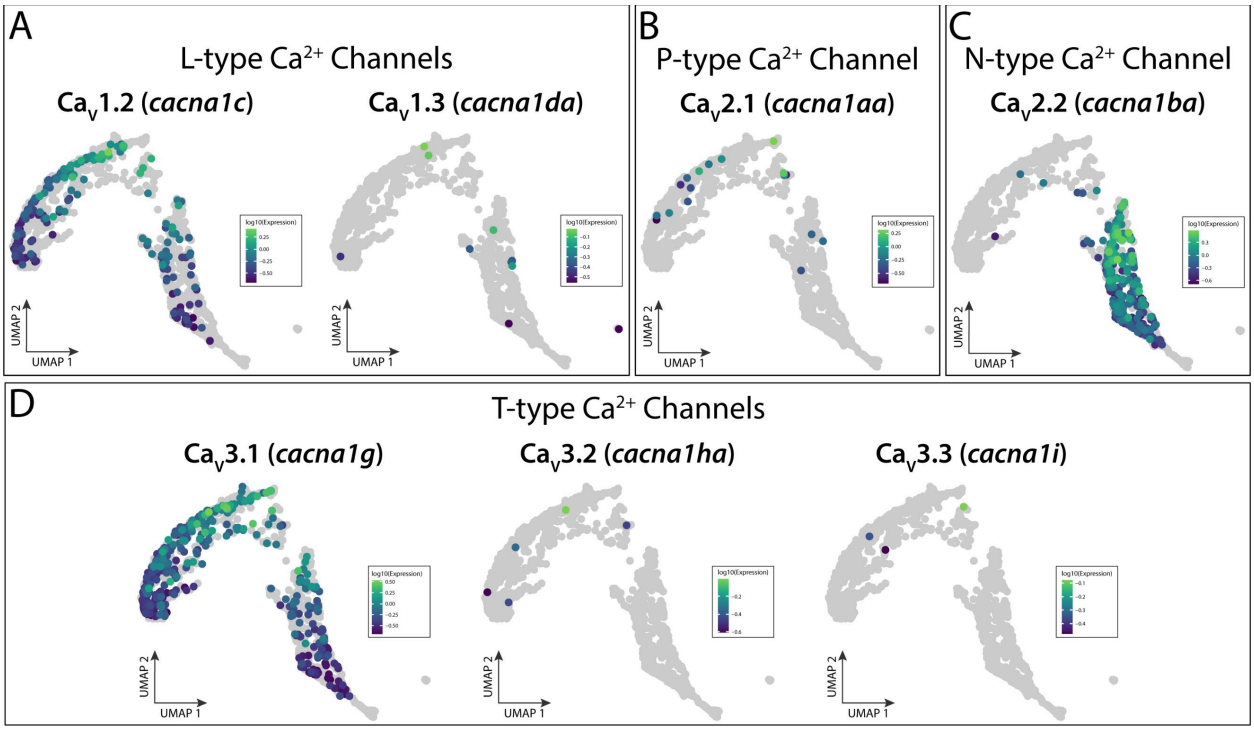

Figure S15. Identifying voltage-gated Ca^{2+} channels expressed in the fibroblast/mesenchyme and osteoblast cluster. (A-D) Candidate voltage-gated Ca^{2+} channel types and UMAP visualization of their corresponding α_1 subunit(s). Each panel represents L- (A), P- (B), N- (C), or T-type (D) voltage-gated Ca^{2+} channels. Only *cacna1c* (L-type), *cacna1ba* (N-type), and *cacna1g* (T-type) genes were predominantly expressed amongst fibroblast-lineage cells and/or osteoblast cells at high levels and in abundance.

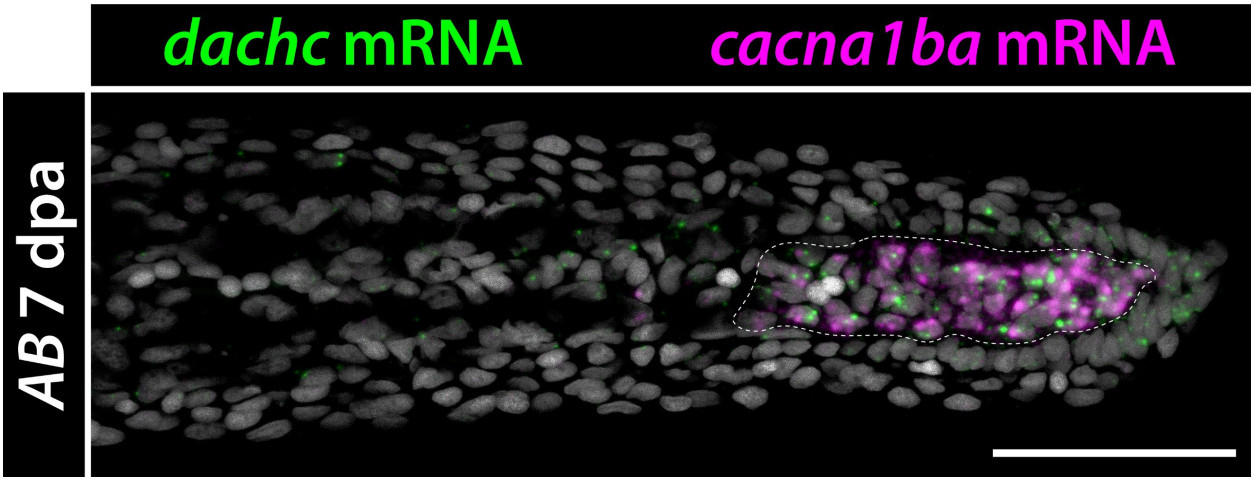

Figure S16. *cacna1ba* is expressed in distal blastema *dachc*$^+$ cells. Representative confocal maximum intensity z-stack image showing double RNAscope in situ hybridization for *dachc* and *cacna1ba* mRNA on 7 dpa wildtype fin section. The dashed white line shows niche-specific *cacna1ba* expression. Hoechst-stained nuclei are in gray. Scale bar is 50 μm.

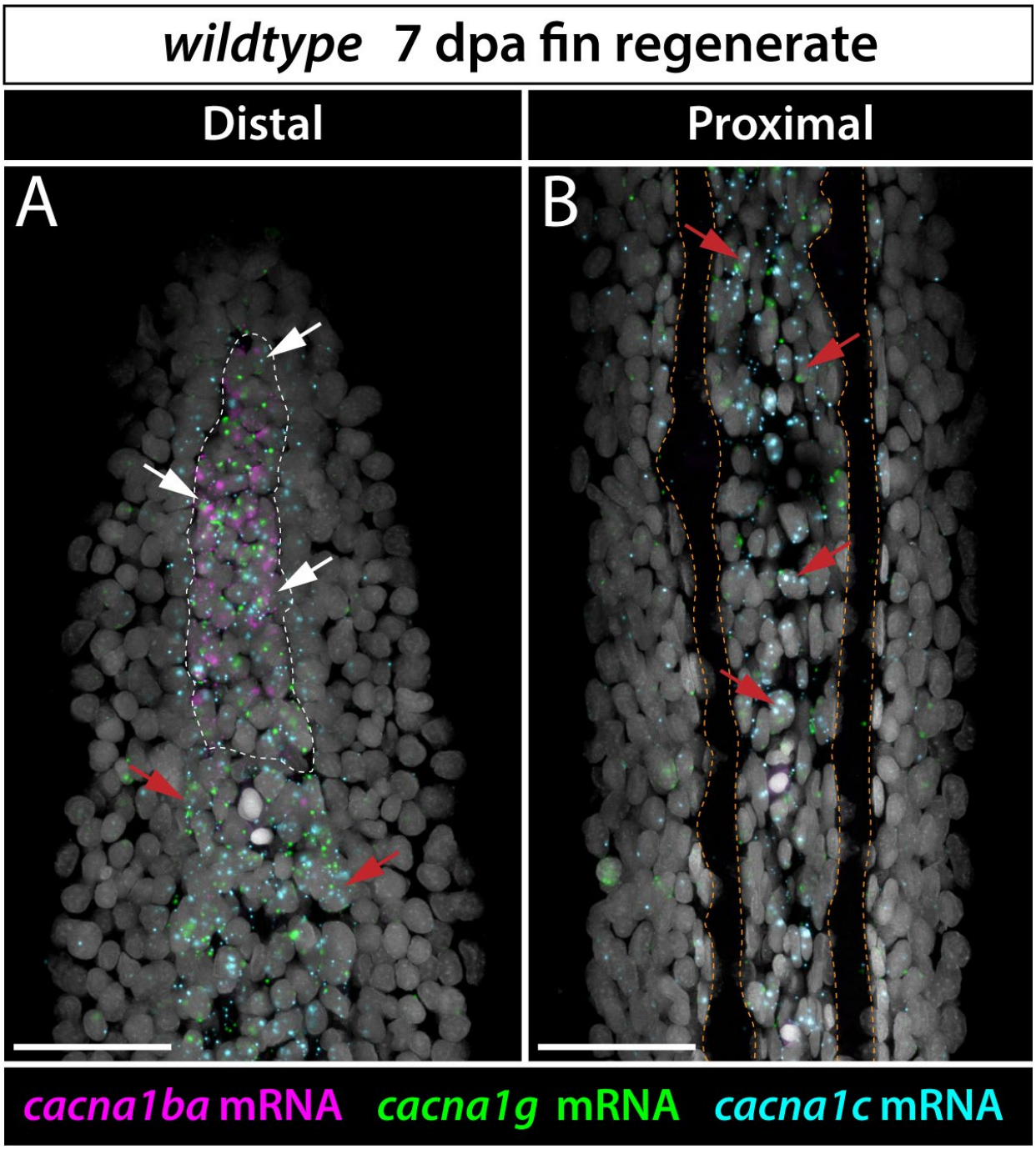

Figure S17. Exclusive co-expression of *cacna1c*, *cacna1ba*, and *cacna1g* to the distal blastema of regenerating fins. Maximum intensity projection images of *cacna1c*, *cacna1ba*, and *cacna1g* RNAscope staining at distal (A) and proximal (B) positions from Figure 9H. Dashed white region outlines distal fibroblast-lineage cells. White arrows point to cells co-expressing *cacna1c*, *cacna1ba*, and *cacna1g* mRNA and red arrows point to cells co-expressing *cacna1c* and *cacna1g* mRNA. Hoechst-stained nuclei are in gray. Dashed orange lines outline fin rays, and the scale bars are 50 μm.

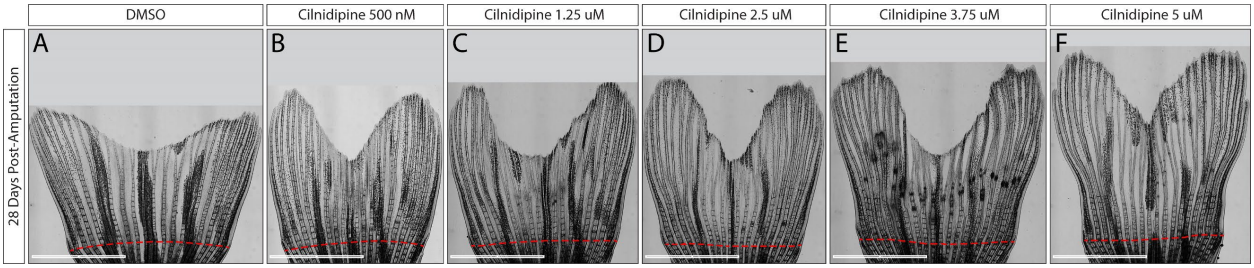

Figure S18. Cilnidipine promotes regenerative fin outgrowth cessation. (A-F) Representative stitched brightfield images of regenerative caudal fin with daily acute treatment of DMSO (A) or 500 nM (B), 1.25 µM (C), 2.5 µM (D), 3.75 µM (E), and 5 µM (F) of cilnidipine from 5 – 28 dpa. The dashed red line indicates amputation plane. The scale bars are 4 mm.

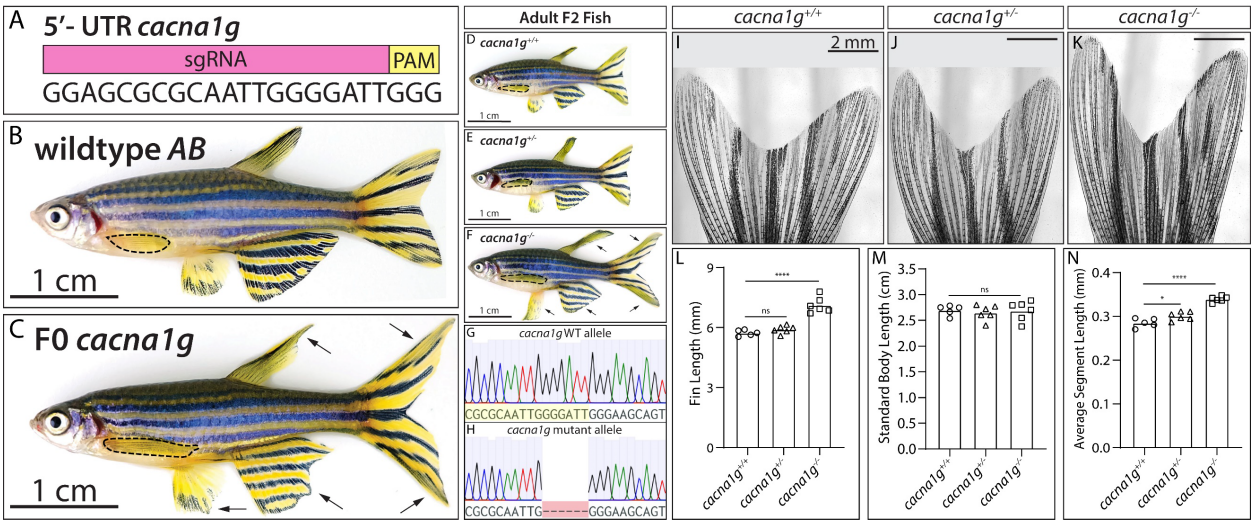

Figure S19. *cacna1g* mutation causes a moderate increase in fin size and shape of developed adult zebrafish fins. (A) Schematic of designed guide RNA to cleave targeted genomic sequence in the 5′UTR of *cacna1g* gene. (B and C) Brightfield lateral whole animal view of control wildtype *AB* (B) and F0 *cacna1g* CRISPant (C). (D-F) Representative brightfield lateral whole animal view of wildtype (D), heterozygous (E), and homozygous mutant (F) *cacna1g* fish from founder in panel C. Black arrows indicate overgrown tissue seen in all fin appendages. Dashed black lines outline the pectoral fin. (G and H) Representative chromatograms of PCR product from WT and mutant *cacna1g* alleles (with expected 6 bp deletion). Deletion in the CRISPR target region is highlighted in yellow in WT allele and evidence of 6 bp deletion is highlighted in pink in the sequence of the mutant allele. (I-K) Representative brightfield stitched images of adult animal caudal fins for each genotype in the clutch *cacna1g*$^{+/+}$ (I), *cacna1g*$^{+/-}$ (J), and *cacna1g*$^{-/-}$ (K); scale bars are 2 mm. (L) Fin length measurements of third ray (starting from the procurrent position to the fin tip) are overgrown in *cacna1g*$^{-/-}$ animals. (M) Standard body length is consistent amongst F2 genotypes. (N) Moderate variation in average segment length measured from the third ray of the caudal fin (N=5 segments/fish) for *cacna1g*$^{+/-}$ and *cacna1g*$^{-/-}$ animals. *$P < 0.05$ and ****$P < 0.5$ vs. the wildtype group (*cacna1g*$^{+/+}$) using one-way ANOVA; ns: not significant.

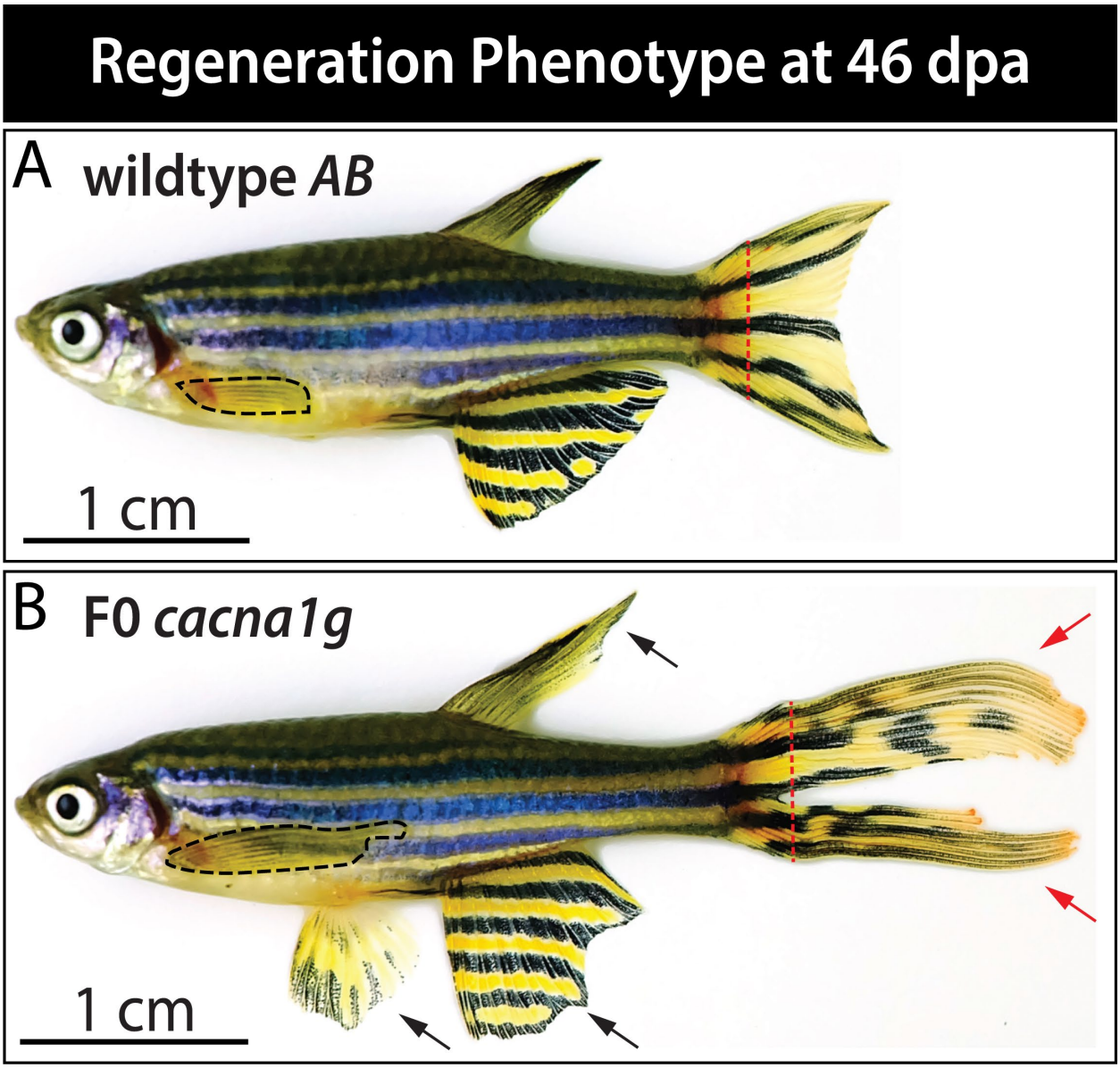

Figure S20. Regenerative fin overgrowth phenotype in *cacna1g* CRISPants. (A and B) The caudal fin of *cacna1g* founder in Supplemental Figure 19 was amputated and screened for regeneration phenotype(s). wildtype *AB* control (A) and F0 *cacna1g* (B) at 46 dpa. Pelvic fin not shown in panel A. Dashed black line outlines pectoral fin. Red dashed line indicates amputation plane. Black arrows point to developmental fin overgrowth and red arrows indicate excessive regenerative caudal fin outgrowth. Scale bars are 1 cm.

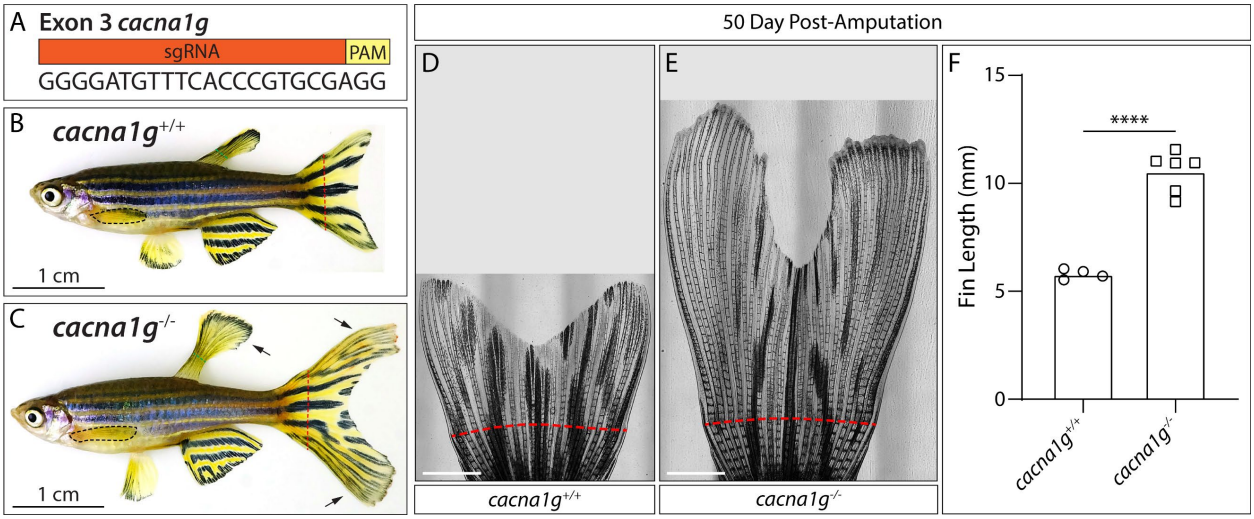

Figure S21. *cacna1g* mutation in exon 3 causes an increase in the size of regenerative fins of adult fish. (A) Schematic of designed guide RNA to cleave targeted genomic sequence in exon 3 of *cacna1g* gene. (B and C) Brightfield lateral whole animal view of control wildtype (B) and homozygous mutant (C) F2 *cacna1g* fish at 70 dpa. Black dashed lines outline the pectoral fin, green dashed lines indicate clipped dorsal fin for genotyping, and the red dashed lines indicate amputation site. Scale bars are 1 cm. (D and E) Representative brightfield stitched images of adult caudal fins at 50 dpa for *cacna1g*$^{+/+}$ (D) and *cacna1g*$^{-/-}$ (E); scale bars are 2 mm. (F) Measurements of fin length of *cacna1g*$^{+/+}$ and *cacna1g*$^{-/-}$ fish at 50 dpa. $^{****}P<0.001$ (unpaired T-test).

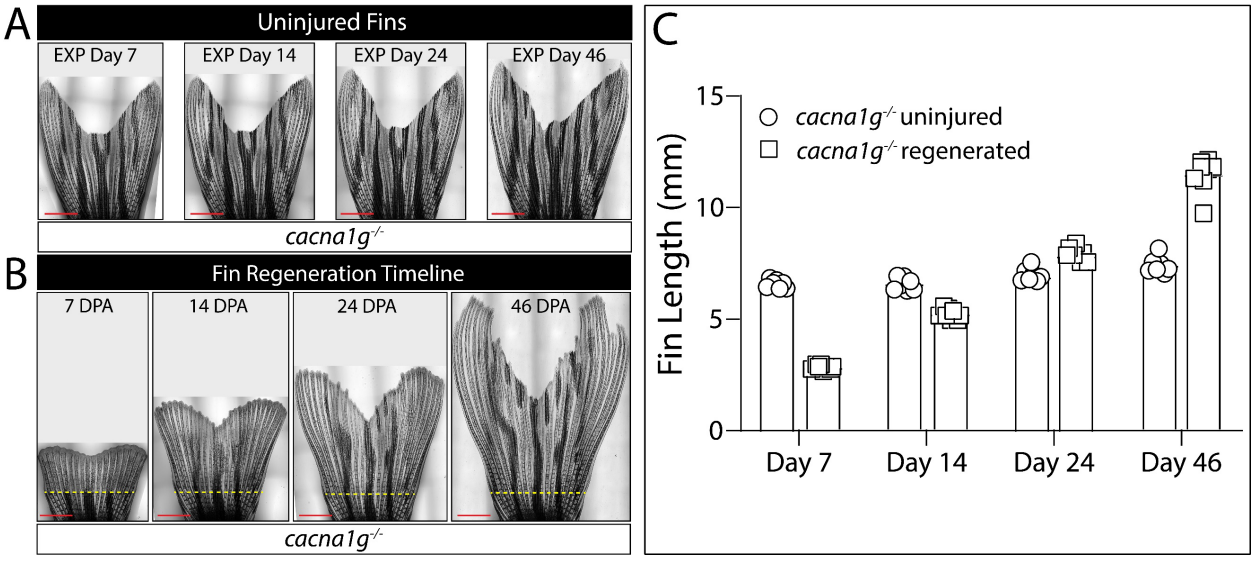

Figure S22. Fin scaling is disrupted in *cacna1g*$^{-/-}$ during regeneration. (A and B) Representative brightfield stitched images of uninjured (A) and regenerating (B) *cacna1g*$^{-/-}$ caudal fins. Fins were captured on days 7, 14, 24, and 46 of experiment (abbreviated as EXP) or day post-amputation (dpa). (C) Individual fin lengths were measured and plotted by treatment group (circles denote uninjured and squares denote regenerated *cacna1g*$^{-/-}$ animals.) Yellow dashed line indicates the amputation plane and red scale bars are 2 mm.

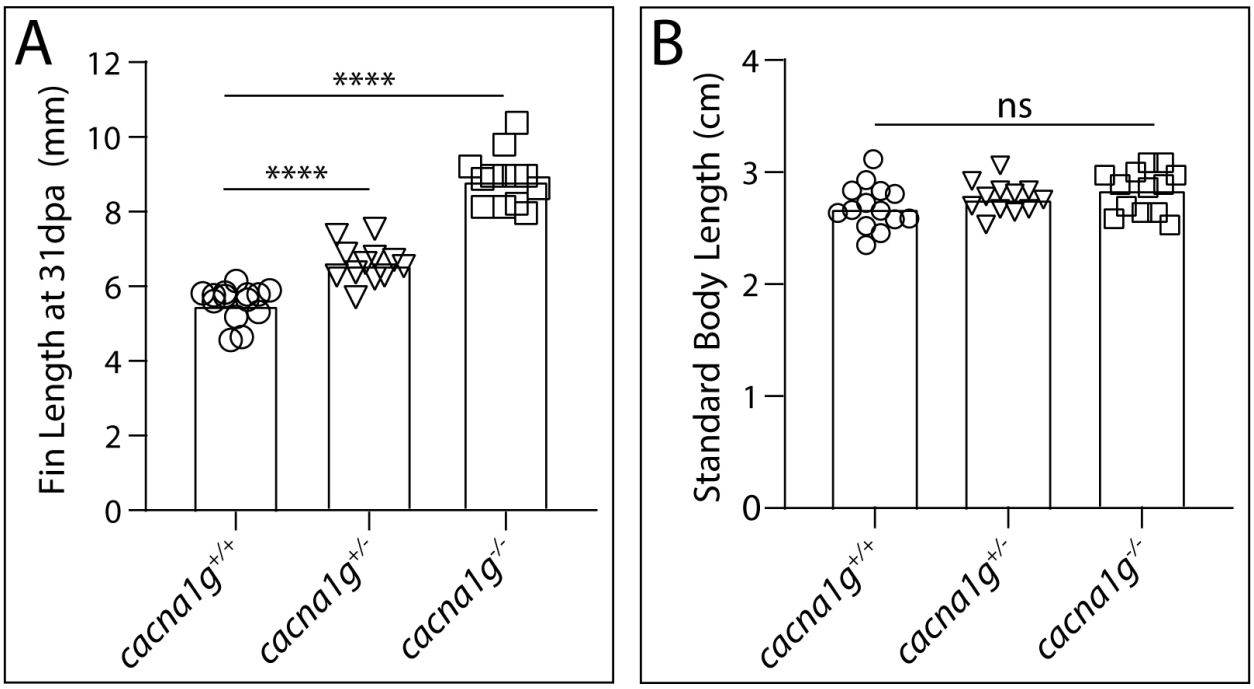

Figure S23. Prolong regenerative outgrowth of *cacna1g* caudal fins. (A and B) Plots show regenerated caudal fin lengths (A) and standard body lengths (B) at 31 dpa for *cacna1g*$^{+/+}$ (circles), *cacna1g*$^{+/-}$ (upside down triangles), and *cacna1g*$^{-/-}$ (squares) fish. Each data point represents an individual animal (N=14 fish per genotype). ****$P > 0.0001$ vs. wildtype group (*cacna1g*$^{+/+}$) using one-way ANOVA; ns: not significant.

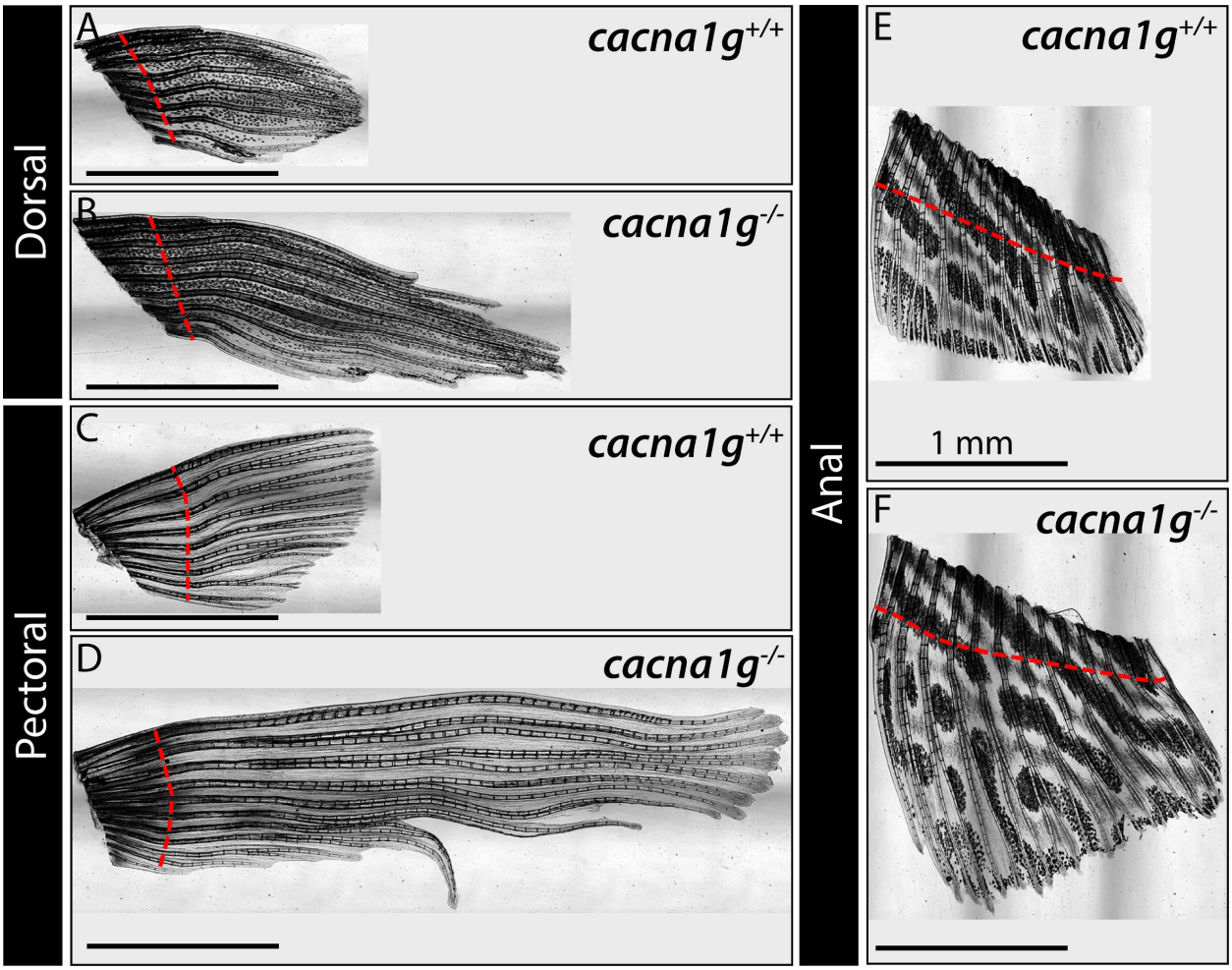

Figure S24. All median and paired fins of *cacna1g*$^{-/-}$ fish regenerate to extraordinary sizes. (A-F) Brightfield stitched images contrasting regenerated fin lengths isolated from *cacna1g*$^{+/+}$ and *cacna1g*$^{-/-}$ fish at 46 dpa. Representative dorsal fins (A and B), pectoral fins (C and D), and anal fins (E and F). Data not shown for pelvic fins. Scale bars are 1 mm.

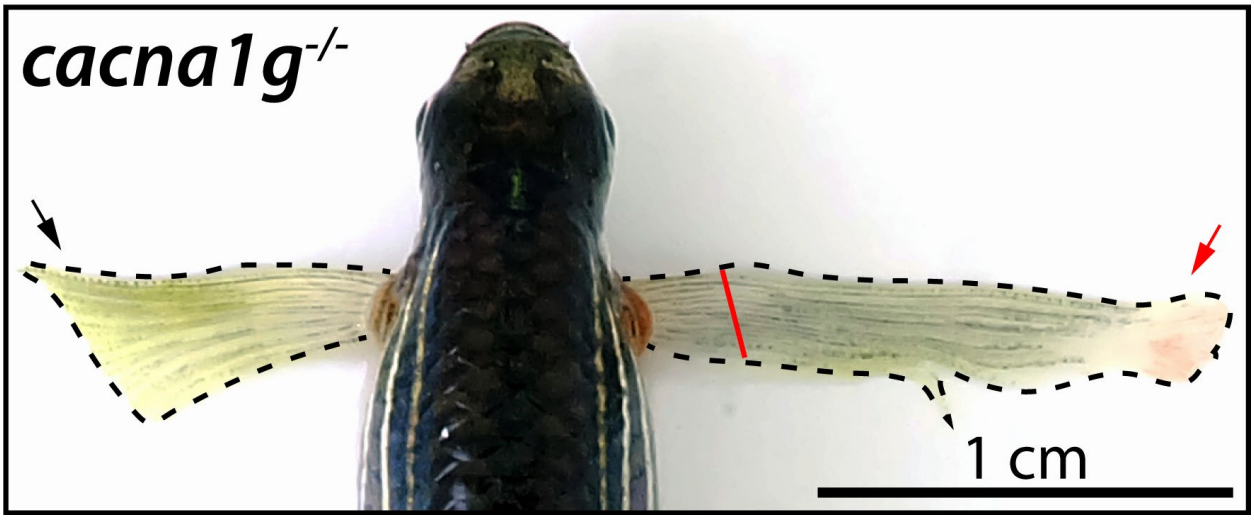

Figure S25. Overgrown pectoral fin reinforces *cacna1g* acts to restrain regenerative fin outgrowth. Brightfield image capturing dorsal whole animal view of a *cacna1g*$^{-/-}$ adult with one paired pectoral fin at 46 dpa. Black dashed line outlines paired pectoral fins. Red line marks amputation site. Red arrow indicates excessively overgrown tissue in regenerating pectoral fin. Black arrow indicates mild outgrowth in its uninjured paired fin. Scale bar is 1 cm.

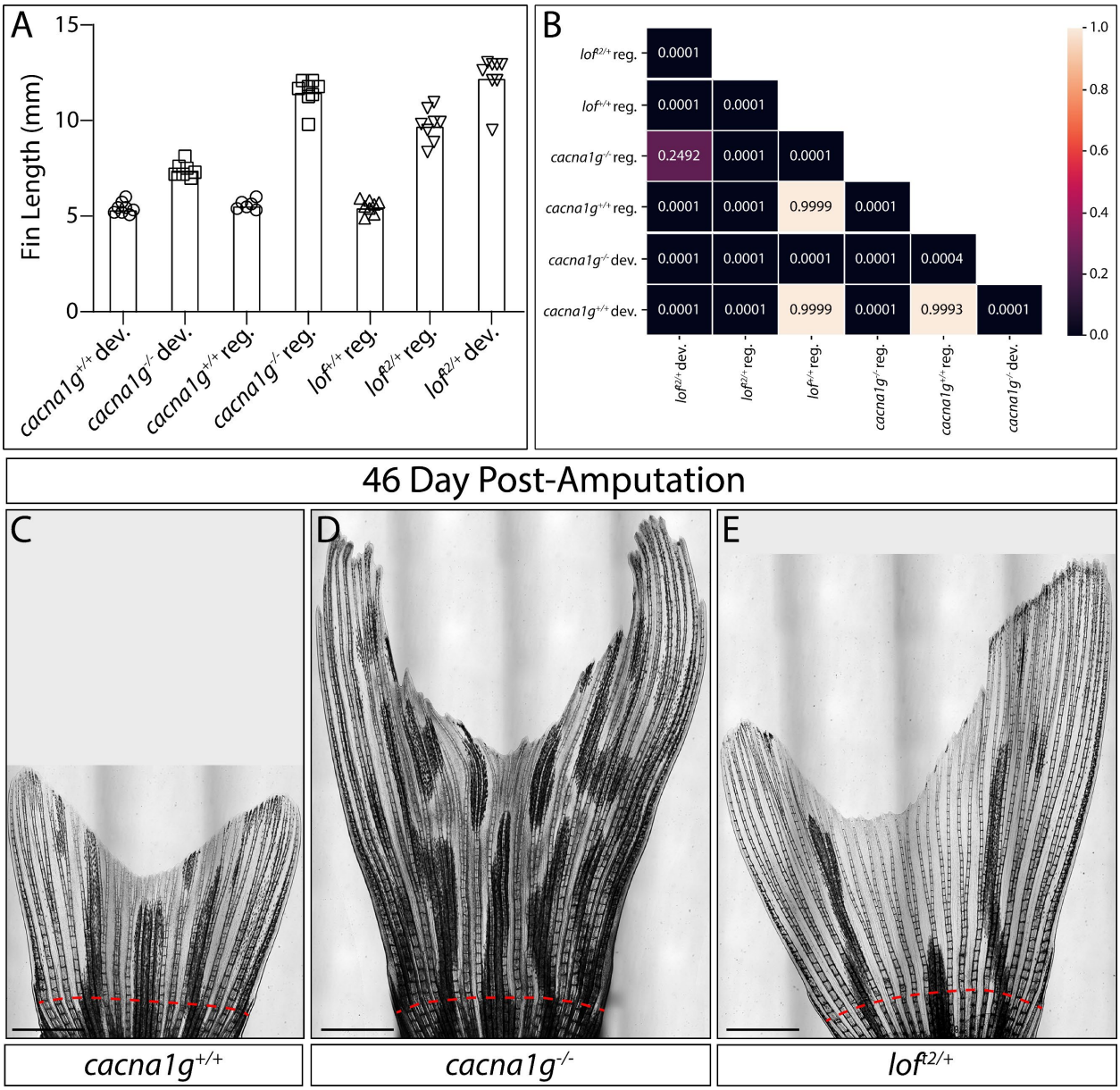

Figure S26. *cacna1g*$^{-/-}$ regenerating caudal fins are comparable in size to *longfin*^{t2}. (A) Fin lengths of *cacna1g*$^{-/-}$ vs. *lof*$^{t2/+}$ animals with corresponding clutchmate controls. *cacna1g*$^{-/-}$ fins regenerated to a similar extent as *lof*$^{t2/+}$ groups. (B) Heatmap depicts p-value significances for a one-way ANOVA Tukey's multiple comparisons test performed using data groups from panel A. (C-E) Representative brightfield stitched images of *cacna1g*$^{+/+}$ (C), *cacna1g*$^{-/-}$ (D), and *lof*$^{t2/+}$ (E) caudal fins at 46 dpa. Red dashed line indicates amputation plane. Scale bars are 1 mm.

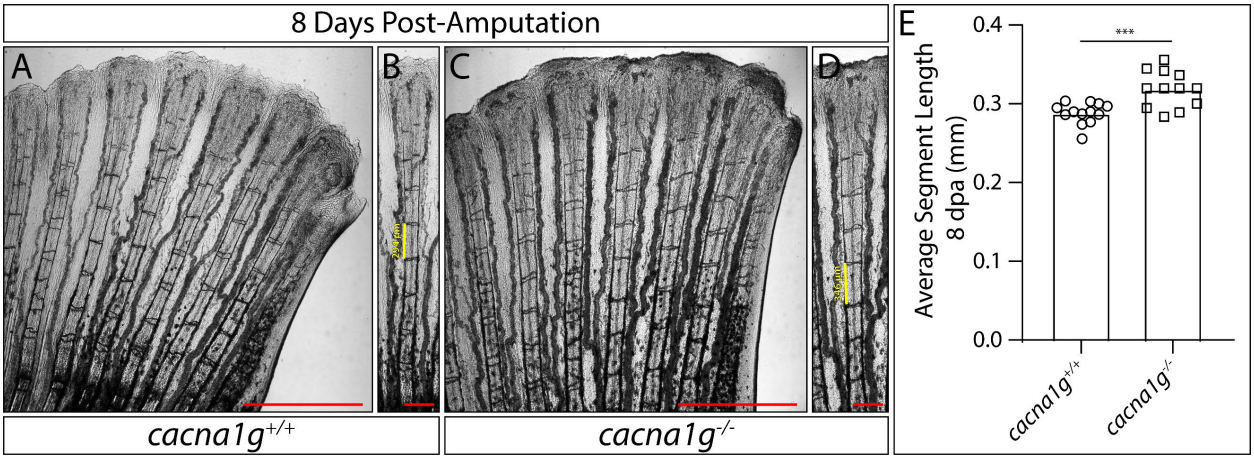

Figure S27. *cacna1g*$^{-/-}$ fish regenerate jointed rays. (A-D) Representative brightfield stitched images of ventral caudal fin lobe of *cacna1g*$^{+/+}$. (A and B) and *cacna1g*$^{-/-}$ (C and D) animals at 8 dpa. Scale bars are 1 mm for panels A and C and 250 µm for B and D. Yellow line represents the length of an individual segment. (E) Quantification of average segment length (N=5 segments/fish) at 8 dpa for each genotype (circles are *cacna1g*$^{+/+}$ and squares are *cacna1g*$^{-/-}$ fish). ***$P<0.001$ vs. the control group (*cacna1g*$^{+/+}$) using unpaired t-test.

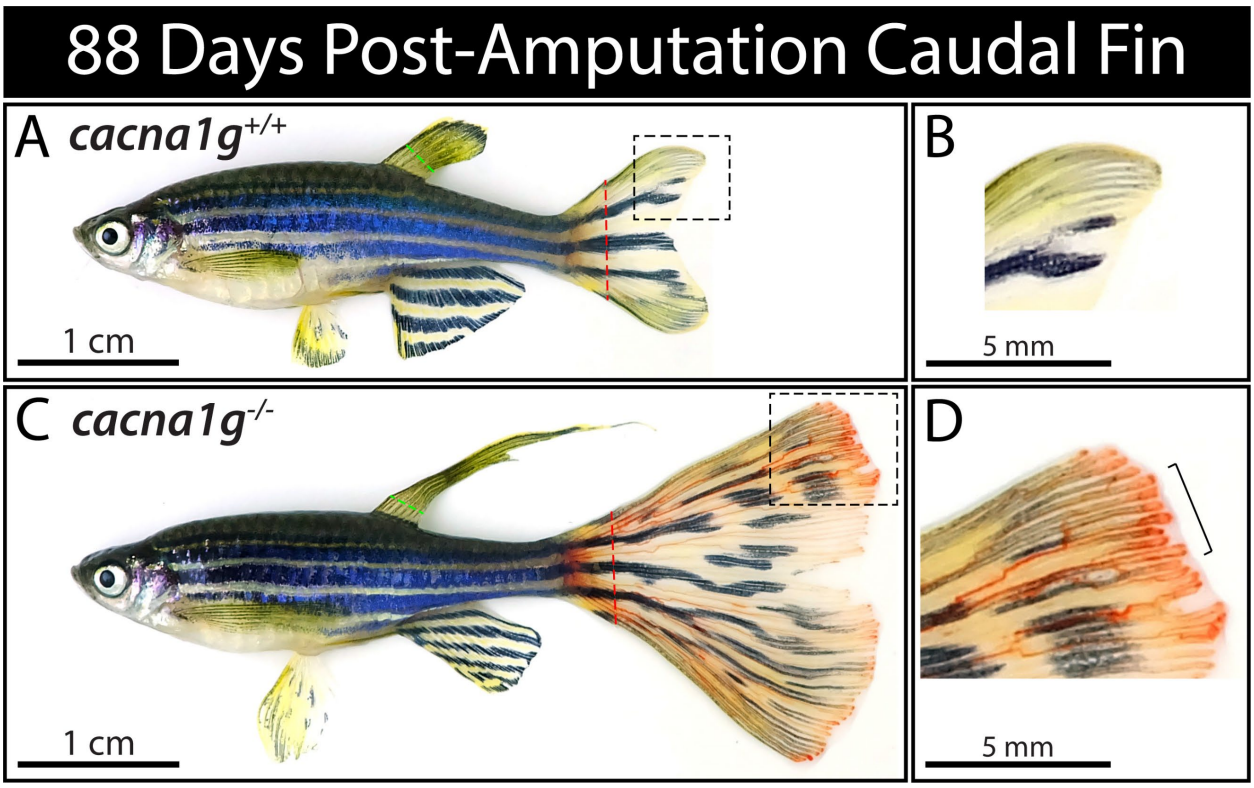

Figure S28. Excessive fin vascularization in *cacna1g*$^{-/-}$ regenerating adult caudal fin. (A-D) Representative brightfield images of lateral whole animal view of *cacna1g*$^{+/+}$ (A and B) and *cacna1g*$^{-/-}$ (C and D) adult fish at 88 dpa. Dashed green line marks clipped dorsal fin for genotyping and red dashed line indicates amputation plane. Black dashed box shows zoomed in areas of caudal fin for *cacna1g*$^{+/+}$ (B) and *cacna1g*$^{-/-}$ (D). Black bar highlights a region of blood pooling at the fin tip of *cacna1g*$^{-/-}$, which is not observed in *cacna1g*$^{+/+}$ fish. Scale bars are 1 cm or 5 mm.

CHAPTER IV: CONCLUSION SUMMARY

For centuries, developmental biologists have been fascinated by the phenomenon of regeneration. Zebrafish fin regeneration has been of particular interest for investigating mechanisms of organ size control. Developmental and regenerative studies have universally implicated ion signaling as a major determinant of fin growth and scaling. Yet, how ion signaling or bioelectricity instructs fin size and shape remained unresolved. This prompted our investigation to determine how the classic *longfin*^{t2} develops and regenerates extraordinarily long fins. We found that *longfin*^{t2} causes *cis*-ectopic expression of the K^+ channel *kcnh2a* in fibroblast fin cells to autonomously prolong the period of fin outgrowth. We revealed that ectopic *kcnh2a* is likely acting upstream Ca^{2+}-dependent calcineurin signaling to disrupt fin cessation. The discovery that *longfin*^{t2} is a gain-of-function model for overgrown fins limited our interpretations regarding how ion signaling controls fin cessation in normal/wildtype fish. Numerous studies have shown that K^+ channels modulate repolarization-depolarization kinetics, ultimately changing intracellular Ca^{2+} dynamics. Therefore, we explored the contribution of voltage-gated Ca^{2+} channel activity and Ca^{2+} signaling in fin regeneration and size control. We showed that voltage-gated Ca^{2+} channels generate Ca^{2+} fluxes in fibroblast-lineage blastema mesenchyme to restrain fin outgrowth. We introduced a genetic loss-of-function of the T-type *cacna1g* channel that directly links Ca^{2+} signaling to mechanisms of normal fin regrowth and tissue scaling. Collectively, our studies support the notion that upstream voltage-gated Ca^{2+} channels interpret electrical signals at the cell membrane level, thereby modulating activity and signaling pathways to regulate downstream pathways controlling cellular behaviors essential for zebrafish fin regeneration.

REFERENCES CITED

Akimenko, M. A., Johnson, S. L., Westerfield, M. and Ekker, M. (1995). Differential induction of four msx homeobox genes during fin development and regeneration in zebrafish. *Development* **121**, 347–357.

Anders, S., Pyl, P. T. and Huber, W. (2015). HTSeq--a Python framework to work with high-throughput sequencing data. *Bioinformatics* **31**, 166–169.

Bassett, A. R., Tibbit, C., Ponting, C. P. and Liu, J. L. (2013). Highly efficient targeted mutagenesis of drosophila with the crispr/cas9 system. *Cell Rep* **4**, 220–228.

Baumgärtel, K. and Mansuy, I. M. (2012). Neural functions of calcineurin in synaptic plasticity and memory. *Learn. Mem.* **19**, 375–384.

Beane, W. S., Morokuma, J., Lemire, J. M. and Levin, M. (2013). Bioelectric signaling regulates head and organ size during planarian regeneration. *Development* **140**, 313–322.

Becht, E., McInnes, L., Healy, J., Dutertre, C. A., Kwok, I. W. H., Ng, L. G., Ginhoux, F., and Newell, E. W. (2018). Dimensionality reduction for visualizing single-cell data using umap. *Nat Biotechnol*. **37**, 38–44.

Bhattacharya, D. and Van Meir, E. G. (2019). A simple genotyping method to detect small crispr-cas9 induced indels by agarose gel electrophoresis. *Sci Rep* **9**, 4437.

Blondel, V. D., Guillaume, J.-L., Lambiotte, R. and Lefebvre, E. (2008). Fast unfolding of communities in large networks. *J. Stat. Mech.* **2008**, P10008.

Bohnen, M. S., Peng, G., Robey, S. H., Terrenoire, C., Iyer, V., Sampson, K. J. and Kass, R. S. (2017). Molecular Pathophysiology of Congenital Long QT Syndrome. *Physiol. Rev.* **97**, 89–134.

Boniface, E. J., Lu, J., Vicotroff, T., Zhu, M. and Chen, W. (2009). FlEx-based transgenic reporter lines for visualization of Cre and Flp activity in live zebrafish. *Genesis (New York, N.Y. : 2000)* **47**, 484–491.

Butler, M. G., Iben, J. R., Marsden, K. C., Epstein, J. A., Granato, M. and Weinstein, B. M. (2015). SNPfisher: tools for probing genetic variation in laboratory-reared zebrafish. *Development* **142**, 1542–1552.

Cao, J., Spielmann, M., Qiu, X., Huang, X., Ibrahim, D. M., Hill, A. J., Zhang, F., Mundlos, S., Christiansen, L., Steemers, F. J., Trapnell, C. and Shendure, J. (2019). The single-cell transcriptional landscape of mammalian organogenesis. *Nature* **566**, 496–502.

Cao, Z., Meng, Y., Gong, F., Xu, Z., Liu, F., Fang, M., Zou, L., Liao, X., Wang, X., Luo, L., Li, X. and Lu, H. (2021) Calcineurin controls proximodistal blastema polarity in zebrafish fin regeneration. *Proc. Natl. Acad. Sci. U.S.A.* **118**, e2009539118.

Catterall, W. A. (2011). Voltage-gated calcium channels. *Cold Spring Harb Perspect Biol* **3**, a003947.

Chen, C. H. and Poss, K. D. (2017). Regeneration Genetics. *Annu. Rev. Genet.* **51**, 63–82.

Chen, J., Xia, L., Bruchas, M. R. and Solnica-Krezel, L. (2017). Imaging early embryonic calcium activity with GCaMP6s transgenic zebrafish. *Dev Biol* **430**, 385–396.

Chen, T. W., Wardill, T. J., Sun, Y., Pulver, S. R., Renninger, S. L., Baohan, A., Schreiter, E. R., Kerr, R. A., Orger, M. B., Jayaraman, V., Looger, L. L., Svoboda, K. and Kim, D. S. (2013). Ultrasensitive fluorescent proteins for imaging neuronal activity. *Nature*, **499**. 295–300.

Crabtree, G. R. (1999). Generic signals and specific outcomes: signaling through Ca2+, calcineurin, and NF-AT. *Cell* **96**, 611–614.

Curran, M. E., Splawski, I., Timothy, K. W., Vincent, G. M., Green, E. D. and Keating, M. T. (1995). A molecular basis for cardiac arrhythmia: HERG mutations cause long QT syndrome. *Cell* **80**, 795–803.

Daane, J. M., Blum, N., Lanni, J., Boldt, H., Iovine, M. K., Higdon, C. W., Johnson, S. L., Lovejoy, N. R. and Harris, M. P. (2021) Modulation of bioelectric cues in the evolution of flying fishes. *Curr Biol* **32**, 5052-5061.

Daane, J. M., Lanni, J., Rothenberg, I., Seebohm, G., Higdon, C. W., Johnson, S. L. and Harris, M. P. (2018). Bioelectric-calcineurin signaling module regulates allometric growth and size of the zebrafish fin. *Sci Rep* **8**, 10391.

DeLaurier, A., Eames, B. F., Blanco Sánchez, B., Peng, G., He, X., Swartz, M. E., Ullmann, B., Westerfield, M. and Kimmel, C. B. (2010). Zebrafish sp7:EGFP: A transgenic for studying otic vesicle formation, skeletogenesis, and bone regeneration. *Genesis* **48**, 505–511.

DeMazumder, D. and Tomaselli, G.F. (2012) Molecular and cellular mechanisms of cardiac arrhythmias. In *Muscle* (ed. A. H. a. E. N. O. Joseph), pp. 583–599. Boston/Waltham: Academic Press.

Dimitriou, R., Jones, E., McGonagle, D. and Giannoudis, P. V. (2011). Bone regeneration: Current concepts and future directions. *BMC Med* **9**, 66.

Eisenhoffer, G. T., Kang, H. and Sánchez Alvarado, A. (2008). Molecular analysis of stem cells and their descendants during cell turnover and regeneration in the planarian schmidtea mediterranea. *Cell Stem Cell* **3**, 327–339.

Elias, J. (1984). *Brachydanio frankei*-Schleierform. *Aquaria* **34**, 81–85.

Farnsworth, D. R., Saunders, L. M. and A. C., Miller. (2020). A single-cell transcriptome atlas for zebrafish development. *Dev Biol* **459**, 100–108.

Gaviño, M. A. and Reddien, P. W. (2011). A bmp/admp regulatory circuit controls maintenance and regeneration of dorsal-ventral polarity in planarians. *Curr Biol* **21**, 294–299.

Gemberling, M., **Bailey, T. J., Hyde, D. R. and Poss, K. D.** (2013). The zebrafish as a model for complex tissue regeneration. *Trends Genet.* **29**, 611–620.

Goldsmith, M. I., Iovine, M. K., O'Reilly-Pol, T. and Johnson, S. L. (2006). A developmental transition in growth control during zebrafish caudal fin development. *Dev Biol* **296**, 450–457.

Haffter, P., Odenthal, J., Mullins, M. C., Lin, S., Farrell, M. J., Vogelsang, E., Haas, F., Brand, M., Van Eeden, F. J., Furutani-Seiki, M., Granato, M., Hammerschmidt, M., Heisenberg, C. P., Jiang, Y. J., Kane, D. A., Kelsh, R. N., Hopkins, N. and Nüsslein-Volhard, C. (1996). Mutations affecting pigmentation and shape of the adult zebrafish. *Dev. Genes Evol.* **206**, 260–276.

Harris, M. P. (2021). Bioelectric signaling as a unique regulator of development and regeneration. *Development* **148**, dev180794.

Harris, M. P., Daane, J. M. and Lanni, J. (2020). Through veiled mirrors: Fish fins giving insight into size regulation. *Wiley Interdiscip Rev Dev Biol* **99**, e381.

Ho, K. Y. L., Khadilkar, R. J., Carr, R. L. and Tanentzapf, G. (2021). A gap-junction-mediated, calcium-signaling network controls blood progenitor fate decisions in hematopoiesis. *Curr Biol* **31**, 4697–4712.

Hou, Y., Lee H.J., Chen, Y., Ge, J., Osman, F. O. I., McAdow, A. R., Mokalled, M. H., Johnson, S. L., Zhao, G. and Wang, T. (2020). Cellular diversity of the regenerating caudal fin. *Sci Adv.* **6**, eaba2084.

Hu, L. Y., Ryder, T. R., Rafferty, M. F., Dooley, D. J., Geer, J. J., Lotarski, S. M., Miljanich, G. P., Millerman, E., Rock, D. M., Stoehr, S. J., Szoke, B. G., Taylor, C. P. and Vartanian, M. G. (1999). Structure-activity relationship of N-methyl-N-aralkyl-peptidylamines as novel N-type calcium channel blockers. *Bioorg Med Chem Lett.* **9**, 2151-2156.

Iaquinta, M. R., Mazzoni, E., Bononi, I., Rotondo, J. C., Mazziotta, C., Montesi, M., Sprio, S., Tampieri, A., Tognon, M. and Martini, F. (2019). Adult stem cells for bone regeneration and repair. *Front Cell Dev Biol* **7**, 268.

Iovine, M. K., Higgins, E. P., Hindes, A., Coblitz, B. and Johnson, S. L. (2005). Mutations in connexin43 (GJA1) perturb bone growth in zebrafish fins. *Dev Biol* **278**, 208–219.

Iovine, M. K. and Johnson, S. L. (2000). Genetic analysis of isometric growth control mechanisms in the zebrafish caudal fin. *Genetics* **155**, 1321–1329.

Iovine, M. K. and Johnson, S. L. (2002). A genetic, deletion, physical, and human homology map of the long fin region on zebrafish linkage group 2. *Genomics* **79**, 756–759.

Kapsimali, M. K., Kaushik, A. L., Gibon, G., Dirian, L., Ernest, S. and Rosa, F. M. (2011). Fgf signaling controls pharyngeal taste bud formation through miR-200 and Delta-Notch activity. *Development* **138**, 3473–3484.

Kawakami, K., Shima, A. and Kawakami N. (2000). Identification of a functional transposase of the Tol2 element, an Ac-like element from Japanese medaka fish, and its transposition in the zebrafish germ lineage. *Proc Natl Acad Sci U S A.* **97**, 11403–11408.

Kim, D., Pertea, G., Trapnell, C., Pimentel, H., Kelley, R. and Salzberg, S. L. (2013). TopHat2: accurate alignment of transcriptomes in the presence of insertions, deletions and gene fusions. *Genome Biol.* **14**, R36.

Kimmel, C. B., Ballard, W. W., Kimmel, S. R., Ullmann, B. and Schilling, T. F. (1995). Stages of embryonic development of the zebrafish. *Dev. Dyn.* **203**, 253–310.

Kimmel, C. B., Warga, R. M. and Schilling, T. F. (1990). Origin and organization of the zebrafish fate map. *Development* **108**, 581–594.

Klee, C. B., Ren, H. and Wang, X. (1998). Regulation of the calmodulin-stimulated protein phosphatase, calcineurin. *Journal of Biological Chemistry* **273**, 13367–13370.

Knopf, F., Hammond, C., Chekuru, A., Kurth, T., Hans, S., Weber, C. W., Mahatma, G., Fisher, S., Brand, M., Schulte-Merker, S. and Weidinger, G. (2011). Bone Regenerates via Dedifferentiation of Osteoblasts in the Zebrafish Fin. *Developmental Cell* **20**, 713–724.

Kujawski, S., Lin, W., Kitte, F., Börmel, M., Fuchs, S., Arulmozhivarman, G., Vogt, S., Theil, D., Zhang, Y. and Antos, C. L. (2014). Calcineurin regulates coordinated outgrowth of zebrafish regenerating fins. *Developmental Cell* **28**, 573–587.

Kwan, K. M., Fujimoto, E., Grabher, C., Mangum, B. D., Hardy, M. E., Campbell, D. S., Parant, J. M., Yost, H. J., Kanki, J. P. and Chein C.B. (2007). The Tol2kit: a multisite gateway-based construction kit for Tol2 transposon transgenesis constructs. *Dev Dyn.* **236**, 3088-3099.

Labun, K., Montague, T. G., Krause, M., Torres Cleuren, Y. N., Tjeldnes, H. and Valen, E. (2019). Chopchop v3: Expanding the crispr web toolbox beyond genome editing. *Nucleic Acids Res* **47**, W171–W174.

Lanni, J. S., Peal, D., Ekstrom, L., Chen, H., Stanclift, C., Bowen, M. E., Mercado, A., Gamba, G., Kahle, K. T. and Harris, M. P. (2019). Integrated K^+ channel and K+Cl- cotransporter function are required for the coordination of size and proportion during development. *Dev Biol* **456**, 164–178.

Lawson, N. D., Li, R., Shin, M., Grosse, A., Yukselen, O., Stone, O. A., Kucukural, A. and Zhu, L. (2020). An improved zebrafish transcriptome annotation for sensitive and comprehensive detection of cell type-specific genes. *Elife* **9**, e55792.

Lee, Y., Grill, S., Sanchez, A., Murphy-Ryan, M. and Poss, K. D. (2005). Fgf signaling instructs position-dependent growth rate during zebrafish fin regeneration. *Development* **132**, 5173–5183.

Lee, Y., Hami, D., De Val, S., Kagermeier-Schenk, B., Wills, A. A., Black, B. L., Weidinger, G. and Poss, K. D. (2009). Maintenance of blastemal proliferation by functionally diverse epidermis in regenerating zebrafish fins. *Dev Biol* **331**, 270–280.

Levin, M. (2014). Molecular bioelectricity: how endogenous voltage potential control cell behavior and instruct pattern regulation in vivo. *Mol Biol Cell* **25**, 3835-3850.

Lewis, V. M., Le Bleu, H. K., Henner, A. L., Markovic, H., Robbins, A. E., Stewart, S. and Stankunas, K. (2023). Insulin-like growth factor receptor / mTOR signaling elevates global translation to accelerate zebrafish fin regeneration. *Dev Biol* **502**, 1–13.

Mardon, G., Solomon, N. M. and Rubin, G. M. (1994). Dachshund encodes a nuclear protein required for normal eye and leg development in Drosophila. *Development* **120**, 3473–3486.

McInnes, L., Healy, J., Saul, N. and Großberger, L. (2018). Umap: Uniform manifold approximation and projection. *Journal of Open Source Software*. arXiv.1802.0342603.

McLaughlin, K. A. and Levin, M. (2018). Bioelectric signaling in regeneration: Mechanisms of ionic controls of growth and form. *Dev Biol* **433**, 177–189.

McMillan, S. C., Zhang, J., Phan, H.-E., Jeradi, S., Probst, L., Hammerschmidt, M. and Akimenko, M.-A. (2018). A regulatory pathway involving retinoic acid and calcineurin demarcates and maintains joint cells and osteoblasts in regenerating fin. *Development* **145**, dev161158.

Morgan, T. H. (1900). Regeneration in teleosts. *Archiv für Entwicklungsmechanik der Organismen* **10**, 120–134.

Morrison, S. J. and Spradling, A. C. (2008). Stem cells and niches: Mechanisms that promote stem cell maintenance throughout life. *Cell* **132**, 598–611.

Nayler, W. G. and Gu, X. H. (1991). The unique binding properties of amlodipine: a long-acting calcium antagonist. *J Hum Hypertens.* **5**, 55–59.

Nelson, J. S., Grande, T. C. and Wilson, M. (2016). *Fishes of the World*. Fifth Edition. John Wiley & Sons.

Noble, D. and Tsien, R. W. (1969). Outward membrane currents activated in the plateau range of potentials in cardiac Purkinje fibres. *J. Physiol. (Lond.)* **200**, 205–231.

Parra, V. and Rothermel, B. A. (2017). Calcineurin signaling in the heart: The importance of time and place. *J. Mol. Cell. Cardiol.* **103**, 121–136.

Paton, D. M. and Webster, D. R. (1985). Clinical pharmacokinetics of H1-receptor antagonists (the antihistamines). *Clin Pharmacokinet* **10**, 477–497.

Perathoner, S., Daane, J. M., Henrion, U., Seebohm, G., Higdon, C. W., Johnson, S. L., Nüsslein-Volhard, C. and Harris, M. P. (2014). Bioelectric signaling regulates size in zebrafish fins. *PLoS Genet* **10**, e1004080.

Perez-Reyes, E. (1998). Molecular characterization of a novel family of low voltage-activated, t-type, calcium channels. *J Bioenerg Biomembr* **30**, 313–318.

Petersen, C. P. and Reddien, P. W. (2009). Wnt signaling and the polarity of the primary body axis. *Cell* **139**, 1056–1068.

Poss, K. D., Shen, J., Nechiporuk, A., McMahon, G., Thisse, B., Thisse, C. and Keating, M. T. (2000). Roles for Fgf signaling during zebrafish fin regeneration. *Dev Biol* **222**, 347–358.

Quint, E., Smith, A., Avaron, F., Laforest, L., Miles, J., Gaffield, W. and Akimenko, M.-A. (2002). Bone patterning is altered in the regenerating zebrafish caudal fin after ectopic expression of sonic hedgehog and bmp2b or exposure to cyclopamine. *Proc. Natl. Acad. Sci. U.S.A.* **99**, 8713–8718.

Rabinowitz, J. S., Robitaille, A. M., Wang, Y., Ray, C. A., Thummel, R., Gu, H., Djukovic, D., Raftery, D., Berndt, J. D. and Moon, R. T. (2017). Transcriptomic, proteomic, and metabolomic landscape of positional memory in the caudal fin of zebrafish. *Proc. Natl. Acad. Sci. U.S.A.* **114**, E717–E726.

Rao, A. (2009). Signaling to gene expression: calcium, calcineurin and NFAT. *Nat. Immunol.* **10**, 3–5.

Robinson, M. D., McCarthy, D. J. and Smyth, G. K. (2010). edgeR: a Bioconductor package for differential expression analysis of digital gene expression data. *Bioinformatics* **26**, 139–140.

Sanguinetti, M. C. and Tristani-Firouzi, M. (2006). hERG potassium channels and cardiac arrhythmia. *Nature* **440**, 463–469.

Sanguinetti, M. C., Jiang, C., Curran, M. E. and Keating, M. T. (1995). A mechanistic link between an inherited and an acquired cardiac arrhythmia: HERG encodes the IKr potassium channel. *Cell* **81**, 299–307.

Santamaría, J. A., Marí-Beffa, M. and Becerra, J. (1992). Interactions of the lepidotrichial matrix components during tail fin regeneration in teleosts. *Differentiation* **49**, 143–150.

Schartl, M., Kneitz, S., Ormanns, J., Schmidt, C., Anderson, J. L., Amores, A., Catchen, J., Wilson, C., Geiger, D., Du, K., Garcia-Olazábal, M., Sudaram, S., Winkler, C., Hedrich, R., Warren, W. C., Walter, R., Meyer, A. and Postlethwait, J. H. (2020). The developmental and genetic architecture of the sexually selected male ornament of swordtails. *bioRxiv* 2020.07.24.219840.

Schulte, C. J., Allen, C., England, S. J., Juárez-Morales, J. L. and Lewis, K. E. (2011). Evx1 is required for joint formation in zebrafish fin dermoskeleton. *Dev Dyn* **240**, 1240–1248.

Sehring, I. M. and Weidinger, G. (2020). Recent advancements in understanding fin regeneration in zebrafish. *Wiley Interdiscip Rev Dev Biol* **9**, e367.

Shen, W. and Mardon, G. (1997). Ectopic eye development in Drosophila induced by directed dachshund expression. *Wiley Interdiscip Rev Dev Biol* **9**, 45–52.

Shibata, E., Yokota, Y., Horita, N., Kudo, A., Abe, G., Kawakami, K. and Kawakami, A. (2016). Fgf signalling controls diverse aspects of fin regeneration. *Development* **143**, 2920–2929.

Silic, M. R., Wu, Q., Kim, B. H., Golling, G., Chen, K. H., Freitas, R., Chubykin, A. A., Mittal, S. K. and Zhang, G. (2020). Potassium Channel-Associated Bioelectricity of the Dermomyotome Determines Fin Patterning in Zebrafish. *Genetics* **215**, 1067–1084.

Singh, S. P., Holdway, J. E. and Poss, K. D. (2012). Regeneration of amputated zebrafish fin rays from de novo osteoblasts. *Developmental Cell* **22**, 879–886.

Smith, A., Avaron, F., Guay, D., Padhi, B. K. and Akimenko, M. A. (2006). Inhibition of BMP signaling during zebrafish fin regeneration disrupts fin growth and scleroblasts differentiation and function. *Dev Biol* **299**, 438–454.

Sousa, S., Afonso, N., Bensimon-Brito, A., Fonseca, M., Simões, M., Leon, J., Roehl, H., Cancela, M. L. and Jacinto, A. (2011). Differentiated skeletal cells contribute to blastema formation during zebrafish fin regeneration. *Development* **138**, 3897–3905.

Stewart, S., Gomez, A. W., Armstrong, B. E., Henner, A. and Stankunas, K. (2014). Sequential and opposing activities of Wnt and BMP coordinate zebrafish bone regeneration. *Cell Reports* **6**, 482–498.

Stewart, S., Le Bleu, H. K., Yette, G. A., Henner, A. L., Robbins, A. E., Braunstein, J. A. and Stankunas, K. (2021). Longfin causes cis-ectopic expression of the kcnh2a ether-a-go-go k+ channel to autonomously prolong fin outgrowth. *Development* **148**, dev199384.

Stewart, S. and Stankunas, K. (2012). Limited dedifferentiation provides replacement tissue during zebrafish fin regeneration. *Dev Biol* **365**, 339–349.

Stewart, S., Yette, G. A., Le Bleu, H. K., Henner, A. L., Braunstein, J. A., Chehab, J. W., Harms, M. J. and Stankunas, K. (2019). Skeletal geometry and niche transitions restore organ size and shape during zebrafish fin regeneration. *bioRxiv* 606970.

Stoick-Cooper C.L., Weidinger G., Riehle K.J., Hubbert C., Major M.B., Fausto N. and Moon R.T. (2007). Distinct Wnt signaling pathways have opposing roles in appendage regeneration. *Development* **134**, 479–489.

Suessbrich, H., Waldegger, S., Lang, F. and Busch, A. E. (1996). Blockade of HERG channels expressed in Xenopus oocytes by the histamine receptor antagonists terfenadine and astemizole. *FEBS Lett.* **385**, 77–80.

Takahara, A. (2012). Dual l/n-type ca^{2+} channel blocker: Cilnidipine as a new type of antihypertensive drug. In *Antihypertensive Drugs* (ed. P. H. Babaei), pp. 29–44. China: InTech.

Timmerman, L. A., Clipstone, N. A., Ho, S. N., Northrop, J. P. and Crabtree, G. R. (1996). Rapid shuttling of NF-AT in discrimination of Ca2+ signals and immunosuppression. *Nature* **383**, 837–840.

Ton, Q. V. and Iovine, M. K. (2013). Identification of an evx1-dependent joint-formation pathway during FIN regeneration. *PLOS ONE* **8**, e81240.

Tornini, V. A., Puliafito, A., Slota, L. A., Thompson, J. D., Nachtrab, G., Kaushik, A.-L., Kapsimali, M., Primo, L., Di Talia, S. and Poss, K. D. (2016). Live Monitoring of Blastemal Cell Contributions during Appendage Regeneration. *Curr. Biol.* **26**, 2981–2991.

Tornini, V. A., Thompson, J. D., Allen, R. L. and Poss, K. D. (2017). Live fate-mapping of joint-associated fibroblasts visualizes expansion of cell contributions during zebrafish fin regeneration. *Development* **144**, 2889–2895.

Tseng, A. S., Adams, D. S., Qiu, D., Koustubhan, P. and Levin, M. (2007). Apoptosis is required during early stages of tail regeneration in xenopus laevis. *Dev Biol* **301**, 62–69.

Tu, S. and Johnson, S. L. (2011). Fate restriction in the growing and regenerating zebrafish fin. *Developmental Cell* **20**, 725–732.

Van Eeden, F. J., Granato, M., Schach, U., Brand, M., Furutani-Seiki, M., Haffter, P., Hammerschmidt, M., Heisenberg, C. P., Jiang, Y. J., Kane, D. A., Kelsh, R. N., Mullins,

M. C., Odenthal, J., Warga, R. M. and Nüsslein-Volhard, C. (1996). Genetic analysis of fin formation in the zebrafish, Danio rerio. *Development* **123**, 255–262.

Vandenberg, J. I., Perry, M. D., Perrin, M. J., Mann, S. A., Ke, Y. and Hill, A. P. (2012). hERG K(+) channels: structure, function, and clinical significance. *Physiol. Rev.* **92**, 1393–1478.

Wang, F., Flanagan, J., Su, N., Wang, L.-C., Bui, S., Nielson, A., Wu, X., Vo, H.-T., Ma, X.-J. and Luo, Y. (2012). RNAscope: a novel in situ RNA analysis platform for formalin-fixed, paraffin-embedded tissues. *J Mol Diagn* **14**, 22–29.

Wehner, D., Cizelsky, W., Vasudevaro, M. D., Özhan, G., Haase, C., Kagermeier-Schenk, B., Röder, A., Dorsky, R. I., Moro, E., Argenton, F., Kühl, M. and Weidinger, G. (2014). Wnt/β-catenin signaling defines organizing centers that orchestrate growth and differentiation of the regenerating zebrafish caudal fin. *Cell Reports* **6**, 467–481.

Wehner, D. and Weidinger, G. (2015). Signaling networks organizing regenerative growth of the zebrafish fin. *Trends Genet.* **31**, 336–343.

Wenemoser, D., Lapan, S. W., Wilkinson, A. W., Bell, G. W. and Reddien, P. W. (2012). A molecular wound response program associated with regeneration initiation in planarians. *Genes Dev* **26**, 988–1002.

Wenemoser, D. and Reddien, P. W. (2010). Planarian regeneration involves distinct stem cell responses to wounds and tissue absence. *Dev Biol* **344**, 979–991.

Wolpert, L. (2016). Positional information and pattern formation. *Curr Top Dev Biol* **117**, 597–608.

Yamaura, T., Kase, N., Kita, H. and Uematsu, T. (1986). Antihypertensive and cardiovascular effects of the new dihydropyridine derivative methyl (E)-3-phenyl-2-propen-1-yl-1,4-dihydro-2,6-dimethyl- 4(3-nitrophenyl)pyridine-3,5-dicarboxylate. *Arzneimittel-Forschung* **36**, 29–34.

Yi, C., Spitters, T. W., Al-Far, E. A.-D. A., Wang, Sen, Cai, S., Yan, X., Guan, K., Wagner, M., El-Armouche, A. and Antos, C. L. (2021). A calcineurin-mediated scaling mechanism that controls a K^+-leak channel to regulate morphogen and growth factor transcription. *Elife*, **10**, e60691.

Yunker, A. M. and McEnery, M. W. (2003). Low-voltage-activated ("T-type") calcium channels in review. *J Bioenerg Biomembr* **35**, 533–575.

Zhou, Z., Vorperian, V. R., Gong, Q., Zhang, S. and January, C. T. (1999). Block of HERG potassium channels by the antihistamine astemizole and its metabolites desmethylastemizole and norastemizole. *J. Cardiovasc. Electrophysiol.* **10**, 836–843.